FAR-INFRARED AND NMR SPECTROSCOPIC STUDIES OF ORGANOMETALLIC COMPOUNDS

Thesis submitted for the degree of
Doctor of Philosophy
at the University of Leicester

by

Zaid Mahmood

Department of Chemistry
University of Leicester

University of Leicester
Department of Chemistry
Leicester, LE1 7RH

June 1996

ProQuest LLC
789 East Eisenhower Parkway
P.O. Box 1346
Ann Arbor, MI 48106-1346

Statement

The experimental work described in this thesis has been carried out by the author in the Department of Chemistry at the University of Leicester, between October 1992 and May 1996. The work has not been submitted for any other degree at this or any other university.

Signed Zaid Mahmood Date 4/9/1996

Dedicated to My Parents

Acknowledgements

I would like to thank my supervisor Dr. D. K. Russell, for all his help, guidance and patience during the cource of this work. My special thanks must go to my supervisor Dr A. M. Ellis, for his help, encouragement, guidance and supervision throughout this work. It is not possible to express in words my gratitude to him having spent invaluable time on many discussions, reading and giving comments during the course of this work.

I would also like to thank Dr. G. Griffith for his help with recording and interpretation of the number of NMR spectra. I also thank to Dr Graham Eaton for his guidance on the MS experiments and Dr. A. C. Jones for his supply of chemicals.

I am also grateful to Dr U. S. Rai for his help. I am also equally grateful to G. P. Mills and S. Sydam for their invaluable help and contributions.

I would also like to thank Ann Crane for drawing a number of the figures in this thesis and Vicky Orson-Wright and Martin Spark for their help. Further, I would like to express my gratitude to Phil Acton and Gerry Butler for their assistance when the equipment failed to function correctly.

I am also extremely grateful to all Chemistry workshop staff without whose expertise, advice and co-operation this thesis would not have been possible. In particular, I would like to express my gratitude to Roy Batchen for the construction of the vacuum line and reaction cells, and to Keith Wilkinson and Jack Patel for the construction of other vital equipment.

Further, I would like to express my gratitude to my wife for her continuous support encouragement throughout the course of this work, and her tolerance during the preparation of this thesis.

Last but by no means least, I would like to thank the Ministry of Education Government of Pakistan for a research studentship.

Far-infrared and NMR spectroscopic studies of organometallic compounds.

Abstract.

Far-infrared and mid-infrared spectroscopy, mass spectrometry and ^1H NMR spectroscopy of various isotopic combinations of $(CH)_3Al$+$(CH_3)_2AlH$ in the gas phase have been recorded to confirm the nature of mixed bridge compounds. IR studies have shown that the major constituent of a labile gas phase equilibrium mixture of trimethylalane and dimethylalane is the heteroleptic pentamethyldialane, $Me_2Al(\mu H)(\mu H)AlMe_2$. A partial normal coordinate analysis of the spectra of isotopic variants reveals that this predominance arises from a significant strengthening of the Al-H-Al bridging bond. IR and NMR studies lead to a similar conclusion for solutions of alane mixtures in toluene, and lend support for a ligand exchange mechanism involving singly bridged species.

Solution mixtures of dimethylgallane and diethylgallane in toluene have been investigated using mass spectrometry and proton NMR spectroscopy. The mass spectrometric observations reveal the presence of dimeric and trimeric species. The NMR results confirm this conclusion, and further suggest that intramolecular exchange processes are fast even at 200 K, whereas intermolecular exchange is significant only abve 250 K.

Vibrational spectra of $C_4H_6Fe(CO)_3$, $CpMn(CO)_3$ and $MeCpMn(CO)_3$ have been measured in the vapour phase in the 500-10 cm^{-1} region using IR spectroscopy and an assignment is given. Low frequency vibrations were investigated in order to determine whether these provide any useful information on the structure and bonding in the aforementioned compounds.

The vibrational spectra of $XMn(CO)_5$ compounds (where X= CH_3, H, CF_3, Br, Cl) in the vapour phase have been studied in the far-infrared region. This study was carried out to ascertain the effect of the non-carbonyl ligand in $XMn(CO)_5$ on the bonding in the $Mn(CO)_5$ group. The number of ν(MC) and δ(MCO) modes active in the infrared in the gas phase was compared with the data available in the liquid phase in the same region and their frequencies were correlated where possible with the frequencies of the ν(CO) modes.

The overall aim of this work was to characterise the structure and interactions (intra- and intermolecular) in a variety of organometallics. Many of these compounds are important precursors in semiconductor fabrication.

Contents

List of Figures. ix

List of Tables. xi

Chapter 1

Introduction. 1

References. 8

Chapter 2. Experimental details and techniques. 10

2.1 Introduction. 11

2.2 The manipulation of air-sensitive compounds. 11

2.3 Sample preparation. 12

2.4 Basic experimental approach. 15

2.5 Infrared Laser Homogeneous Pyrolysis IR LPHP. 15

2.5.1 Basics of IR LPHP. 15

2.5.2 The carbon dioxide laser. 17

2.6 Reaction cells. 20

2.7 Window materials. 21

2.7.1 ZnSe windows. 21

2.7.2 Polyethylene windows. 22

2.8 Spectroscopic methods. 25

2.8.1 Fourier Transform Infrared Spectroscopy. 25

2.8.2 Fourier Transform NMR Spectroscopy. 30

2.9 Chemicals. 33

Chapter 3. Mixtures of Trimethylaluminium and Dimethylaluminiumhydride.

3.1 Introduction. 37

3.2 Review. 39

3.3 Experimental details. 43

3.3.1 Chemicals employed and their characterization. 43

3.3.2 Sample preparation. 53

3.4 Gas phase Mid-IR Investigations. 53

3.4.1 DMAlH + TMAl mixture. 53

3.4.2 DMAlD + TMAl mixture. 54

3.5 Gas phase far-infrared study. 60

3.5.1 Far-infrared spectra of TMAl, d_9-TMAl, DMAlH, and DMAlD. 60

3.5.2 Mixture of TMAl + DMAlH and TMAl + DMAlD. 61

3.6 Liquid Phase FTIR spectra of DMAlH + TMAl mixture in cyclopentane. 66

3.7 ^{1}H NMR spectra of DMAl + TMAl mixture in d_8-toluene. 72

3.8 Discussion and Conclusion. 76

Chapter 4. Spectroscopic studies of exchange and pyrolysis reactions of Trimethylamine alane, Trimethylgallane and Triethylgallane mixtures. 85

4.1 Introduction. 86

4.2 Synthesis and properties of mixed alkyl Group compounds. 88

4.3 Experimental details. 91

4.4 Exchange studies of TMGa and TMAA mixtures. 92

4.4.1 Synthesis of Dimethylgalliumhydride, Me_2GaH. 92

4.4.2 FTIR spectrum of TMGa + TMAA mixture. 93

4.4.3 ^{1}H NMR spectra of Dimethylgalliumhydride. 94

4.5 Synthesis of Diethylgalliumhydride by IR LPHP. 98

4.6 ^{1}H NMR spectra of a MeGaH + EtGaH mixture. 101

4.7 IR LPHP studies of TMGa + TEtGa mixture. 105

4.7.1 FTIR studies of the pyrolysis products of TMGa + TEGa. 105

4.7.2 ^{1}H NMR studies of the pyrolysis products of TMGa+TEGa mixtures.

4.7.3 Mass spectra of pyrolysis product of TMGa +TEGa mixtures. 111

4.8 Discussion and Conclusion. 115

Chapter 5. Comparative far-infrared studies of η-bonded carbonyls. 122

5.1 Introduction. 123

5.2 Experimental. 126

5.3 Results and Discussion. 127

5.3.1 Butadiene Iron Tricarbonyl. 127

5.3.2 Cyclopentadienylmanganese Tricarbonyl and Methylcyclopentadienylmanganese Tricarbonyl. 133

5.4 Conclusion. 141

Chapter 6. Comparative studies of $Mn(CO)_5X$ compounds.

6.1 Introduction. 145

6.2 Experimental details. 149

6.2.1 Sample preparations. 149

6.2.2 Infrared spectroscopy. 151

6.3 Results and Discussion. 151

6.3.1 $BrMn(CO)_5$ and $ClMn(CO)_5$. 151

6.3.2 $HMn(CO)_5$ and $DMn(CO)_5$. 160

6.3.3 $CH_3Mn(CO)_5$ and $CD_3Mn(CO)_5$. 166

6.3.4 $CF_3Mn(CO)_5$. 172

6.4 Conclusion. 176

Chapter 7. Overall Conclusions. 181

List of Figures.

2.1	Schematic diagram of vacuum manifold.	13
2.2	Schematic diagram of the sample tube used.	14
2.3	Schematic diagram of the essential elements of the IR LPHP technique.	16
2.4	Schematic diagram of CO_2 laser.	18
2.5	Block diagram of the vibrational energy levels used in the CO_2 laser.	19
2.6	Schematic diagram of the standard reaction cell.	23
2.7	Schematic diagram of the reaction cell used for low vapour pressure compounds.	24
2.8	Optical path of FTS-40V far-infrared spectrometer.	27
2.9	Schematic diagram of kinetically moveable mylar beamsplitters.	28
2.10	Schematic diagram of the Michelson interferometer.	29
3.1	FTIR spectrum of $(CH_3)_3Al$.	45
3.2	FTIR spectrum of $(CD_3)_3Al$.	46
3.3	FTIR spectrum of $(CH_3)_2AlH$.	47
3.4	FTIR spectrum of $(CH_3)_2AlD$.	48
3.5	FTIR spectrum of $(CD_3)_2AlH$.	49
3.6	FTIR spectrum of mixture $(CH_3)_2AlH$ and $(CH_3)_3Al$.	56
3.7	FTIR spectrum of mixture $(CH_3)_2AlD$ and $(CH_3)_3Al$.	57
3.8	FTIR spectrum of mixture of $(CD_3)_2AlH$ and $(CD_3)_3Al$.	58
3.9	Far-infrared spectrum of $(CH_3)_3Al$.	62
3.10	Far-infrared spectrum of $(CD_3)_3Al$.	63
3.11	Far-infrared spectrum of $(CH_3)_2AlH$.	64
3.12	Far-infrared spectrum of $(CH_3)_2AlD$.	65
3.13	Far-infrared spectrum of a mixture of $(CH_3)_2AlH$ and $(CH_3)_3Al$.	68
3.14	Far-infrared spectrum of a mixture of $(CH_3)_2AlH$ and $(CH_3)_3Al$.	69
3.15	FTIR spectrum of a mixture of $(CH_3)_2AlH$ and $(CH_3)_3Al$ in cyclopentane solution.	
3.16	^1H NMR spectrum of a 1:1 mixture of $(CH_3)_2AlH$ and $(CH_3)_3Al$ in d_8-toluene at 191 K. Only the regions of Al-H and CH_3 resonances are shown.	74
3.17	Temperature variation of the Me resonances (D-G) of figure 3.16.	75

4.1 FTIR spectrum of mixture of TMAA and TMGa in the ratio 1:3(A) and 1:1(B).
4.2 FTIR spectrum of DMGaH produced by a mixture of TMAA and TMGa in the ratio 1:3. 96
4.3 ^{1}H NMR spectrum of DMGaH in d_8-toluene solution. 97
4.4 FTIR spectrum of DEGaH produced by IR LPHP of TEGa. 99
4.5 FTIR spectrum of a mixture SF_6 and TEGa before (A) and after (B) irradiation at 2 W of laser power for 45 seconds. Feature assigned to Et_2GaH is indicated.
4.6 ^{1}H NMR spectrum of mixture of DMGaH and DEGaH at 203 K. Only the region Ga-H (a) and Ga-CH_3 (b) resonances are shown. 103
4.7 FTIR spectrum of the products of the IR LPHP of mixture of SF_6, TMGa and TEGa before (A) and after (B) exposure to 2 W of laser power for 300 s. Features assigned to Me_2GaH (o) are indicated. 106
4.8 FTIR spectrum of the product of IR LPHP of TMGa and TEGa mixture. 107
4.9 ^{1}H NMR spectrum of the pyrolysis products of the IR LPHP of TMGa and TEGa at 203 K. Only the region of Ga-H (A) and Ga-CH_3 (B) resonance are shown, with features arising from $Me_6Ga_3H_3$ and $Me_5EtGa_3H_3$ identified. 109
4.10 Ga-Me and Ga-H environments in $Me_5EtGa_3H_3$ (A) and $Me_4Et_2Ga_3H_3$ (B = gem diethyl, C = cis diethyl, and D = trans diethyl). The Ga_3-H_3 is assumed to be planar in each case. 110
4.11 Mass spectrum (m/z from 160 to 400) of solution in d_8-toluene of a mixture of Me_2GaH and Et_2GaH (Me;Et approximately 2:1). 113
5.1 FTIR spectrum of $C_4H_6Fe(CO)_3$. 130
5.2 Far-infrared spectrum of $C_4H_6Fe(CO)_3$. 131
5.3 Far-infrared spectrum of $CpMn(CO)_3$. 138
5.4 Far-infrared spectrum of $MeCpMn(CO)_3$. 139
6.1 Far-infrared spectrum of $BrMn(CO)_5$. 156
6.2 Far-infrared spectrum of $ClMn(CO)_5$. 157
6.3 Far-infrared spectrum of $HMn(CO)_5$. 163
6.4 Far-infrared spectrum of $DMn(CO)_5$. 164
6.5 Far-infrared spectrum of $CH_3Mn(CO)_5$. 169
6.6 Far-inrared spectrum of $CD_3Mn(CO)_5$. 170

6.7 Far-infrared spectrum of $CF_3Mn(CO)_5$. 174

List of Tables

2.1	List of slush baths used in this study.	32
2.2	List of chemicals used.	33
2.3	Chemicals which were synthesised	34
3.1	FTIR data for Trimethylalane (cm^{1}).	50
3.2	FTIR data for Deuterated Trimethylalane (cm^{-1}).	51
3.3	FTIR data for Dimeethylalane Dimer (cm^{-1}).	52
3.4	Al-H Stretching and Me_2Al rocking vibration in bridged systems.	58
3.5	Far-infrared data for TMAl, d_9-TMAl, DMAlH, d_6-DMAlH and their mixtures.	
3.6	Force constant in H-Bridged Alanes.	80
3.7	Result from the ab initio calculations for H-bridged Alanes.	81
4.1	FTIR spectral data for Et_2GaH (cm^{-1}).	104
4.2	FTIR spectral data for Me_2GaH (cm^{-1}).	114
5.1	Frequencies and assignment of vapour phase spectrum of $BdFe(CO)_3$.	132
5.2	Far-infrared data for $CpMn(CO)_3$ and $MeCpMn(CO)_3$.	140
6.1	Far-infrared data for $BrMn(CO)_5$.	158
6.2	Far-infrared data for $ClMn(CO)_5$.	159
6.3	Far-infrared data for $HMn(CO)_5$ and $DMn(CO)_5$.	165
6.4	Far-infrared data for $CH_3Mn(CO)_5$ and $CD_3Mn(CO)_5$.	171
6.5	Far-infrared data for $CF_3Mn(CO)_5$.	175

Some of the work contained in this thesis may found in the following publications:

1. Bonding and ligand exchange in pentamethyldialane; an IR, NMR, and ab initio study.
   D.K.Russell, T.A.Claxton, A. S.Grady, R.E.Linney, Zaid Mahmood and R.D.Markwell, J. Chem. Soc. Faraday Trans 1995, 91(18) 3015.
2. Association and exchange in Dialkylgallane in toluene solution.
   D.K.Russell, A.S.Grady, R.E.Linney, Zaid Mahmood and R.D.Markwell J. Organomet. Chem 1996, 506, 327.

Far-infrared and NMR Spectroscopic Studies of Organometallic Compounds.

CHAPTER 1

INTRODUCTION

The work in this thesis falls into two sections. The first part is devoted to IR and NMR studies of bonding in heterobridged $Me_2Al(\mu H)(\mu Me)AlMe_2$ and association and exchange reactions of dialkylgallanes, while the remainder is concerned with comparative studies of metal carbonyls in the vapour phase by far-infrared spectroscopy.

Interest in the chemistry of simple alkyl derivatives of alane and gallane has recently undergone something of a renaissance. One factor influential in this revival is the widespread utilisation of these compounds as precursors to the deposition of Al and Ga in semiconductor materials via processes such as Metal Organic Chemical Vapour Deposition, (MOCVD) [1]. Thus both trimethylalane (Me_3Al or TMA) and trimethylgallane (Me_3Ga or TMGa) have been used as sources of the corresponding metal in compound semiconductors such as GaAs or AlGaAs [2]. However, these methyl compounds have not proved entirely satisfactory, largely because of the incorporation of considerable quantities of highly deleterious carbon, particularly in the case of aluminium [3]. This effect has initiated a search for viable and economical alternative precursors. In the case of Ga, this problem has largely been solved by the use of triethylgallium, Et_3Ga, where the lower activation energy β-elimination decomposition route by-passes the production of alkyl radicals, [4,5] widely held to be the principal culprit in carbon contamination. Unfortunately, the low vapour pressure of triethylalane renders this solution impracticable for Al. This has led to searches in other directions, one of which has identified dimethylalane (DMA), Me_2AlH, as a possible candidate for MOCVD purposes [6].

In this study, we have employed FTIR spectroscopy as a versatile and non-invasive technique for monitoring the progress of a reaction, coupled with NMR for further characterisation of reaction products. This work has resulted in the spectroscopic characterisation of a number of novel species involved in this study. In addition a more thorough investigation of the spectroscopy of some of the materials involved has resulted in a reappraisal of earlier work [7]. A detailed analysis of the IR spectrum of dimethylalane and its deuterated isotopomers following pyrolysis has shown that one of the pyrolysis products of dimethylalane, (DMA), is trimethylalane, (TMA) [8,9], which then undergoes rapid ligand exchange with the parent compound in the gas phase. Exchange processes of this sort have been extensively studied in solution, principally by ^{1}H NMR spectroscopy [10]. On the other hand, rather little is known of these processes in the gas phase. What evidence there is suggests that the eventual outcome may be quite different; for example, studies of the gas phase exchange reaction between alane trimethylamine, $AlH_3.NMe_3$, and Me_3Ga and Et_3Ga indicate the presence of a number of novel gallane species which enjoy at most a fleeting existence in solution [11,12]. The most versatile investigation tool in gas phase chemistry is IR spectroscopy; unfortunately, its application to the alane system has often been hampered by incomplete understanding of their IR spectra. With the analysis of the vibrational spectrum of dimethylalane, DMA, however, this obstacle has now been removed [8]. Here we report a detailed investigation of the interaction between TMA and DMA by FT IR spectroscopy in the gas phase and by ^{1}H NMR in toluene solution. We have also undertaken an *ab initio*

investigation of the compounds $H_2Al(\mu H)(\mu Me)AlH_2$ and $H_2Al(\mu H)_2AlH_2$, in order to support the conclusion of the experimental studies.

The technique of Infrared Laser Powered Homogeneous Pyrolysis (IR LPHP, see chapter 2 for detail) has been shown to be highly suitable for studying the thermal decomposition mechanisms of organometallic compounds. IR LPHP, as the name implies, involves the pyrolysis of a gas sample by passing an infrared laser beam through it; when the sample includes a photosensitiser such as SF_6, this will absorb the radiation and ultimately distribute the energy as heat in the gas. The nature of this process results in heating only in the gas phase i.e the surrounding wall remains unheated and this technique has been used for the pyrolysis studies of mixed trialkylgallane systems [7,13,14]. This is of some interest, since there have been reports in the literature of the use of mixed group III alkyl precursors. Jones *et al.* have reported the use of dimethyl isobutyl aluminium [15], and Stringfellow *et al.* have described the advantages of dimethyl ethyl indium [16]. In short it was hoped that such compounds would exhibit the volatility of methyl compounds, and the reduced carbon contamination characteristic of higher alkyl precursors. It also appeared that IR LPHP technique would be ideally suited to the study of such a system [17,18]. We have therefore undertaken a study of the pyrolysis (IR LPHP) of a mixture of TEGa and TMGa, in which the behaviour of the two starting components was well understood. The FT IR spectrum following the mixing of equal partial pressures of TEGa and TMGa clearly indicates that the mixture contained species other than the starting materials, which were exchange product such as $MeEt_2Ga$ and

Me_2EtGa [7]. It is significant that these exchange processes are formed in the gas phase by a fairly rapid process.

The class of transition metal compounds which involve CO as a ligand are known as metal carbonyls. These compounds are interesting for a number of reasons. Some are specific catalytic agents in important organic reactions. Some are also precursors in metal deposition processes. In addition, the simplicity of the CO ligand makes metal carbonyls perhaps the most important class of transition metal complexes for fundamental studies of metal-ligand bonding. Techniques such as IR spectroscopy, particularly in the CO stretching region, have provided valuable information. Metal carbonyls are commonly soluble in the solvents (e.g CCl_4 and CS_2) and some are volatile enough to allow investigation of their vapour phase spectra. A large number of metal carbonyls have been investigated by infrared and Raman spectroscopy [19-28]. However, although there have been many reports of infrared spectra of metal carbonyls, most of the studies have been in the 5 μm region (around 2000 cm^{-1}) of the infrared. In the 5 μm region, the principal absorption bands are due to C-O stretching vibrations. In general, there are relatively few bands in this region, and these bands are essentially isolated energetically. Thus, it is usual to treat these vibrations as being independent of other vibrational modes. The vibrational spectra of metal carbonyls are characteristically divided into three regions. There is the high frequency region, usually around 5 μm (2000 cm^{-1}), which as already stated covers primarily the C-O stretching vibrations. The middle frequency region, about 700-400 cm^{-1}, contains bands due to several types of vibrations,

including M-C-O bending motion, M-C stretching motions and combinations of these motions with one another and with other motions. This region commonly contains a considerable number of bands, depending upon the molecular symmetry of the compounds. The low frequency region, 400-10 cm^{-1}, contains bands due to OC-M-CO bending vibrations as well as others.

Tha main difficulty in making assignments in the low frequency region (400-10 cm^{-1}) is due to the fact that it contains bands due not only to M-C stretching and M-C-O bends, but also to combinations or mixture of these motions. Nevertheless, extensive work performed earlier on metal carbonyls in solution and Nujol mulls [19-25,28,29] has resulted in a good understanding of the vibrational assignments in these molecules.

Far-infrared spectra of $BdFe(CO)_3$, $CpMn(CO)_3$ and $MeCpMn(CO)_3$ have been studied in the present work in the range 500-10 cm^{-1}. In contrast to the previous work on these compounds [24,30,31], our spectra were recorded in the vapour phase where possible complications such as solute-solvent interaction are avoided. This investigation involved measurement of far-infrared spectra in order to determine whether these provided any useful information on the structure and bonding in these compounds.

Compounds of the type $XMn(CO)_5$ have also been extensively studied by IR spectroscopy in the CO stretching region. In the far-infrared, much less work has been done and that which has been carried out was in condensed phase, i.e. solid sample in Nujol Mull and also solution work. In this work we have obtained the first vapour phase far-infrared spectra of a range of $XMn(CO)_5$

complexes, where X= CH_3, CD_3, H, D, CF_3, Br and Cl. Accurate values of the frequencies for all the bands in the low frequency region in the vapour phase have been obtained for all these complexes. The numbers of ν(MC) and δ(MCO) modes active in the infrared are compared with the condensed phase spectra of these complexes.

This thesis is arranged as follows. In chapter two, the experimental equipment and overall operational procedures are described in detail. In chapter three, the work on the gas phase exchange reactions between mixtures of dimethylalane, (DMAlH), and trimethylalane, (TMAl) is presented. This is followed in chapter four by the results of IR LPHP of mixtures of dimethylgallane and diethylgallane. In chapter five, comparative studies of η-bonded metal carbonyls e.g, $C_4H_6Fe(CO)_3$, $CpMn(CO)_3$, $MeCpMn(CO)_3$ in the far-infrared region are presented, while a similar study of $XMn(CO)_5$ compounds (where X=CH_3, H, CF_3, Br, Cl) is reported in chapter six. Finally, chapter seven draws together all the conclusions reached from the above studies.

References.

[1]. N. J. Mason, in The Chemistry of the Semiconductor Industry, ed. S.J. Mason and A. Ledwith, Blackie, London, 1987.

[2]. G. B. Stringfellow, Organometallic Vapour Phase Epitaxy- Theory and Practice, Acadmic Press, San Diego, 1989.

[3]. T. F. Keuch, E. Veuhoff, T. S. Kuan, V. Delin and R. Poteuski, J. Cryst Growth, 1986, **77**, 257.

[4]. A. S.Grady, A. L.Mapplebeck, D. K. Russell, and M. G. Taylorson, J. Chem. Soc., Chem. Commun., 1990, 257.

[5]. A. S. Grady, R. D. Markwell, and D.K.Russell, J. Chem. Soc., Chem. Commun., 1991, 14.

[6]. R. Bhat, M. A. Koza, C.C. Chang, S. A. Schwartz, and T. D. Harris, J. Cryst. Growth, 1986, **77**, 7.

[7]. A. S. Grady, R. E. Linney, R. D.Markwell, and D. K. Russell, J. Mater. Chem., 1993, **3**, 483

[8]. A. S. Grady, S. G. Puntambekar, and D. K. Russell, Spectrochim. Acta 1991, **47A**, 47.

[9]. G. A. Atiya, A. S. Grady, D. K. Russell and T. A. Claxton. Spectrochim Acta, 1991, **47A**, 467.

[10]. M. Fishwick, C. A. Smith, and M. G.H. Wallbridge, J. Organomet. Chem. 1970,**21**, P9.

[11]. A. S.Grady, R. D. Markwell, D. K. Russell, and A.C. Jones, J. Cryst. Growth, 1990, **106**, 239.

[12]. A. S. Grady, R. D. Markwell, D. K. Russell, and A. C Jones, J. Cryst Growth 1991, **110**, 739.

[13]. G. A. Atiya, Ph.D. Thesis (University of Leicester) 1990.

[14]. A. S. Grady, R. E. Linney, R. D. Markwell, G. P. Mills, D. K. Russell, P. J. Williams and A. C. Jones. J. Mater.Chem., 1992, **2**, 539.

[15]. A. C. Jones, P. R. Jacobs, S. A. Rushworth, J. S. Roberts, C. Button, P.J. Wright, P. E.Oliver, and B. Cockayne, J. Cryst. Growth, 1989. **96**, 769.

[16]. K. L. Fry, C.P Kuo, C. A. Larsen, R. M. Cohen, G. B. Stringfellow, and A. Melas, J. Electron. Mater.,1986, **15,** 91.

[17]. D.K. Russell, Chem. Soc. Rev. 1990, **19**, 407.

[18]. D. K. Russell, Coord. Chem. Rev. 1992, **112**, 131.

[19]. W. F. Edgell, W. E. Wilson and R. Summitt, Spectrochim. Acta, 1963, **19**, 863.

[20]. W. F. Edgell and M. P. Dunkle, J. Phys. Chem., 1964, **68**, 452.

[21]. F. A. Cotton, A. Musco, and G. Yagupsky, Inorganic Chem, 1967, **6**. 1357.

[22]. F. J. Paul, Yvon L e Page, S. Jacqueline and I. S. Butler, Inorg. Chem. 1981, **20**, 2852.

[23]. A. Danti and F. A. Cotton, J. Chem. Phys., 1957. **28**, 736.

[24]. D. M.Adams and A. Sauir, J. Chem. Soc. 1970, 814.

[25]. I. M. T. Davidson, A. M. Ellis, G. P. M. Mills, M. Pennington, I. M. Povey, J. B. Raynor, D. K. Russell, S. Saydam and A. D. Workman. J. Mater. Chem,. 1994, **4**, 13.

[26]. L.H. Jones and R.S. McDowell, Spectrochim. Acta, 1964. **20**. 248.

[27]. R. S. McDowell and L. H. Jones, J. Chem. Phys., 1962, **36**, 3321.

[28]. M. A. Andrews, J. Eckert, J. A. Goldstone, L. Passell and B. Swanson, J. Am. Chem. Soc., 1983, **105**, 2262.

[29]. G. P. McQuillan, D. C. McKean, C. Long, A. R. Morrisson and I. Torto., J Am. Chem. Soc. 1986, **108**, 863.

[30]. G. Davidson, Inorganic Chemica Acta. 1969, **3**, 596.

[31]. D. M. Adams and A.Squire, J. Organometallic Chem. 1973, **63**, 381.

Chapter 2

2.1: INTRODUCTION

In this chapter the equipment, experimental procedures and the main chemical reagents used in all the experiments will be described. More specific experimental details will, in some cases, be given in the appropriate results chapter. Much of the equipment (e.g. the experimental arrangment for IR LPHP) was designed by G.A.Atiya [1] and A.S.Grady [2] and has been modified where necessary to suit the type of experiment required for the work described in this thesis. The details of these changes are described in the relevant section below.

2.2: Manipulation of air sensitive compounds.

Many of the compounds used in this investigation were air and moisture sensitive, circumstances which necessitated the use of inert-atmosphere and vacuum techniques for their manipulation. These techniques have been well-described elsewhere [3,4] and are therefore only briefly described here. A specially constructed vacuum line was employed for sample handling; this is illustrated in figure 2.1. The manifold was constructed from pyrex glass (2mm thick, 15mm diameter) and was fitted with J.Young O-ring vacuum taps (POR-5-RA) and P.T.F.E. high vacuum screw cap joints (DOY-1). The latter were for the connection of a sample tube and the reaction cell (see later). It was also equipped with a liquid nitrogen cooled U-trap preceeding an Edwards EO2 oil diffusion pump and an Edwards E2M5 two stage rotary pump combination. The typical vacuum obtained using the rotary pump was around 10^{-2} mbar; however, with the oil diffusion pump 10^{-5} mbar could be attained. This vacuum was measured using two gauges: a Pirani PRL10K gauge (for pressure in the range 10 down to 10^{-4} mbar) and a Penning CP25K gauge for measuring lower pressures more accurately. Measurement of the sample pressure introduced into the line was by means of an MKS-122A baratron gauge (of range 0-100 torr). Low temperatures were achieved by the use of liquid nitrogen or slush baths consisting of a solid-

liquid equilibrium mixture of a suitable organic material. Table 2.1 lists some of the slush baths used in this study.

Those compounds which are moderately-moisture sensitive and essentially involatile at ambient temperature were manipulated by either Schlenk or standard glove box techniques using dry nitrogen as the inert atmosphere [3].

2.3: Sample Preparation.

After removal from their respective containers the organometallic compounds were distilled and stored under vacuum in standard pyrex sample tubes of the type shown in figure 2.2. If a pyrolysis experiment was to be performed, SF_6 photosensitiser needed to be added to the sample cell. The SF_6 was stored in a U-tube on the vacuum line. Prior to each experiment, the SF_6 was pumped on at 77 K , in order to remove any oxygen present; this was then followed by the removal of residual water vapour at 197 K.

Before commencing each experiment, all samples were subjected to several freeze-pump-thaw cycles at 77 K; the purpose of this was to remove any traces of oxygen or thermal decomposition products. This is particularly important for the organometallic compounds as leakage of air through the vacuum tap causes the production of hydrocarbons from hydrolysis and/or oxidation.

Before filling the reaction cell, residual adsorbed water or oxygen were removed by conditioning the reaction cell and the vacuum line with a small pressure of the compounds to be studied. After several minutes of exposure, both the reaction cell and the vacuum line were evacuated and then the reaction cell was filled with the required pressure of the compounds. An FTIR spectrum of the contents of the cell was then recorded to confirm the sample purity. Pyrolysis studies were carried out using the technique of Infrared Laser Power Homogeneous Pyrolysis (IR LPHP), as detailed in the next section.

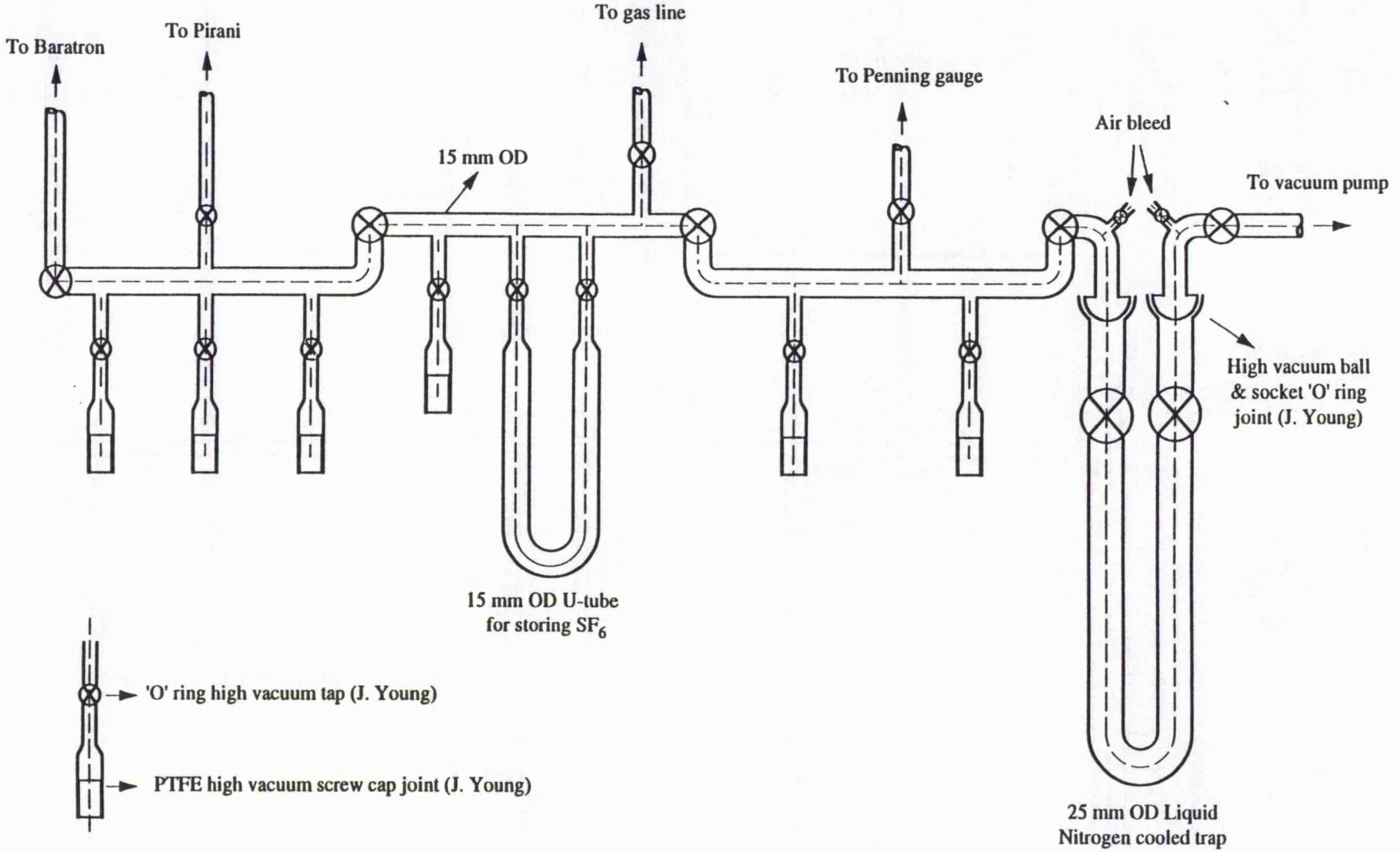

Figure 2.1. Schematic diagram of Vacuum Manifold

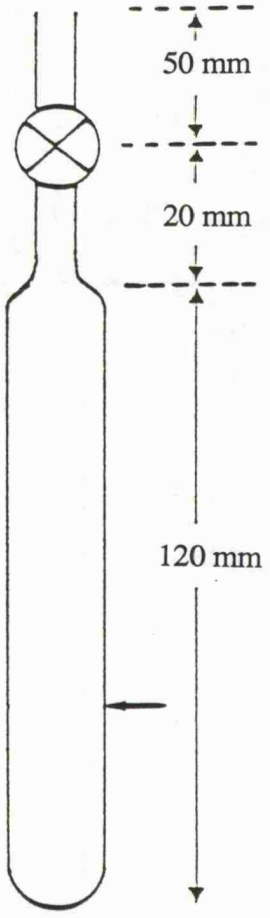

Figure 2.2 Schematic diagram of the sample tube used

2.4: Basic Experimental Approach.

Naturally, the precise experimental details are dependent upon the nature of the investigation, but the general approach is described here. The basic experimental arrangement is illustrated in Figure 2.3 and is similar to that used by G.Atiya and A.S.Grady. In this arrangement, a mixture of the reagent gas or gases and, for a pyrolysis experiment, an inert IR absorber (SF_6), is injected to a pressure of a few torr into a static pyrex cell. The cell is fitted with a filling port, and in some cases an additional port is present for sample isolation and investigation by, for example, NMR spectroscopy. In addition, both ends of the cell are fitted with windows of the appropriate material for transmission of infrared and, where appropriate, laser radiation. For samples having very low volatility the liquid material may be retained in a cylindrical hollow in the cell, as illustrated in Figure 2.3. This feature leads to considerable enhancement of reaction products, and therefore aids their detection. Changes in chemical composition were monitored by one or more of a number of spectroscopic methods which were described below. As indicated above, pyrolysis experiments were also performed in some cases using the type of cell shown in figure 2.3. In these experiments, pyrolysis was achieved by laser-induced heating and this is briefly described in the next section.

2.5: Infrared Laser Powered Homogeneous Pyrolysis (IR LPHP)

2.5.1: Basics of IR LPHP

The basic principle of this method is that a specific vibrational mode of the photosensitiser absorbs energy from the laser radiation and then rapidly converts this energy into heat via efficient collisional relaxation processes.

The major advantage of this technique is that it is an entirely homogeneous process. This generates a static temperature profile in which the center of the pyrolysis cell may reach as high as 1500 K while the cell walls

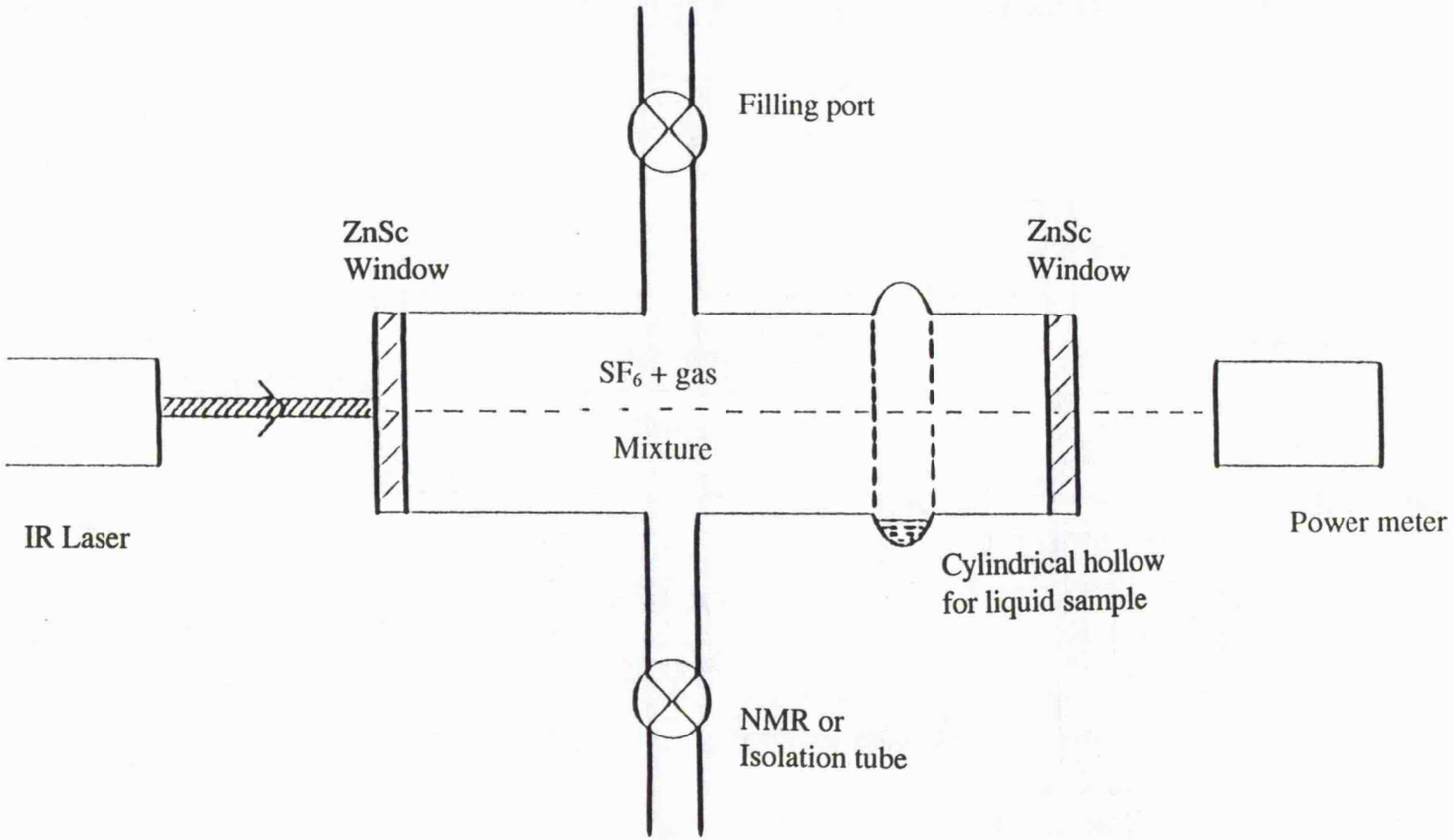

Figure 2.3. Schematic diagram of the essential elements of the IR LPHP technique.

remain at room temperature. However, the disadvantage associated with the production of this non-uniform temperature distribution is that detailed kinetic data cannot be derived. Despite this the IR LPHP process still has significant advantages over conventional hot-walled pyrolysis techniques, where the principal drawbacks are that the primary reaction products tend to decompose on the reactor walls and that this deposition of solid material may provide a highly auto-catalytic surface for further reaction. This was clearly demonstrated by Ashworth *et al.* in the oxidation of tetramethyl tin [5]. The inability to trap primary products, such as free radicals, means that reaction mechanisms must be deduced from the final products, which are usually hydrocarbons and deposited materials.

2.5.2: The Carbon Dioxide Laser.

An Edinburgh Instruments PL4 free-running carbon dioxide gas laser [6] was used for the IR LPHP in this work. A schematic diagram of the CO_2 laser is illustrated in Figure 2.4. A water-cooled pyrex discharge tube (C) with an active length of 130 cm sits within the laser cavity, the overall cavity length of the instrument is 180 cm (D). Both ends of the discharge tube are sealed with anti-reflection coated ZnSe windows (W) which allow the transmission of 10.6 μm of IR radiation. The output coupling mirror (OC) of the laser has a reflectivity of 75% and is mounted on a piezo-electric transducer (PZT), which by its adjustment the cavity can be fine tuned and stabilized.

The laser was operated using a mixture of 9% CO_2,, 13.5% N_2 and 77.5% He, which was continuously flowed through the discharge tube at a pressure regulated by a metering valve (MV) and measured on a vacuum gauge (G). The electric discharge was provided by an Edinburgh Instrument (PS4R) power supply rated at 30 kV, 30 mA. By controlling the current supplied to the laser and the pressure of the gas flowing through it, laser powers ranging from 1.25 to

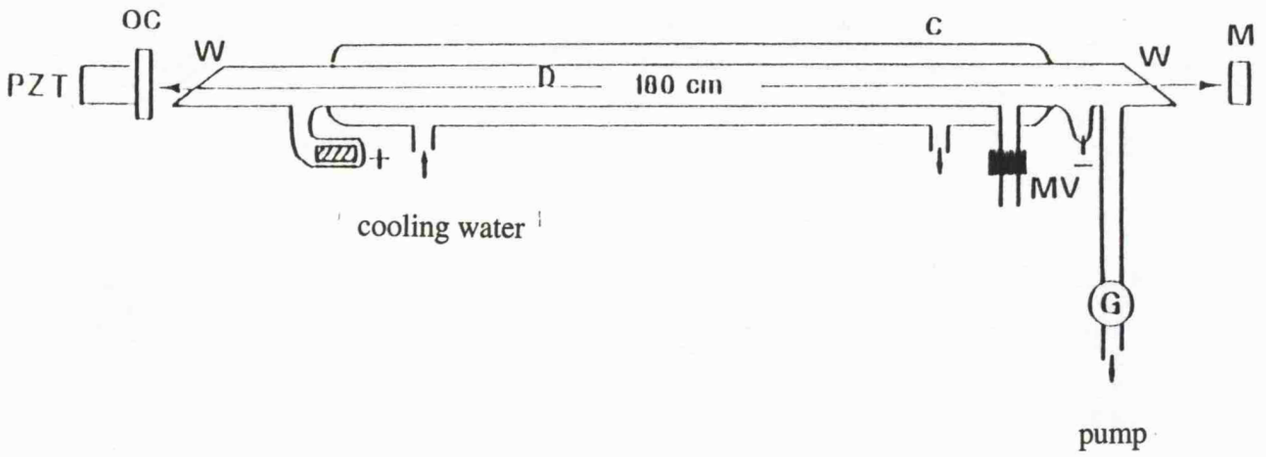

Figure 2.4 Schematic diagram of CO_2 laser

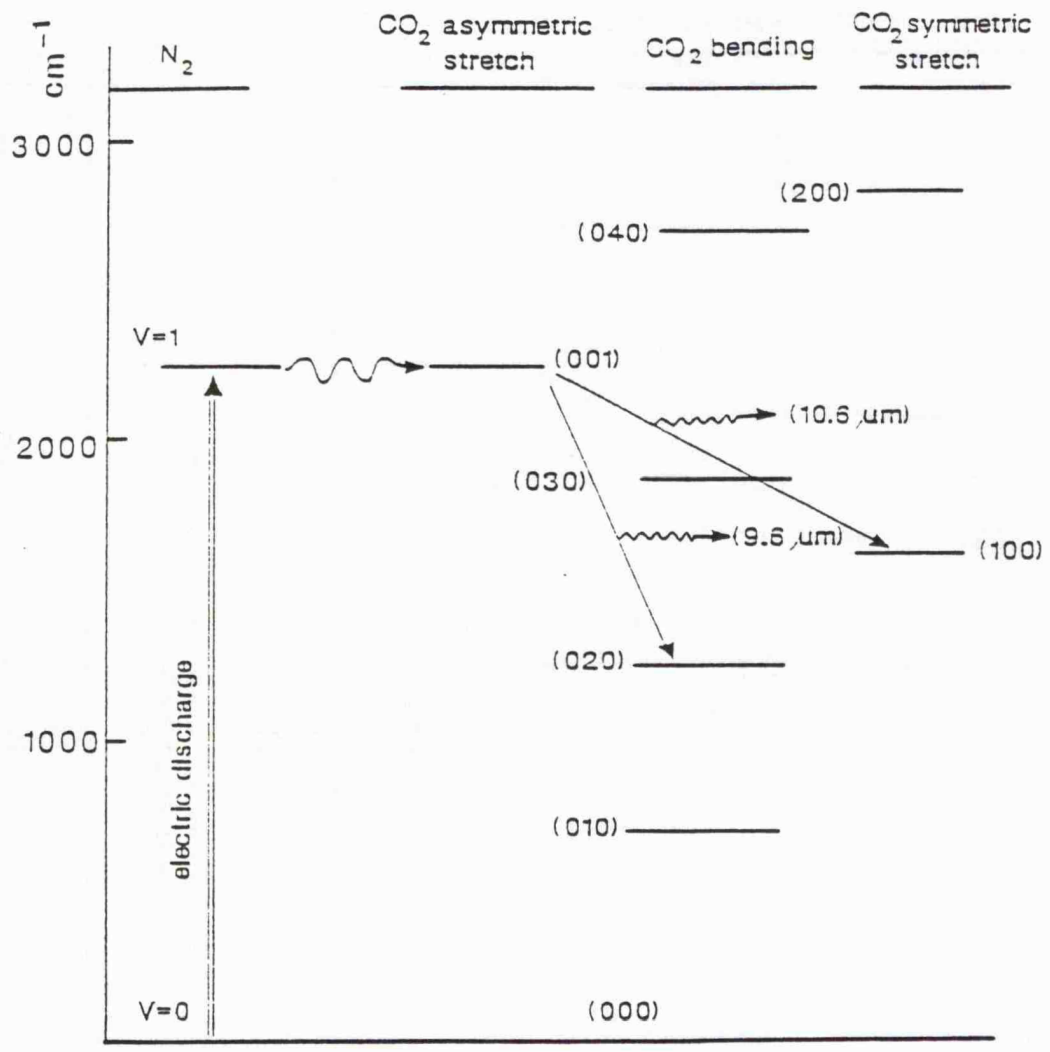

Figure 2.5. Block diagram of the vibrational energy levels used in the CO_2 laser.

40 W could be obtained. The diameter of the emerging beam was 7.5 mm with a divergence of less than 2 milliradians. The laser power was monitored by a Coherent power meter (Model 201), calibrated to give a signal of 0.4 mV/W of power absorbed with a rise time of approximately 1 second.

The carbon dioxide laser is a gas laser which is capable of generating extremely intense mid-infrared radiation . It is based on vibrational energy level transitions in the carbon dioxide molecule. On passing an electric discharge through the carbon dioxide laser gas mixture. helium produces electrons and collision impact of these cause the nitrogen molecules to become vibrationally excited to the v=1 level. This is metastable as optical transitions back down to the v=0 level are forbidden. The v=1 vibrational level of nitrogen almost coincides with the antisymmetric stretching (001) vibrational level of CO_2, and therefore facile near-resonant energy transfer from N_2(v=1) to CO_2(001) is possible during collision. This results in a population inversion in CO_2 which causes laser action to take place between the (001) level of CO_2 and the unpopulated lowest excited level of the symmetric stretch (100) and the second lowest excited level of the CO_2 bending mode (020). This generates 10.6 μm and 9.6 μm infrared radiation respectively. A block diagram of the vibrational energy levels used in the CO_2 laser is shown in Figure 2.5.

2.6: Reaction Cell.

A variety of reaction cells were employed for these experiments. As indicated above, these also serve as IR sample cells. They were constructed from pyrex glass (usually 2 mm thick) and fitted with Young O-ring high vacuum taps for connection to the vacuum line. ZnSe windows at both ends of the cell were used for mid-infrared work, while polyethylene windows were used for the far-infrared region (see next section). The cell design illustrated in Figure 2.6 was used for the majority of experiments. This was the most basic design,

with typical dimensions being a length of 7 cm and diameter 3.6 cm for mid-infrared work and 15 cm length and 4.5 cm diameter for far-infrared work respectively. For isolation of pyrolysis products for further analysis by NMR spectroscopy the cell illustrated in Figure 2.3 was used. This was of similar design to that above, but was fitted with an additional port for connection of 5 mm NMR tubes fitted with greaseless and rotationally symmetrical valves (J.Young) [7]. These valves were vacuum sealed to the port by O-rings. This reaction cell was of similar design to that used by G.Atiya [1] and A.S.Grady [2]. The cell illustrated in Figure 2.7 was used for compounds which have very low vapour pressures. Once again this is of a similar design to that above but in addition there is heating jacket around the cell for heating the sample with the help of heated liquid (e.g water, liquid paraffin).

2.7: Window Materials.

2.7.1: ZnSe windows.

The choice of window material was important for the success of these experiments. The material must be highly transparent to the infrared radiation from both the CO_2 laser and FTIR spectrometer (see below), and should also preferably possess a high degree of mechanical strength and thermal stability, as well as being chemically inert. These requirements, coupled with economic considerations, have led to the establishment of NaCl and KCl as the materials used by the majority of workers [8]. However, there are a number of drawbacks associated with their use. In the case of laser transmission, one is the generation of hot spots, caused by absorption of laser radiation by solid deposited on the windows, which can easily lead to thermal stress and subsequent failure of the windows [9] . Another problem, which is directly related to this work, is that alkali halide materials are hygroscopic; even traces of absorbed water can drastically alter the course of reaction in moisture-sensitive organometallic

compounds. Fortunately, these problems are circumvented by the use of ZnSe windows (for mid-IR region), which have lower absorption around 10 μm, lower thermal expansion, and higher thermal conductivity than alkali halides [10]. However, such windows need to be provided with anti-reflection coatings because of their high refractive index, and are rather expensive. Their great durability and non-hygroscopic nature, however, makes them very attractive for use with air- and moisture- sensitive organometallic compounds and they have been used extensively in this work.

2.7.2: Polyethylene windows.

Polyethylene is the most generally useful window material for the far-infrared region and it was therefore used throughout the far-IR experiments described here. In many ways it comes close to being an ideal window material. It is very cheap and has a low refractive index of 1.5 which is reasonably constant beyond 150 μm. It is quite inert, surprisingly strong mechanically, and can be used as a vacuum seal even at liquid nitrogen temperatures. All these benefits make it very attractive for use in far-infrared spectroscopy. It softens rapidly above 70 ^{o}C and melts above 120 ^{o}C, so it is not used much above room temperature. Polyethylene is finding increasing use in the far-infrared region, particularly as a substrate material for components like metal mesh filters and polarisers. This is undoubtedly the cheapest and most versatile window material in current use and is commercially available in various high density forms. However, there are various mechanical disadvantages inherent in the use of polyethylene; in particular, if the spectrometer is evacuated the elasticity of the material is sufficient to cause outward bowing of the windows with consequent uncertainty in the cell path length. It is possible to use increased thicknesses of window material to counteract this and plates up to 1/4 inch thickness have been used by Wills *et al* [11].

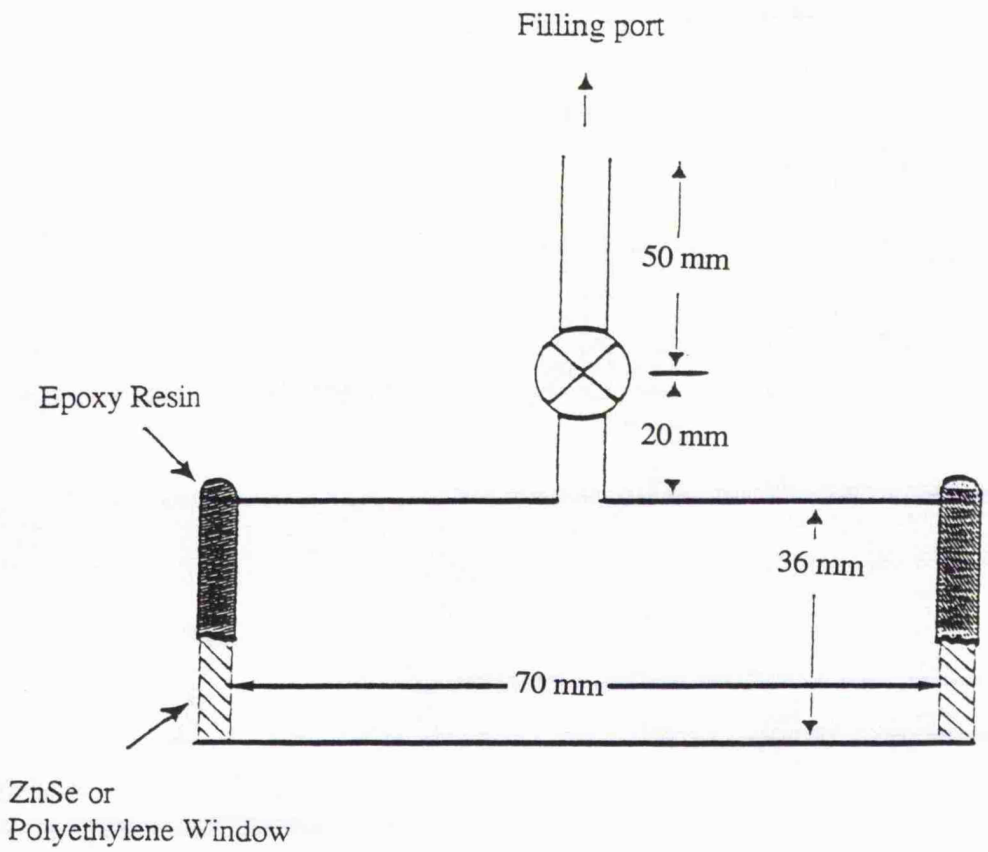

Figure 2.6 Schematic diagram of the standard reaction cell

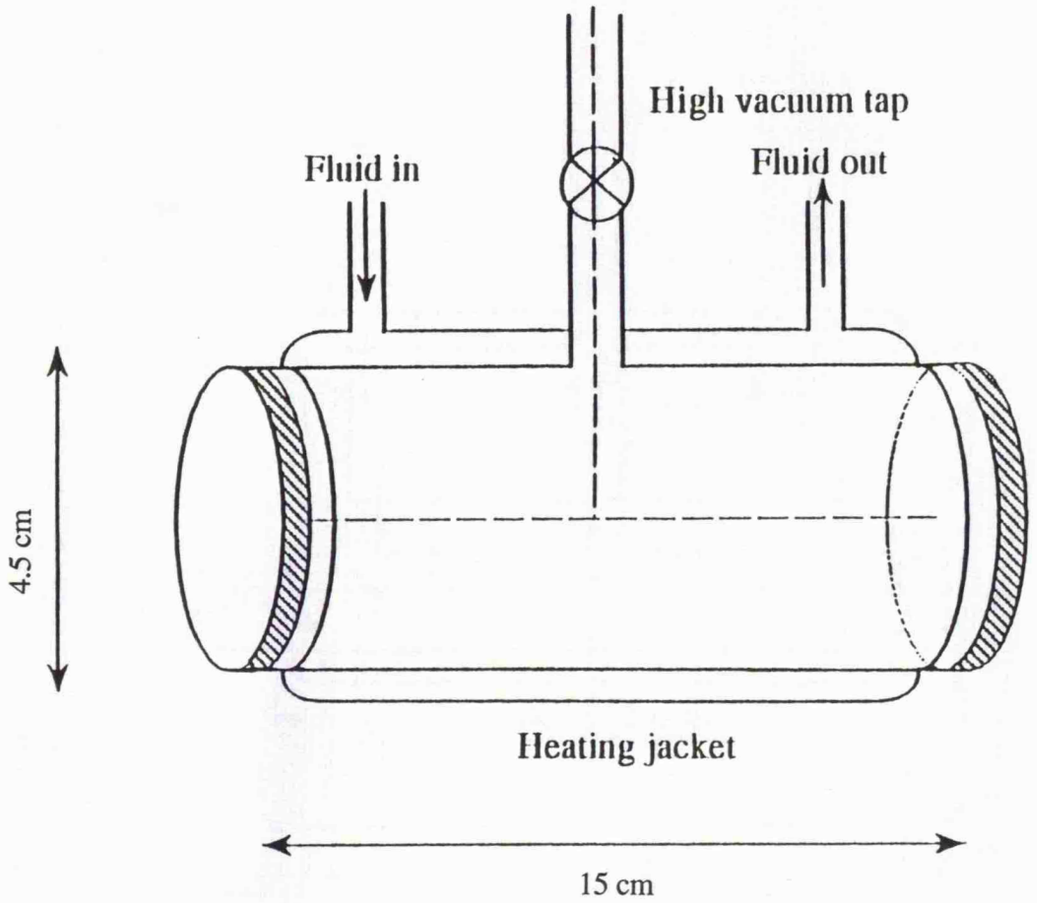

Figure 2.7 Schematic diagram of the reaction cell used for low vapour pressure compounds

2.8: Spectroscopic methods

2.8.1: Fourier Transform Infrared Spectroscopy.

Two infrared spectrometers were used during the course of this research work, these being a Biorad FTS40 FTIR spectrometer and FTS40V FTIR spectrometer. All the mid-infrared spectra presented in this work were recorded using the FTS40 machine while the far-infrared spectra were recorded using the FTS40V spectrometer. The FTS40V system comes standard with a mercury arc lamp mounted in a water-cooled cast-bronze housing. This source emits the bulk of its IR radiation in the range 500 to 10 cm^{-1} and has a higher output intensity than a ceramic source below 100 cm^{-1} (the ceramic source is intended for use from 5000 to 80 cm^{-1}). Figure 2.8 shows the optical schematic for the FTS40V bench. In the far-IR spectrometer a set of removeable Mylar beamsplitters (figure 2.9) were employed; these are mounted onto a magnetic frame which interfaces with magnets on the beamsplitter mounting surface. The operation of the FTS40 is similar to the FTS40V in many respects, although it contains a single fixed KBr beamsplitter.

As with all FTIR spectrometers, the central component of the instrument is an interferometer based on an original design by Michelson in 1891[12]. In its simplest form, the Michelson interferometer has the arrangement shown in figure 2.10. It is comprised of two mutually perpendicular plane mirrors, one of which can move at constant velocity along an axis perpendicular to its plane. A beamsplitter is located between the mirrors which partially transmits a beam of radiation from an external source to the moving mirror M and partially reflects some towards the fixed mirror F. After each beam has been reflected back to the beamsplitter they are combined, and once again partial reflection or transmission is possible. Thus a portion of each beam returns back to the source, while a portion travels to the detector via the sample compartment. The intensity of the beam passing to the detector is dependent on the path difference of the two

beams in each arm of the interferometer which is modulated by the moving mirror.

When more than one frequency is emitted by the source, the measured interferograms will be a combination of the interferogram of each frequency. This then can be transformed into a spectrum of the IR source by a Fourier transformation. The beam travelling to the detector is passed through the sample compartment where absorption can occur. By recording the interferogram with the compartment empty (i.e. the background) computer subtraction of the two will yield the IR spectrum of the sample.

The speed with which an infrared spectrum can be attained in FT IR spectroscopy is given by the scan time of the moving mirror plus the digitisation rate of the data and subsequent calculation of the Fourier transform. Using modern computers and efficient computational alogorithms this can be achieved within a few seconds or less.

There are a number of advantages of FTIR over conventional IR spectroscopy. These can be summarised as follows.

i) Increased sensitivity compared to conventional spectrometers where most of the light from the source is rejected due to the narrowness of entrance and exit slits;

ii) Great speed of data acquisition, i.e. able to scan the whole wavelength range in essentially one mirror pass.

iii) Excellent levels of accuracy. Conventional machines suffer from wavelength inaccuracies due to backlash from mechanical movement, such as rotation of mirrors or gratings, whereas FTIR spectrometers use continous calibration by an internal He/Ne laser.

iv) Fewer moving parts, therefore less susceptible to vibrations.

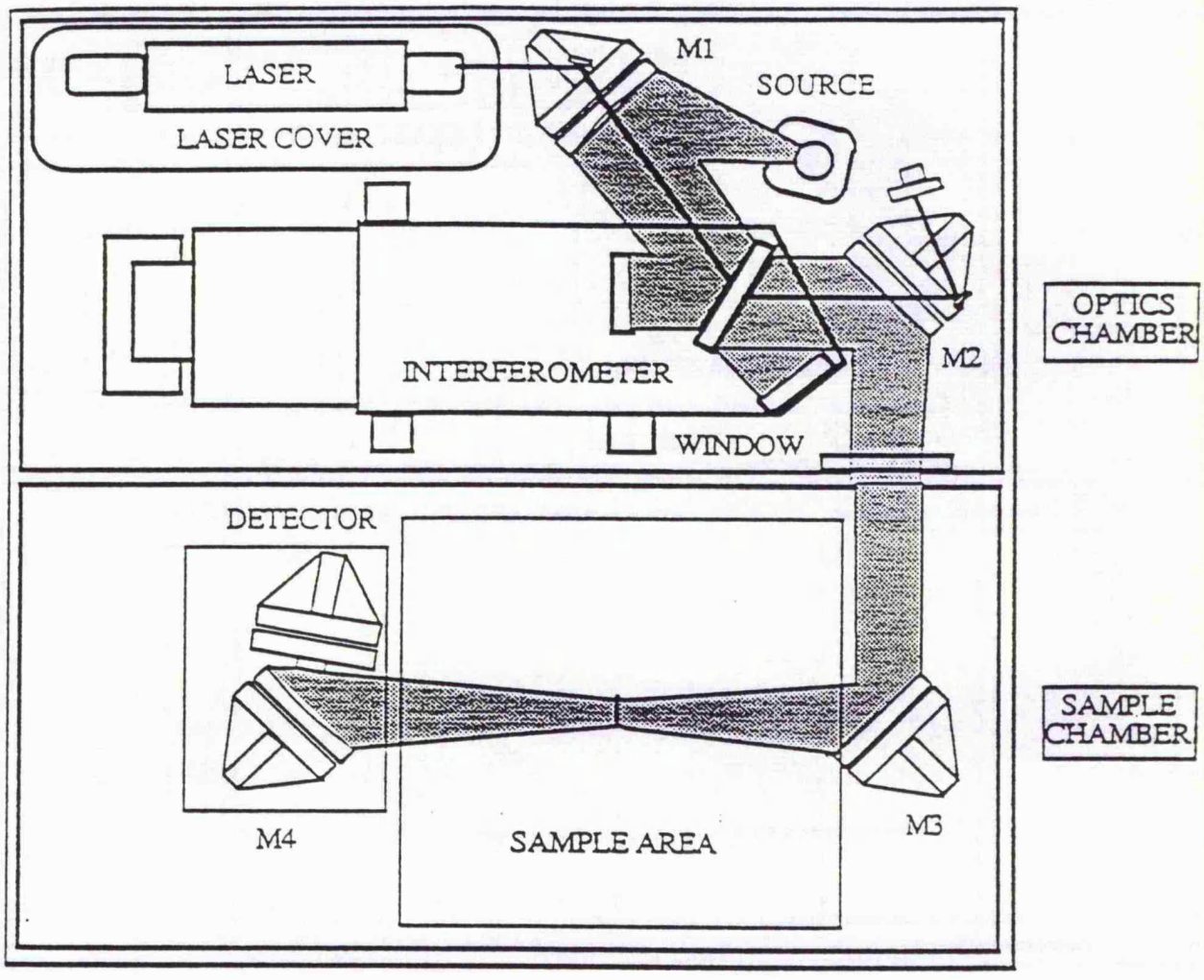

Figure 2.8 Optical path of FTS-40V far-infrared Spectrometer

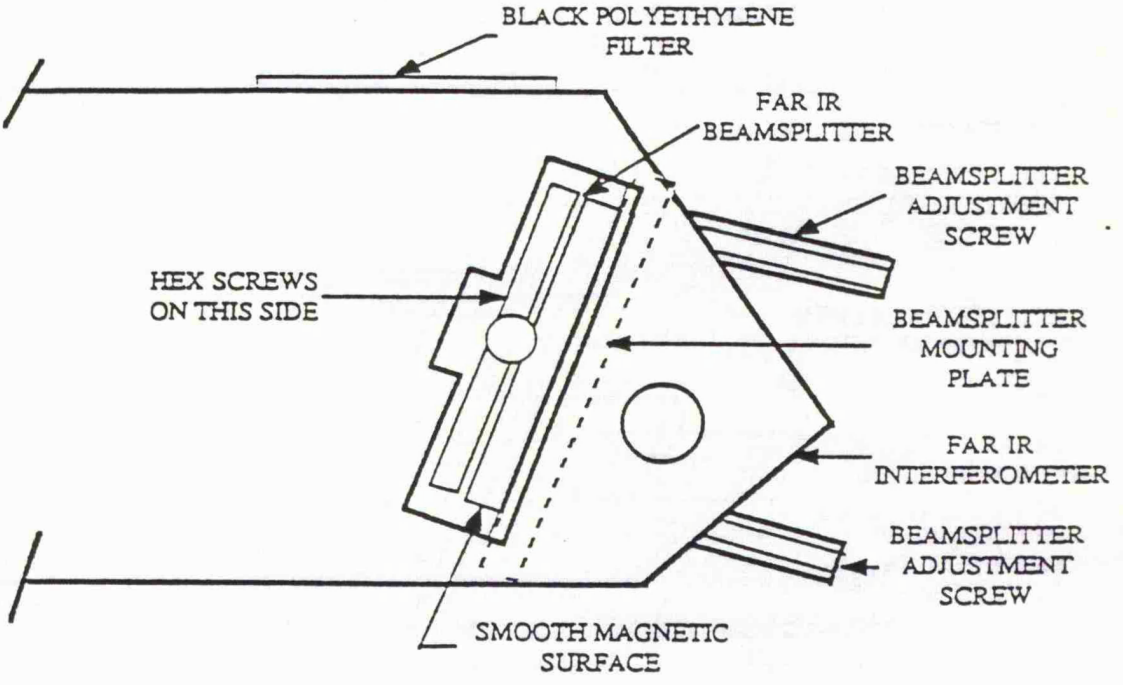

Figure 2.9. Schematic diagram of kinematically moveable mylar beam splitters

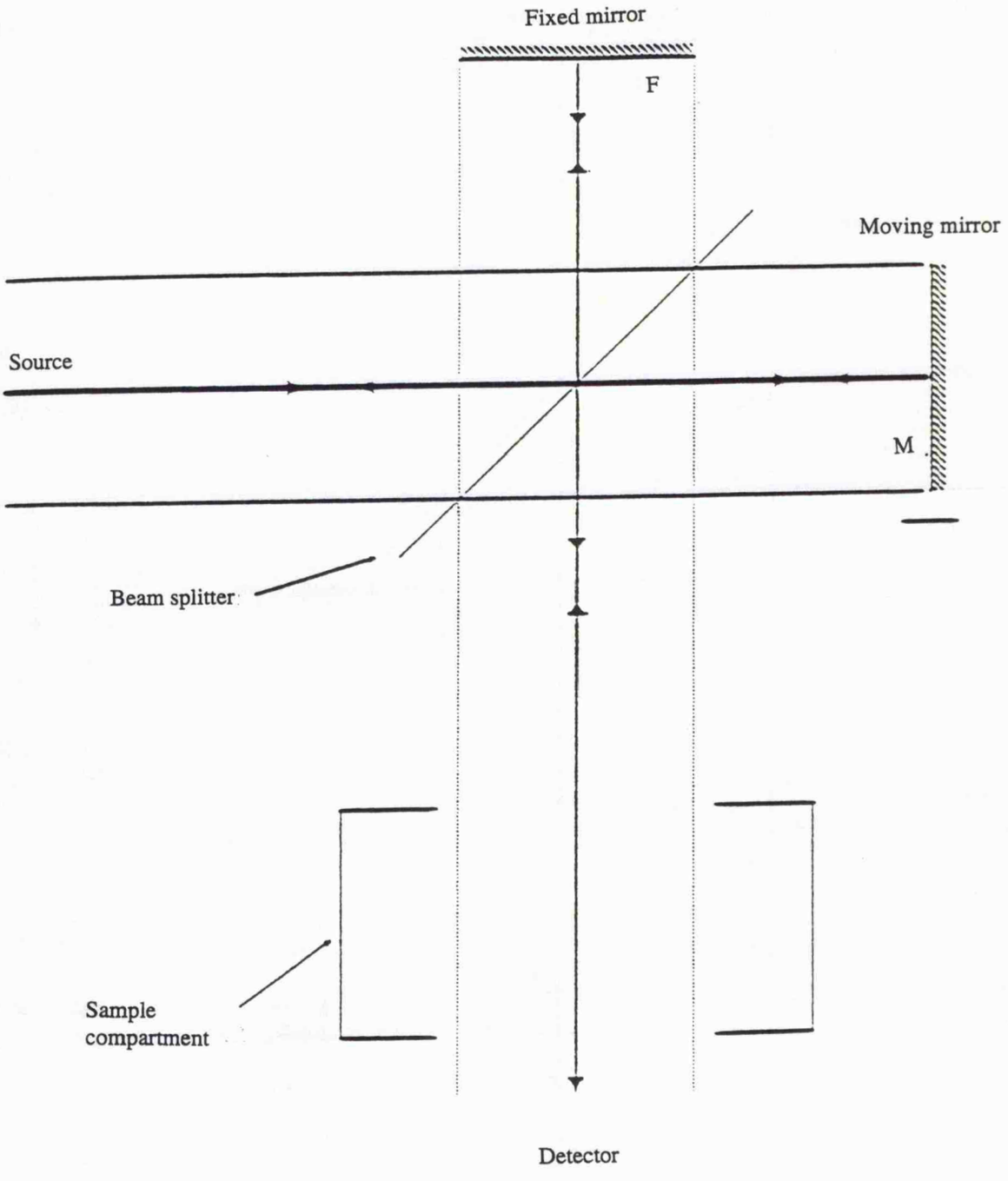

Figure 2.10 Schematic diagram of the Michelson interferometer

v) Computer manipulation of spectra, for example, water vapour contributions can be subtracted out of a spectrum, or spectra can easily be added to improve the signal-to-noise ratio.

2.8.2: Fourier Transform NMR Spectroscopy.

All the ^1H NMR spectra presented in this thesis were recorded at 300 MHz using a Bruker AM300 FT-NMR spectrometer. Fourier transform NMR spectroscopy offers similar advantages to Fourier transform IR spectroscopy, in terms of both the speed of acquisition of spectra and the computer manipulation of spectra [13]. In the present work high field ^1H NMR spectroscopy has been extremely important in confirming many of the conclusions drawn from the infrared spectroscopic observations. The main areas of importance have included;

i) High sensitivity for samples at low concentrations (μg quantities);

ii) Opportunity for applying double resonance techniques, e.g. spin decoupling. This was particularly helpful in the TEG + TMGa system (see chapter 5);

iii) Detection of alkyl groups on different metal centres; this was essential in the exchange reactions studied (see chapter 3);

iv) Accurate measurement of integrals; this enabled the relative abundance of hydrocarbon pyrolysis product to be determined in several cases.

v) The most important feature of the Bruker AM300 FT-NMR spectrometer was the variable temperature probe; this uses cold nitrogen gas from boiling liquid nitrogen and an electric heater, to produce temperatures as low as 191 K. These temperatures were produced with an estimated accuracy of 1-2 K. The most significant use of this was for low temperature spectra of thermolabile materials, such as dialkylgallanes. Also exchange reactions such as those in the TEG+TMGa (chapter 4) and TMAl+DMAlH (chapter 3) mixtures could be investigated over a whole range of temperatures.

2.9: Chemicals

In tables 2.2 and 2.3 the chemicals purchased for the experiments and those which were synthesised are listed. Their common acronyms are also given as the compounds will often be abbreviated to these in later chapters in this thesis. The chemicals from Epichem Ltd were gifts, which are gratefully acknowledged.

Table 2.1 List of some of the slush baths used in this study

Coolant	temperature °C
Ice+Water	0
Liquid nitrogen+Carbon tetrachloride	-22.9
Liquid Nitrogen+Hexanol	-48.0
Dry ice+Acetone	-78.5
Dry ice+Propanol	-78.5
Liquid Nitrogen	-196

Table 2.2: List of chemicals used.

ACRONYM	NAME	FORMULA	SOURCE
TMAl	Trimethylalane	$(CH_3)_3Al$	Epichem Ltd
dTMAl	Deuterated TMAl	$(CD_3)_3Al$	Epichem Ltd
TMGa	Trimethylgallane	$(CH_3)_3Ga$	Epichem Ltd
TEGa	Triethylgallane	$(C_2H_5)_3Ga$	Epichem Ltd
TIPGa	Triisopropylgallane	$(C_3H_7)_3Ga$	Epichem Ltd
TIBGa	Triisobutylgallane	$(C_4H_9)_3Ga$	Epichem Ltd
TTBGa	Tri-tert-butylgallane	$(C_4H_9)_3Ga$	Epichem Ltd
TMAA	Trimethylamine alane	$AlH_3.N(CH_3)_3$	Epichem Ltd

Name	Formula	Source
1,3-Butadiene	$H_2C=CHCH=CH_2$	Aldrich Chemical Co
1,3-Butadiene Irontricarbonyl	$C_7H_6FeO_3$	Janssen Chimica
Cyclopentadienyl Manganesetricarbonyl.	$C_8H_5MnO_3$	Aldrich Chemical Co
Methylcyclopentadiene-manganese tricarbonyl	$C_9H_7MnO_3$	Adrich Chemical Co
Iron pentacarbonyl	$Fe(CO)_5$	Aldrich Chemical Co
Dimanganese decacarbonyl	$Mn_2(CO)_{10}$	Aldrich Chemical Co
Methyl iodide	CH_3I	Aldrich Chemical Co
d_3-Methyl iodide	CD_3I	Aldrich Chemical Co
Calcium Hydride	CaH_2	Aldrich Chemical Co
d_8-Toluene	C_7D_8	Aldrich Chemical Co
Sulphur Hexafluoride	SF_6	British Oxygen

Table 2.3. Chemicals which were synthesised.

Name	Formula
Dimethyl aluminum hydride	$(CH_3)_2AlH$
Dimethyl aluminiun dueteride	$(CH_3)_2AlD$
Dimethyl gallium hydride	$(CH_3)_2GaH$
Diethyl gallium hydride	$(C_2H_5)_2GaH$
Methylmanganese pentacarbonyl	$CH_3Mn(CO)_5$
d_3-Methylmanganese pentacarbonly	$CD_3Mn(CO)_5$
Manganese pentacarbonylhydride	$Mn(CO)_5H$
d-Manganese pentacarbonylhydride	$Mn(CO)_5D$
Trifluromethylmanganese pentacarbonyl	$CF_3Mn(CO)_5$
Manganese pentacarbonylchloride	$Mn(CO)_5Cl$
Manganese pentacarbonylbromide	$Mn(CO)_5Br$

REFERENCES

[1]. G.A.Atiya, Ph.D thesis (University of Leicester) 1990.

[2]. A.S.Grady, Ph.D thesis (University of Leicester) 1991.

[3]. D.F.Shriver, The Manipulation of Air-Sensitive compounds, 1969, Mc Graw-Hill.

[4]. R.T.Sanderson, Vacuum Manipulation of Volatile Compounds, 1940, Chapman and Hall.

[5]. A.P.Ashworth. E.N.Clark and P.G.Harrison, J.Chem.Soc., Chem. Commu., 1987 782; Trans. Faraday Soc,. 1990, 86, 4059.

[6]. Manufacturers Handbook, Edinburgh Instruments Ltd.

[7]. W.Gambler and H.Winer, International laboratory, 1984, 14,84.

[8]. W.M.Shaub and S.H.Bauer, Int. J.Chem. Kinet.,1975, 7, 509.

[9]. N.J.Bristow, B.D.Moore, M. Poliakoff, G.J. Ryott and J.J.Turner, J.Organomet. Chem;1984, 260 181.

[10]. Manufacturers Catalogue, Specac Ltd., 1989.

[11]. Willis,H.A., Miller,R.G.J., Adams,D,M., and H.A.Gebbie. Spectrochim. Acta. 1963, 19, 1457.

[12]. P.R.Griffiths, Chemical Infrared Fourier Transform Spectroscopy, New York Wiley, 1975.

[13]. J.K.Sanders and B.K.Hunter Modern NMR Spectroscopy. A Guide for Chemists, Oxford University Press, New York, 1987.

Chapter 3

3.1. Introduction.

The growth of AlGaAs by MOVPE has traditionally been carried out using TMAl, TMGa and AsH_3 [1]. However, there are several problems associated with the use of methyl-containing aluminium precursors [2]. First is the fact that aluminium forms very strong bonds with oxygen and water vapour and these can therefore be adsorbed on to the growing interface and become incorporated into the solid. Recently this problem has been largely overcome by improvements in reactor design. Second, and most important, is the problem of carbon contamination; the source of this is almost certainly TMAl because GaAs layers grown using TMGa under otherwise identical conditions show considerably less incorporated carbon [1].

One approach to solving the Al precursor problem has been the development of new compounds with appropriate properties. The initial step in this direction was the use of dimethylalane (DMAlH) by Bhat *et al.* [3]. These workers carried out decomposition studies, and also investigated the growth and characterization of AlGaAs layers using this compound. The preliminary results obtained suggested that there was very little, if any, carbon contamination in the films that were grown.

Jones *et al.* [4, 5] have investigated a number of alternative Al precursors including $Me_3Al.NMe_3$, $(Me_2AlNMe_2)_2$ and $(^tBuAlMe_2)_2$. None of these showed any advantage over TMAl in lowering carbon incorporation, and some of these precursors are even less convenient to use, i.e in terms of vapour pressure, preparation and purification. Jones *et al.* have also re-examined the work of Bhat on DMAlH. These workers found that AlGaAs layers grown from DMAlH, or the adduct $DMAlH.NMe_3$, contained similar levels of carbon to those obtained with TMAl and the degree of compositional uniformity was low, which was consistent with the large amount of darkening in the reactor upstream from the substrate [6]. This is due to the lower thermal stability of DMAlH relative to TMAl.

Another Al precursor is triethylalane (TEAl), which is thermally less stable than TMAl due to the facile β-hydride elimination of ethyl groups and therefore

might undergo a cleaner, more rapid, pyrolysis than TMAl. Keuch *et al.* [7] grew AlGaAs using TEAl, TEGa and AsH_3 in a low pressure MOVPE reactor which led to non-detectable levels of carbon. However, ethyl-based precursors are extremely susceptible to parasitic gas phase reactions and, in addition, the low vapour pressure of TEAl (0.04 Torr at 300 K) requires both the source and reactor lines to be heated, which subsequently leads to its premature decomposition. The growth of AlGaAs using the ethyl aluminium adducts $Et_3Al.NMe_3$ and $Et_2AlH.NMe_3$ has been examined by Jones *et al.* [6, 8]. It was thought that these precursors would be less susceptible to pre-reaction with AsH_3 and more stable than TEAl. However, it was found that neither of these precursors had any significant advantages over TMAl.

Another potential Al precursor is trimethylamine alane (TMAA) $AlH_3.NMe_3$, which is a reasonably volatile solid. It was found that atmospheric pressure growth using TMAA and TMGa [9] resulted in AlGaAs in which there was no significant reduction in carbon and that carbon incorporation increased with TMGa mole fraction. Poor layer uniformity and deposition on the reactor inlet were also found. However, low pressure growth using these mixtures resulted in excellent layer uniformity, with no evidence of pre-reaction, but there was again no reduction in the amount of carbon incorporated [10]. Under the same growth conditions, AlGaAs was grown using TMAA and TEGa. In this system no carbon was detected; despite this, the thickness uniformity was poorer than in the TMGa case, and there was a downstream decrease in the aluminium content of the film [11].

It would seem probable that gas phase processes are responsible for this carbon incorporation, a hypothesis which is borne out by the evidence of deposition prior to the susceptor in atmospheric pressure growth [9]. In order to shed further light on this hypothesis, the gas phase exchange reactions in both TMAA+TMGa and TMAA+TEGa mixtures were investigated by A.S.Grady [12] and R. Linney [13]. In the TMAA+TMGa system features ascribed to the following species were observed: free Me_2GaH, $Me_2GaH.NMe_3$, $MeGaH_2.NMe_3$, GaH_3NMe_3, Me_3AlNMe_3 and

$Me_2AlH.NMe_3$. It is evident that the hydrogen preferentially migrates to the more electronegative gallium centre, and the corresponding increase in the number of methyl groups bound to aluminium explains the observation of carbon contamination [9]. The TMAA+TEGa exchange reaction resulted in the formation of Et_2GaH, $Et_2GaH.NMe_3$ and $EtGaH_2.NMe_3$ coupled with the presence of the following species of very low volatility: Et_3Al, $Et_3Al.NMe_3$ and $Et_2AlH.NMe_3$. From these observations the result of the growth study using TMAA+TEGa [11] can be rationalized in terms of a facile β-hydride elimination of ethyl groups on the aluminium centre.

Exchange process between alanes, and also between alanes and gallanes have been extensively studied in solution, principally using ^1H NMR spectroscopy; on the other hand, very little is known of such processes in the gas phase. Recently the IR spectrum of DMAlH [13] has been analysed in detail. Building on this, the gas phase exchange reactions between DMAlH and TMAl, DMAlD and TMAl, DMAlH and d_3-TMAl have been investigated using mid-IR and far-IR spectroscopy in this work. The results of this study are presented in this chapter together with supporting NMR studies of toluene solutions of DMAlH and TMAl mixtures.

3.2. Review.

As early as 1962, Hoffmann [15] reported the detection of alkyl group exchange reactions in aluminium trialkyls using variable temperature ^1H NMR spectroscopy. Hoffmann extensively studied mixtures of triisobutylalane and trimethylalane in cyclopentane solution. In this system, exchange of alkyl groups takes place, producing dimers which are strongly associated by virtue of their methyl groups. Hoffmann concluded from this study that the tendency for bridging is in the order H ⟩ Me ⟩ ^{i}Bu. Furthermore, he also listed the ^1H NMR chemical shifts

for a number of $Me_3Al + Me_2AlX$ systems, where X= H, Cl, OMe, OEt and O^{t}Bu. These systems are complex not only because of exchange, but also because of the different molecularities involved.

In 1966 Williams and Brown investigated the exchange of methyl groups between the trimethyl derivatives of group III metals [16]. They initially studied the exchange of bridging and terminal methyl groups in TMAl in toluene solution using variable temperature ^{1}H NMR spectroscopy. The spectra recorded were similar to those previously reported in cyclopentane solution [17]. At 208 K, resonances ascribed to both bridging and terminal methyl groups were clearly identified. It was concluded that the rate of exchange is a first order process with respect to the TMAl dimer. Williams and Brown proposed that TMAl is involved in a two step equilibrium of the form

$$\underset{\text{Dimer}}{Al_2(CH_3)_6} \leftrightarrow \underset{\text{solvent-caged monomers}}{2Al(CH_3)_3} \leftrightarrow \underset{\text{solvent-separated monomers}}{Al(CH_3)_3 + Al(CH_3)_3} \qquad (3.1)$$

Similar results were obtained for both the TMAl + TMGa and TMAl + TMIn systems in toluene. The rate of exchange was found to depend on the ratio of concentration of the two components. Williams and Brown concluded that the overall rate-determining process in the above two systems is the formation of solvent separated monomeric TMAl followed by the rapid exchange of methyl groups with the other trimethyl compound.

Jeffrey and Mole [18] re-examined the exchange reaction between TMAl+TMGa in cyclopentane and toluene solutions using ^{1}H NMR spectroscopy. Although their kinetic data was very similar to those of Williams and Brown [16],

the interpretation of the result was different in several important respects. However, Jeffrey and Mole were in agreement with one of the most important postulates of Williams and Brown, in that the dissociation of the TMAl dimer determines the rates of both bridge-terminal equilibrium and of exchange with TMGa. The significant differences in interpretation are centred around the fact that William and Brown proposed that a solvent cage restricted the rate of exchange between TMAl and TMGa; in other words the rates of the bridge-terminal equilibration in cyclopentane and toluene are similar. The second discrepancy is that TMAl and TMGa exchange only take place after the TMAl monomers have become separated. Jeffrey and Mole on the other hand suggested that TMAl and TMGa exchange reaction occurs before the two TMAl monomers become separated, and also that both the recombination of TMAl monomers and exchange between the TMAl monomers and TMGa are collision-controlled processes. Jeffrey and Mole then went on to provide further evidence for their postulated mechanism, which is,

$$Al_2(CH_3)_6 \leftrightarrow \underset{\text{monomer pair}}{2Al(CH_3)} \qquad (3.2)$$

$$2Al(CH_3)_3 + (CH_3)_3M \rightarrow (\text{exchange}), \qquad (3.3)$$

by investigation of the ^1H NMR kinetics of exchange between DMZn and TMAl in cyclopentane solution, and also by re-examining the TMAl and TMAl + TMGa system [19]. Studies of this nature are always hindered by the possible involvement of the solvent, so it is therefore advantageous to study the reactions in the gas phase.

A number of hetero-bridge organoaluminium species of the general form $R_2Al(\mu X)(\mu Y)AlR_2$ have been identified by a number of workers in exchange reactions of the type

$$\{R_2AlX\} + \{R_2AlY\} \rightarrow \{R_2AlX.R_2AlY\} \qquad (3.4)$$

where R=Me or Et, and the braces indicate an unspecified degree of aggregation. Whether the resultant hetero-bridged compound enjoys a stable existence, or is simply a component in an exchange equilibrium, evidently depends on the rates of reaction (3.4) and its reverse. Smith and Wallbridge have identified an ordering of exchange rates for X and Y groups in such compounds as

$$Me > Et > Cl, Br, I > SMe, OEt > NMe_2, CN, F \qquad (3.5)$$

an order in keeping with the relative strengths of bridging bonds formed by such groups [20]. Subsequently, Fishwick and co-workers were able, with the aid of mass spectrometry and ^1H NMR spectroscopy, to demonstrate the synthesis and isolation of compounds featuring groups towards the slow exchange end of the range given in (3.5) simply by heating mixtures of the constituents to about 373-473 K. The list of species produced included R=Et, X=NMe_2, and Y= Cl, Br, I, OEt, and SMe [21]. Jeffrey *et.al.* [22] carried out a similar study of exchange reactions between dimeric organoaluminium compounds. Based on the results obtained, these workers placed the X and Y groups in order of decreasing capacity for bridge formation as follows: PrO > Cl > Br > PhCC > Ph > Me. The groups at the beginning of the series differ from those towards the end in terms of electronegativity, availabilty of lone pairs of electrons, and bridge geometry which may result in a higher aluminium-aluminium distance.

Eisch and Rhee [23,24] have studied the stoichiometry of exchange reactions in mixtures of $^iBu_2AlH$ and $^iBu_2AlCl$, and $^iBu_3Al$ and $^iBu_2AlH$, by variable temperature ^1H NMR and IR spectroscopy. In the latter system, two Al-H resonances were observed; a new peak at δ_H 3.9 ppm was assigned to the mixed bridge compound, this being considerably shifted downfield from that of pure $^iBu_2AlH$ at δ_H 2.92 ppm. These workers proposed a number of dimeric and trimeric heterobridged structures based on their results.

3.3. Experimental Details.

3.3.1. Chemicals Employed and their characterization.

i) $(CH_3)_3Al$, Trimethylalane, was a gift from Epichem Ltd.

ii) $(CD_3)_3Al$, fully deuterated trimethylalane, was prepared from $(CD_3)_2Hg$ and Al powder subjected to ultrasound [25].

The FTIR spectrum of $(CH_3)_3Al$ vapour phase is shown in figure 3.1 and the assignment of the spectrum is listed in table 3.1. The vibrational spectrum of TMAl in vapour phase has been extensively studied [27-29]. At room temperature, $(CH_3)_3Al$ is largely dimerized through bridging methyl groups, but at elevated temperatures becomes almost entirely monomeric [29-31]. The FT IR spectrum of $(CD_3)_3Al$ is shown in figure 3.2 and the band assignments are listed in table 3.2.

iii) The dimethylalanes $(CH_3)_2AlH$, $(CH_3)_2AlD$ and $(CD_3)_2AlH$

Dimethylalane, $(CH_3)_2AlH$ was synthesised using the following procedure [26]. Purified TMAl (1.53 g, 0.02 mol) was condensed into a sample tube containing 1 g of fresh $LiAlH_4$ (0.026 mol) at 77 K. On warming to room temperature, the sample was heated in a silicon oil bath to 90-95 °C under an atmosphere of dried (over P_2O_5) oxygen-free nitrogen for 20 minutes. The volatile DMAlH (85.4% yield) was then collected from the reaction tube at 233 K by trap-to-trap distillation under vacuum, and purified by repeated vacuum distillation. The ^1H NMR spectrum of DMAlH at 298 K was in complete agreement with that reported by Jones et al.[6] and there was no evidence of TMAl. Samples of $(CH_3)_2AlD$ and $(CD_3)_2AlH$ were prepared similarly using TMAl+$LiAlD_4$ and $(CD_3)_3Al$+$LiAlH_4$ respectively.

FTIR spectra of the above compounds in the vapour phase are shown in figure 3.3, 3.4 and 3.5 respectively. As mentioned earlier, the IR and Raman spectra of these species have been re-investigated by Grady *et al.* [14] and the results are listed in table 3.3. DMAlH has been extensively studied by IR and Raman spectroscopies, electron diffraction and molecular weight studies by a number of

other workers [32]-[33, 34]. In the vapour phase at room temperature DMAlH is largely dimeric, with contributions from higher species. On the other hand, in solution it is mainly trimeric in structure, again with contributions from higher degrees of aggregation
[14]. The purity of the DMAlH was checked by recording a ^1H NMR spectrum at 298 K. This revealed the presence of a broad singlet, characteristic of protons bound to Al, at δ_H 3.10 ppm and a sharp singlet at δ_H -0.02 ppm which arises from methyl protons. ^1H NMR spectra for $(CD_3)_2AlH$ and $(CH_3)_2AlD$ were also recorded in order to confirm the absence of $(CD_3)_3Al$ and $(CH_3)_3Al$ respectively and were considered to be of sufficient purity for the experiments in this work.

All materials were handled at all times on a rigorously pre-conditioned vacuum line as described in chapter 2. The isotopic purity of all compounds was checked using ^1H NMR and was estimated to be >99 % for all species.

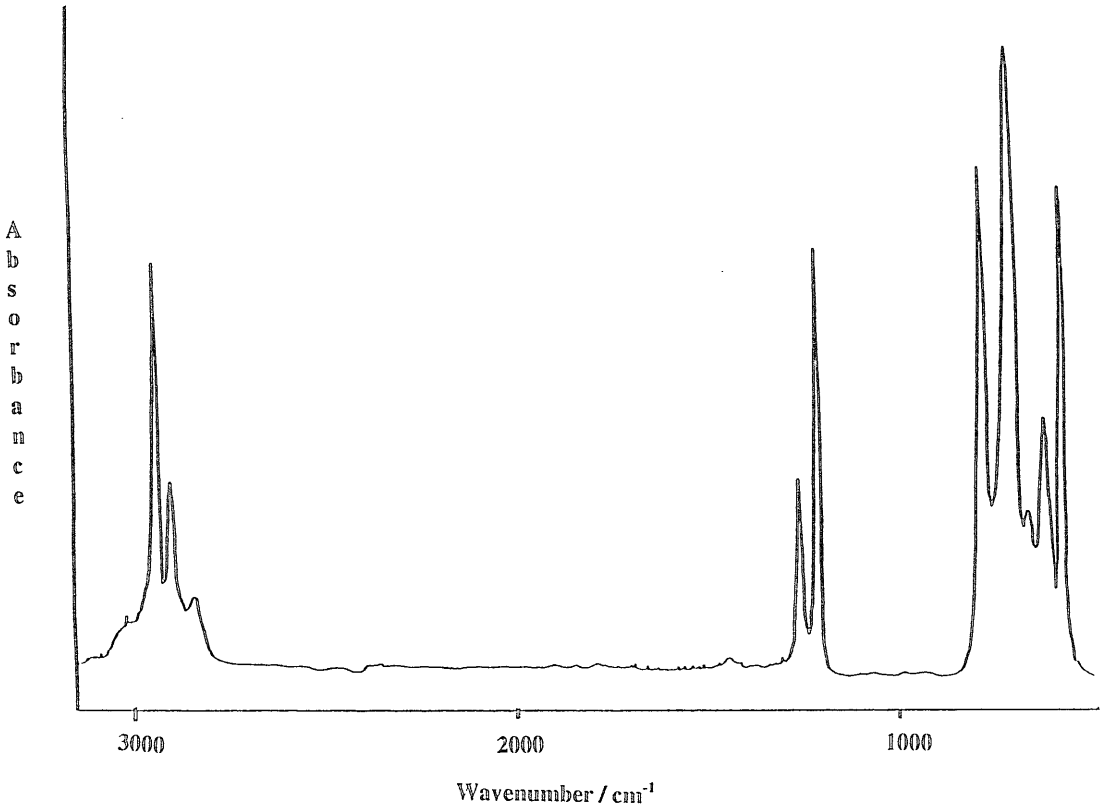

Figure 3.1: FTIR spectrum of $(CH_3)_3Al$

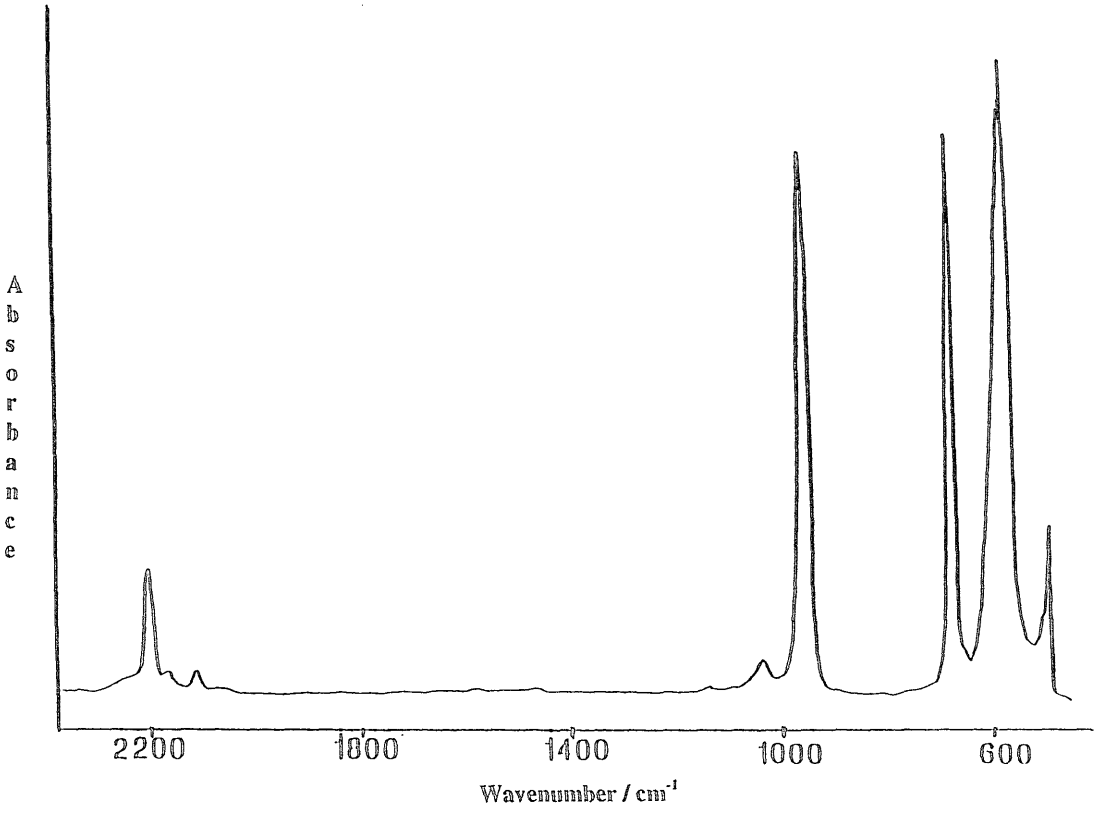

Figure 3.2: FTIR spectrum of $(CD_3)_3Al$

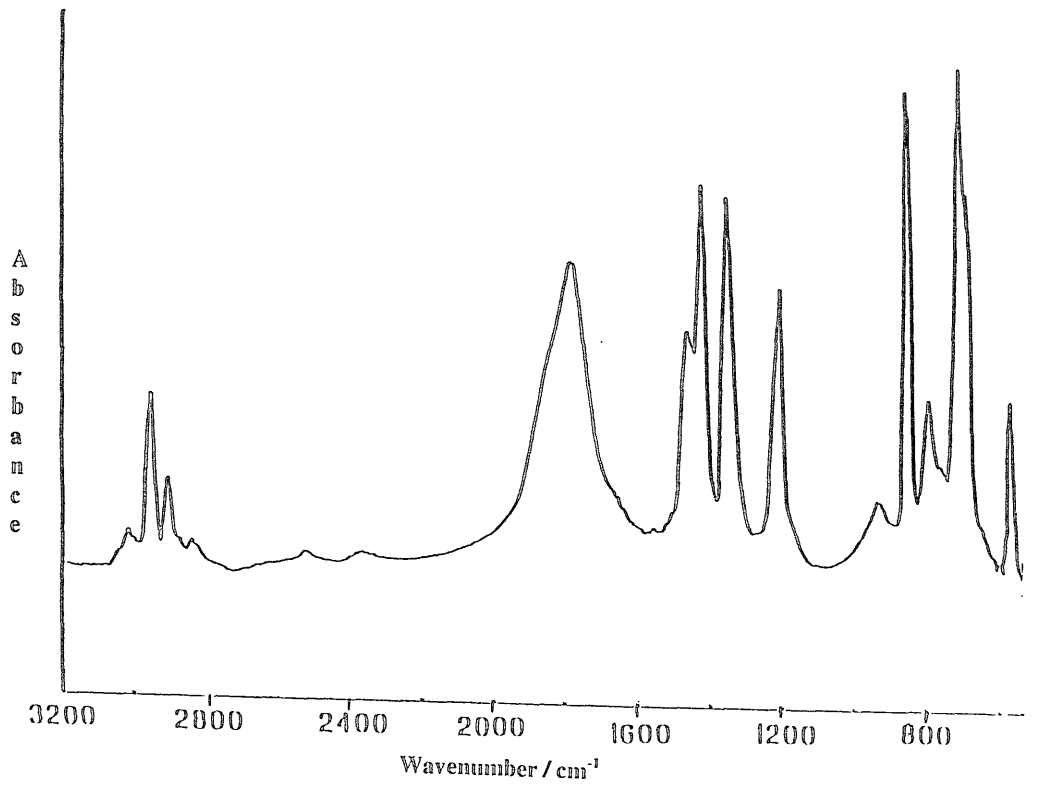

Figure 3.3: FTIR spectrum of $(CH_3)_2AlH$

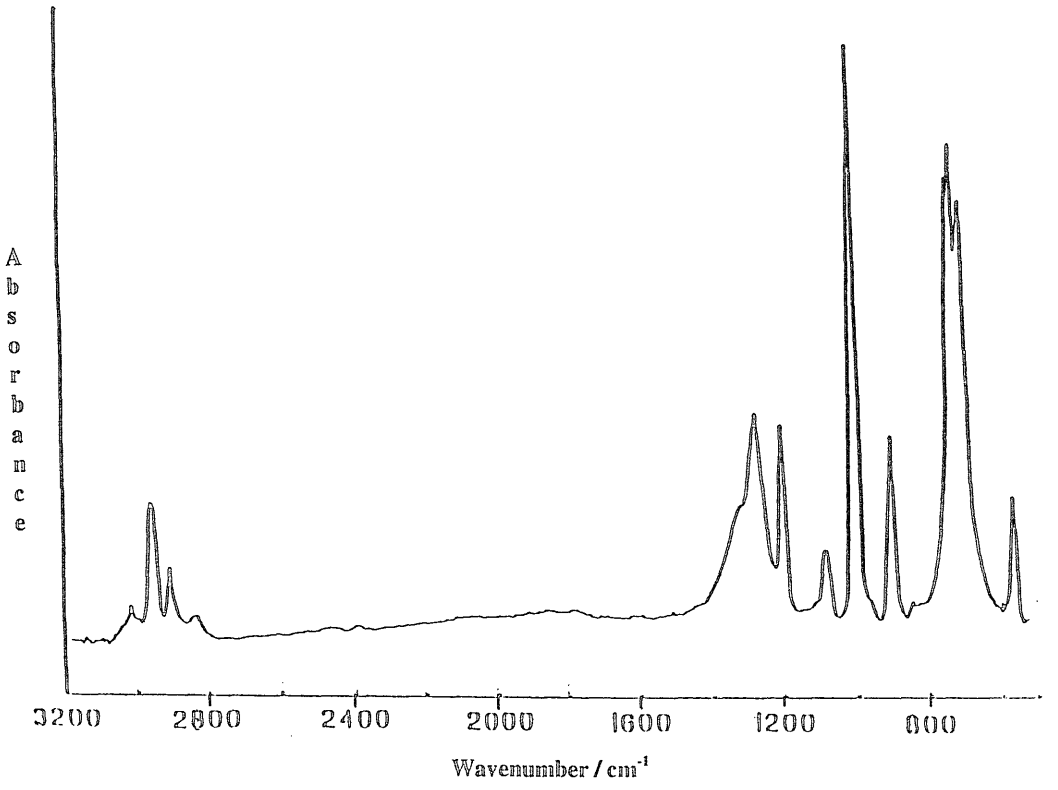

Figure 3.4: FTIR spectrum of $(CH_3)_2AlD$

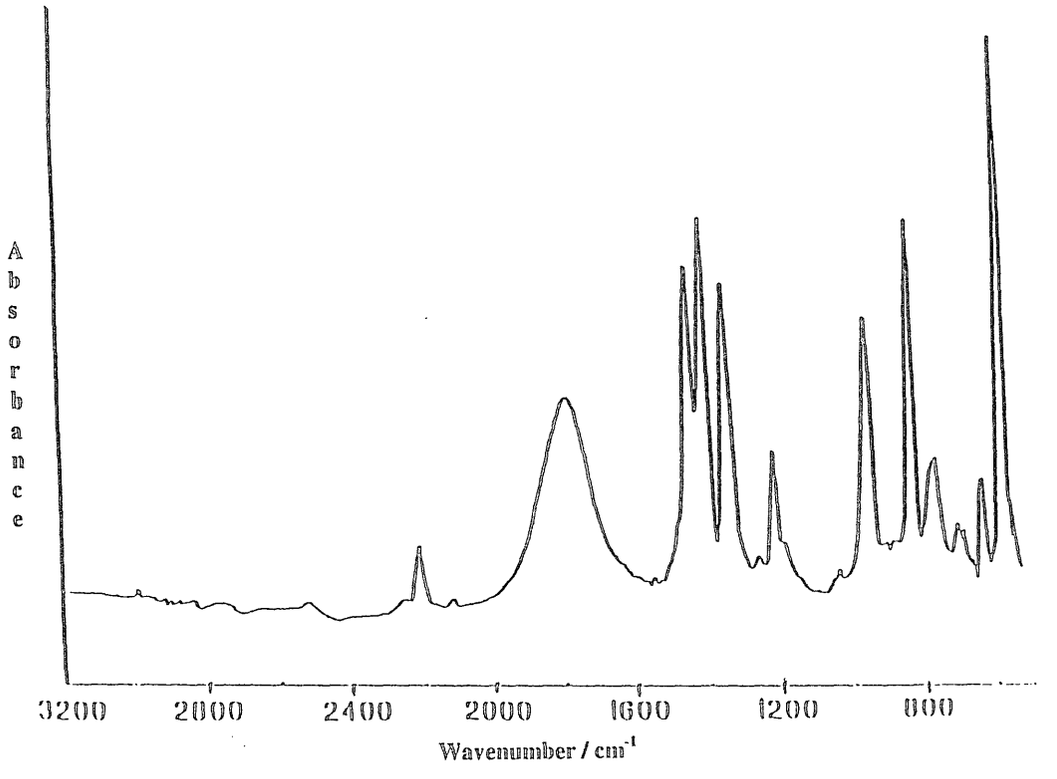

Figure 3.5: FTIR spectrum of $(CD_3)_2AlH$

Table 3.1. FT IR Data for Trimethylalane (cm^{-1})

FTIR*	Ref.[29]	ASSIGNMENT#
2943 (s)	2944 (s)	$\nu_{as}(CH_3)$
2903 (s)	2904 (m)	$\nu_s(CH_3)$
2842 (m)	2845 (w)	$\delta_{as}(CH) \times 2$
1254 (m)	1255 (m)	$\delta_s(CH_3)_b$
1208 (s)	1208 (s)	$\delta_s(CH_3)_t$
777 (vs)	774 (s)	$\rho(CH_3)_t$
702 (vs)	700 (vs)	$\nu(AlC_2)$
653 (m)	650 (vw)	$\rho(CH_3)_t$
610 (s)	609 (m)	$\rho(CH_3)_b$
567 (s)	567 (s)	$\nu(AlC_2)_b$

*** Vapour phase FTIR spectrum of dimeric TMAl at 298 K obtained in this work.**

 # b=bridge and t=terminal

Table 3.2: FT IR Data for Deuterated Trimethylalane (cm^{-1})

FTIR	Ref [28]	Assignment
2200 (s)	2200	
2116 (w)	2170	$\nu_{as,\ s}\ (CD_3)$
2110 (w)	2110	
1139 (w)	1140	$\delta_{as}\ (CD_3)_t$
1038 (m)	1036	$\delta_s\ (CD_3)_b$
957 (vs)	955	$\delta_s\ (CD_3)_t$
679 (vs)	677	$\rho\ (CD_3)_b$
579 (vs)	579	$\rho\ (CD_3)_t + \nu\ (AlC_2)_t$

 # Assignments are those of reference [28]

Table 3.3. FT IR Data for Dimethylalane Dimers (cm^{-1})

$(CH_3)_2AlH$	$(CD_3)_2AlH$	$(CH_3)_2AlD$	Assignment*
2955	2250	2955	ν_{as} (CH_3)
2905	2112	2905	ν_s (CH_3)
1444	1036	1440	δ_{as} (CH_3)
1206	955	1204	δ_s (CH_3)
709	-	708	ρ (CH_3)
692	-	708	$\omega(CH_3)$
#	#	-	ν_{as} (Al-H)
1215	1217	-	ν_s (Al-H)
-	-	1006	ν_{as} (Al-H)
-	-	905	ν_s (Al-D)
-	638	-	ν_{as} (AlC_2)
571	578	567	ν_s (AlC_2)
851	832	737	ρ (AlC_2)

* **Assignments are those of reference [14]**

\# **Perturbed by Fermi resonance**

3.3.2. Sample preparation.

i) Gas phase FTIR and Far-IR Spectroscopic studies

Vapours of dimethylalane or one of its isotopomers were introduced into the reaction cell followed by the addition of an overpressure of trimethylalane, i.e. ~5 torr, such that on briefly opening the cell to the line the pressure throughout the cell dropped to 5 torr. In order to achieved the required ratio of reactants, it was often necessary to add a further pressure of trimethylalane. This method does not take into account the fact that species might be lost from the gas phase, resulting in a decrease in the pressure inside the cell. Therefore the stated ratios can only be regarded as an approximate guide.

ii) ^{1}H NMR Study.

Samples for NMR spectroscopy were prepared by mixing the component in the gas phase as above, followed by condensation and addition of out-gassed, fully dried, solvent at 77K. Spectra in d_8-toluene were referenced to the Me-protonated impurity of the solvent at δ_H 2.10 ppm, and those in cyclopentane to the solvent at δ_H 1.50 ppm. Variable temperature spectra were recorded with an estimated accuracy of 1-2 K.

iii) Liquid Phase FTIR study.

A 1:1 mixture of DMAlH and TMAl was prepared first in the gas phase; this was then condensed into sample tube, followed by the addition of excess cyclopentane.

3.4. Gas Phase Mid-IR Investigations.

3.4.1. DMAlH+TMAl mixture

An FT IR spectrum of a mixture of dimethylalane and trimethylaluminium between 500 and 2000 cm^{-1} is shown in figure 3.6. The region above 2000 cm^{-1} contains only the uninformative methyl C-H stretching vibrations, and the cutoff of the ZnSe window material prevents meaningful measurements below 500 cm^{-1}. Spectrum 3.6(a) is a computer addition of the prerecorded spectra of the two

individual components, and spectrum 3.6(b) is that of a 1:1 mixture of the two. It is readily apparent from an inspection of these two spectra that the mixture contains very different species from the two starting materials; indeed some features uniquely assignable to dimethylalane or trimethylalane are almost undetectable in the mixture. In particular, the strong broad feature around 1800 cm^{-1} ascribed to the Al-H-Al asymmetric stretching mode in trimeric dimethylalane (DMAlH), has disappeared, to be replaced by two somewhat weaker and narrower peaks between 1500 and 1600 cm^{-1}.

A particularly striking and highly informative change is observed near 800 cm^{-1}; the strong and sharp doublet at 851 cm^{-1} (this feature is highly characteristic of the Me_2Al rocking vibration in the dimeric bridge species $Me_2Al(\mu H)(\mu H)AlMe_2$), is almost completely replaced by a similar, but even stronger, feature at 815 cm^{-1}. A similar band was also observed in both IR spectra of a mixture of DMAlH and DMAlD [14] and in the spectrum following IR LPHP of DMAlH [12]. In both cases it was assigned to the Me_2Al rocking vibration in a dimeric mixed bridged species, $Me_2Al(\mu H)(\mu H)AlMe_2$. There are also other less clearly defined changes in the region of Al-H symmetric and antisymmetric stretching modes in the dimeric form of DMAlH (between 1200 and 1500 cm^{-1}) and also in the region of Al-C stretching and Me rocking modes around 800 cm^{-1}. In order to obtained a clearer picture of the changes produced, an IR spectrum was recorded of a mixture containing an excess of dimethylalane. This was followed by the subtraction of excess DMAlH using the clear peak at 851 cm^{-1} as a guide.

3.4.2. DMAlD + TMAl Mixture

An FTIR spectrum of a mixture of $(CH_3)_2AlD$ and $(CH_3)_3Al$ is shown in figure 3.7 after features due to excess DMAlD have been subtracted out. In this system, both the symmetric Al-D stretch (at 1006 cm^{-1}) and its asymmetric counterpart (905 cm^{-1}) are replaced by similar bands at slightly higher wavenumber (1038 and 994 cm^{-1}

respectively); this was accompanied by the disappearance of the asymmetric Al-D stretching mode in trimeric DMAlD at 1280 cm^{-1}. This is coupled with a shift in the MeAl rocking vibration from 737 cm^{-1} (in dimeric DMAlD) to 758 cm^{-1}, which makes this new peak mid-way between the methyl rocking vibrations in DMAlD and TMAl.

The mixture of $(CD_3)_2AlH$ and $(CD_3)_3Al$ has been examined previously [13,36]. The spectrum obtained in the present work is shown in figure 3.8. It is very evident from this spectrum that there are no Al-H vibrations near 1210 cm^{-1}; indeed all such vibrations occur above 1300 cm^{1}. These spectra are all consistent with the assignment above, and this conclusion is confirmed by a partial normal coordinate analysis (carried out by D.K.Russell) of the significant vibrations. Table 3.4 summarises the Al-H stretching and Me_2-Al rocking vibrations in the above three mixed bridged systems.

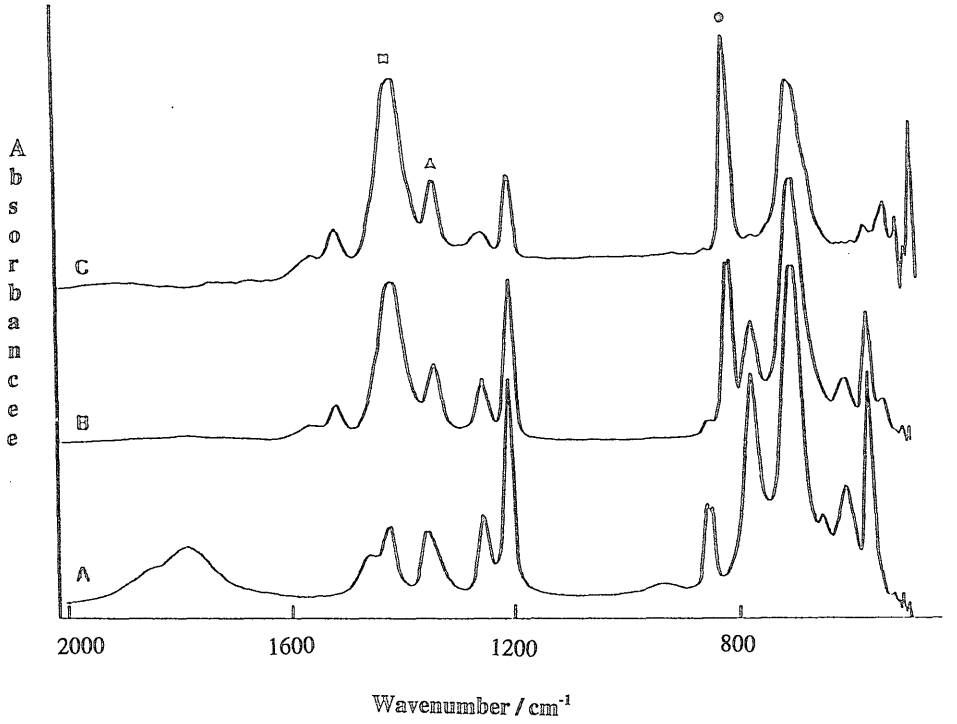

Figure 3.6: FTIR spectra of mixture of $(CH_3)_2AlH$ and $(CH_3)_3Al$. A = computer co-added spectra; B = spectrum of 1:1 mixture; C = spectrum of 1.6:1 mixture. The peaks marked (○), (△), (□) are those assigned to vibrations fitted in the normal coordinate analysis.

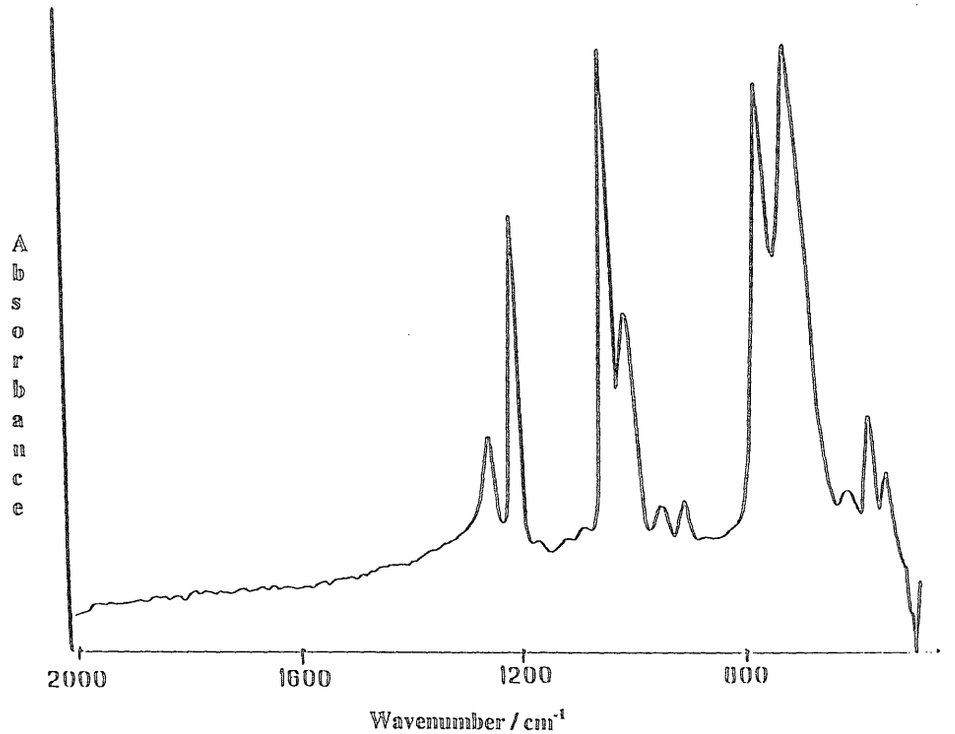

Figure 3.7: FTIR spectrum of mixture of $(CH_3)_2AlD$ and $(CH_3)_3Al$

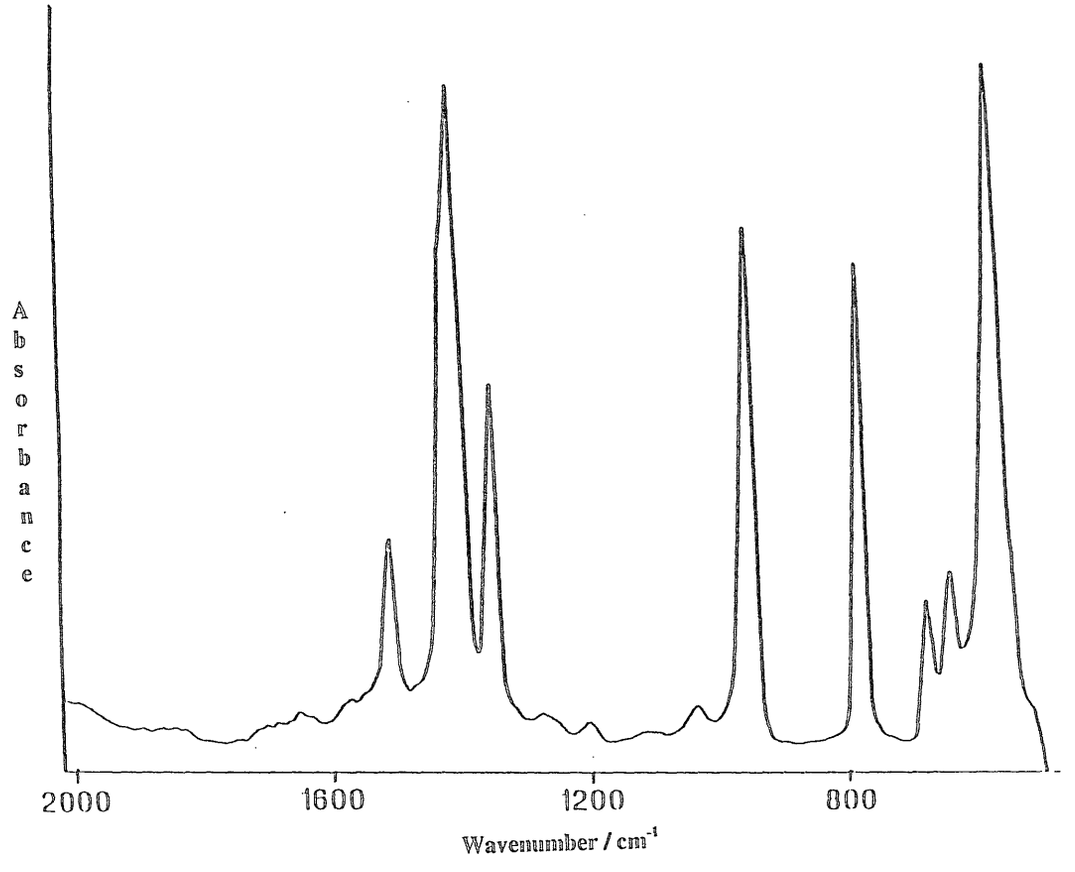

Figure 3.8: FTIR spectrum of mixture of $(CD_3)_2AlH$ and $(CD_3)_3Al$

Table 3.4.

Al-H Stretching and Me_2Al Rocking Vibrations in Bridge Systems.

System[a]	Vibration[b]	Observed	Calculated	Observed in DMAlH[c]
CH_3, H	ν_{as}(AlH)	1416	1416	1353[d]
CH_3, H	ν_s(AlH)	1339	1345	1215
CH_3, H	$\rho(AlMe_2)$	815	803	851
CD_3, H	ν_{as}(AlH)	1411	1415	e
CD_3, H	ν_s(AlH)	1352	1345	1217
CD_3, H	$\rho(AlMe_2)$	784	793	832
CH_3, D	ν_{as}(ALD)	1038	1032	1006[f]
CH_3, D	ν_s(AlD)	994	995	905[f]
CH_3, D	$\rho(AlMe_2)$	758	757	737[f]

a. CH_3 , H = $(CH_3)_2$ Al (μCH_3) (μH) Al $(CH_3)_2$, etc

b. ν = stretch, ρ = rock, s = symmetric, as = asymmetric.

c. From reference [14]

d. For $(CH_3)_2$Al (μH) (μD)Al $(CH_3)_2$

e. Perturbed by Fermi resonance.

f. For $(CH_3)_2$ Al $(\mu D)_2$Al $(CH_3)_2$.

3.5. Gas Phase Far-IR Results

3.5.1. Far-IR Spectra of TMAl, d_3-TMAl, DMAlH and DMAlD

The molecular structure of the dimer of trimethylaluminium is a bridge structure and two methyl groups lie between two aluminium atoms [35]. The vibrational spectra and their assignments have been studied by several authors [27,28,31,36]. Onishi *et al.* [27] have measured the infrared spectra in the region 700-280 cm^{-1} and have calculated the normal vibrational frequency on the basis of a modified Urey-Bradley field. Ogawa *et al.* [36,37] have measured far-infrared spectra (in the region 700 to 65 cm^{-1}) in the liquid phase and have also performed a normal coordinate analysis using a procedure similar to that adopted previously for diborane [38]. In the present study we measured far-infrared spectra of TMAl, DMAlH and their deuterated species and their mixtures in the gas phase (in the region 500-10 cm^{-1}) and the treatment of their normal vibrations were refined and vibrational spectra were reassigned. Far-infrared spectra of TMAl , DMAlH and their deuterated species are shown in figures 3.9, 3.10, 3.11, 3.12 and spectral data for these species and their assignments are shown in table 3.5. In this study the vibrational assignment were carried out with reference to the results of the vibrational frequency calculations of Onishi and Ogawa [27,28,38] In the case of trimethylalane the bands at 163 and 328 cm^{-1} are due to Me-Al-Me rocking vibrations. The rocking vibrations of bridged methyl groups have one in-plane mode and one out-of plane mode and both have been observed by mid-infrared and Raman data [14]. The bands at 377 and 475 cm^{-1} are assigned to Al-Me-Al bridging vibrations. Therefore the following structure is expected

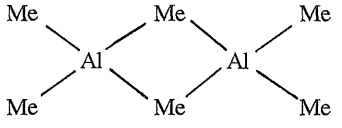

DMAlH and DMAlD also show a signal at 163 cm^{-1} due to an Me-Al-Me bending vibration in the structure given below

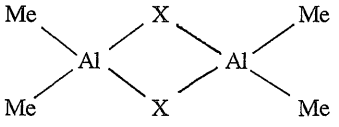

X= H, D

The absence of absorptions at 328, 377 or 475 cm^{-1} for DMAlH and DMAlD confirm the lack of Al-Me-Al bonds in these compounds

3.5.2. Far-IR study of mixtures of TMAl+DMAlH and TMAl+DMAlD.

Far-IR spectra of mixtures of TMAl+DMAlH and TMAl+DMAlD are shown in figures 3.13 and 3.14 and their band assignments are summarised in table 3.5. For these mixtures, the following dimeric bridge structures are possible

a.

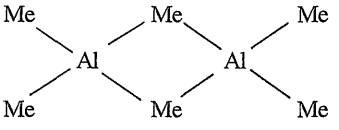

b.

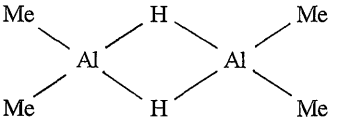

c.

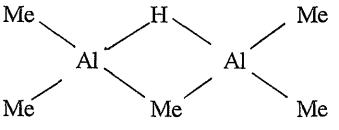

The bands at 166 and 326 cm^{-1} are attributed to the Me_2Al (Me-Al-Me) rocking vibrations in the dimeric bridge structure (c) and the band at 367 cm^{-1} is assigned to the Al-Me-Al stretching vibration [28,36]. The Al-H-Al gives a prominant absorption in the mid-infrared region near 1200 cm^{-1} [14]. The replacement of H by a heavy

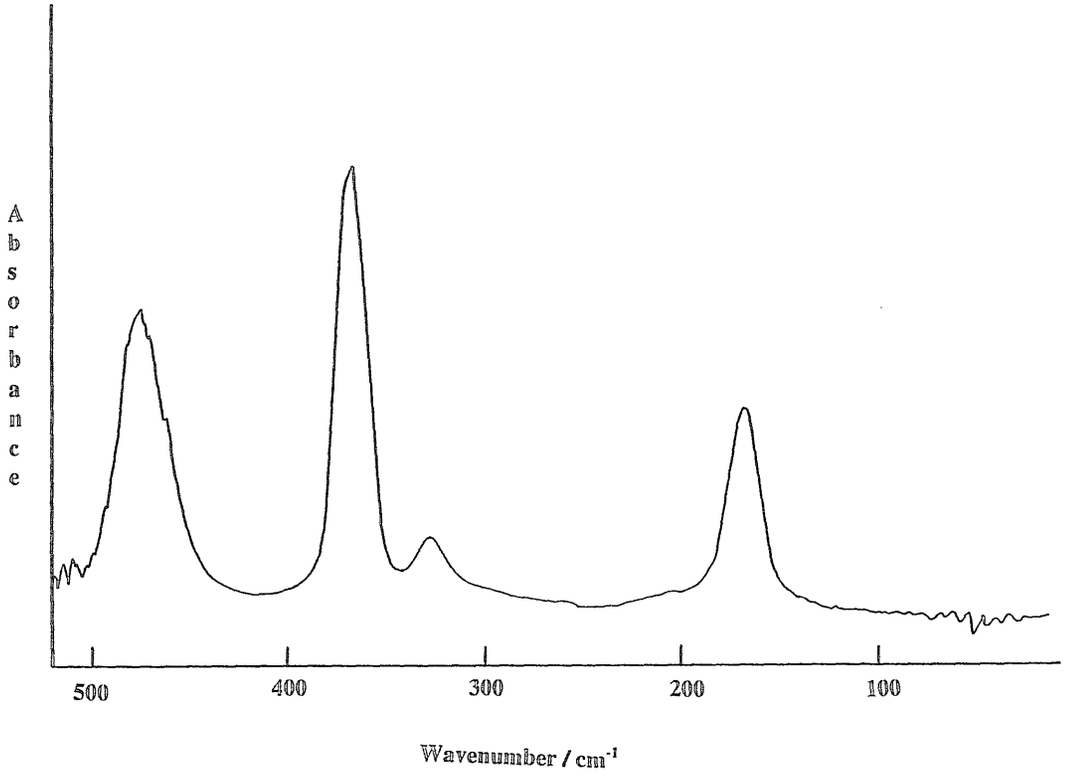

Figure 3.9: Far-infrared spectrum of $(CH_3)_3Al$

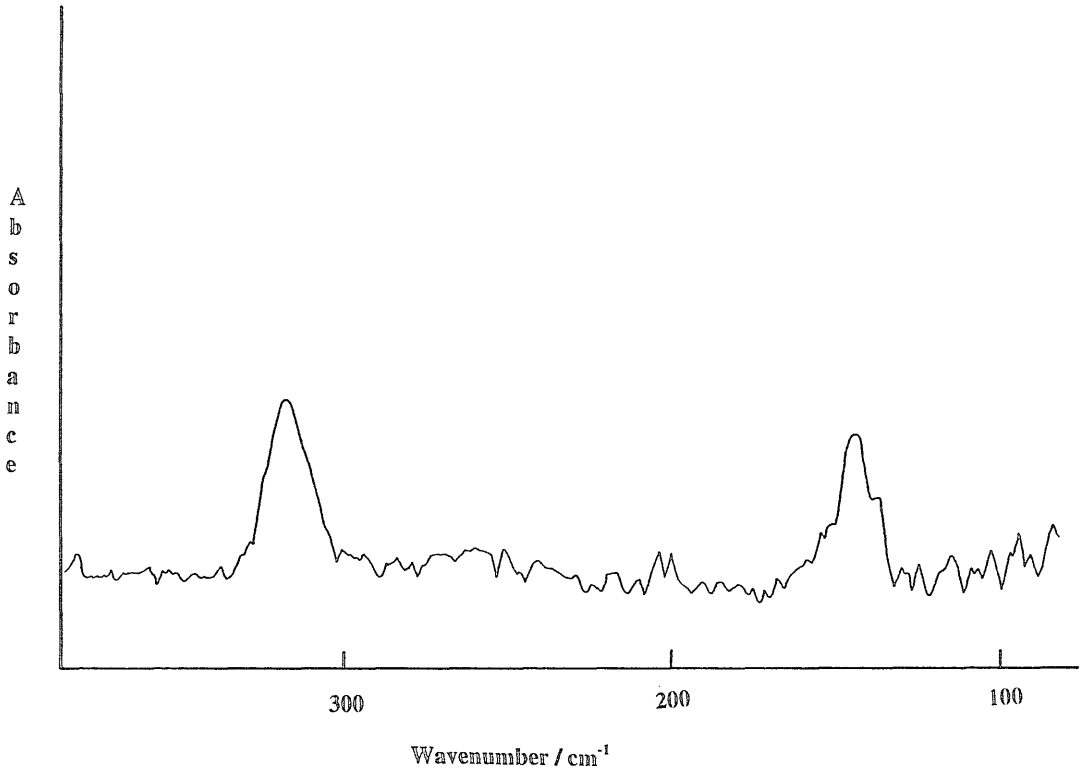

Figure 3.10: Far-infrared spectrum of $(CD_3)_3Al$

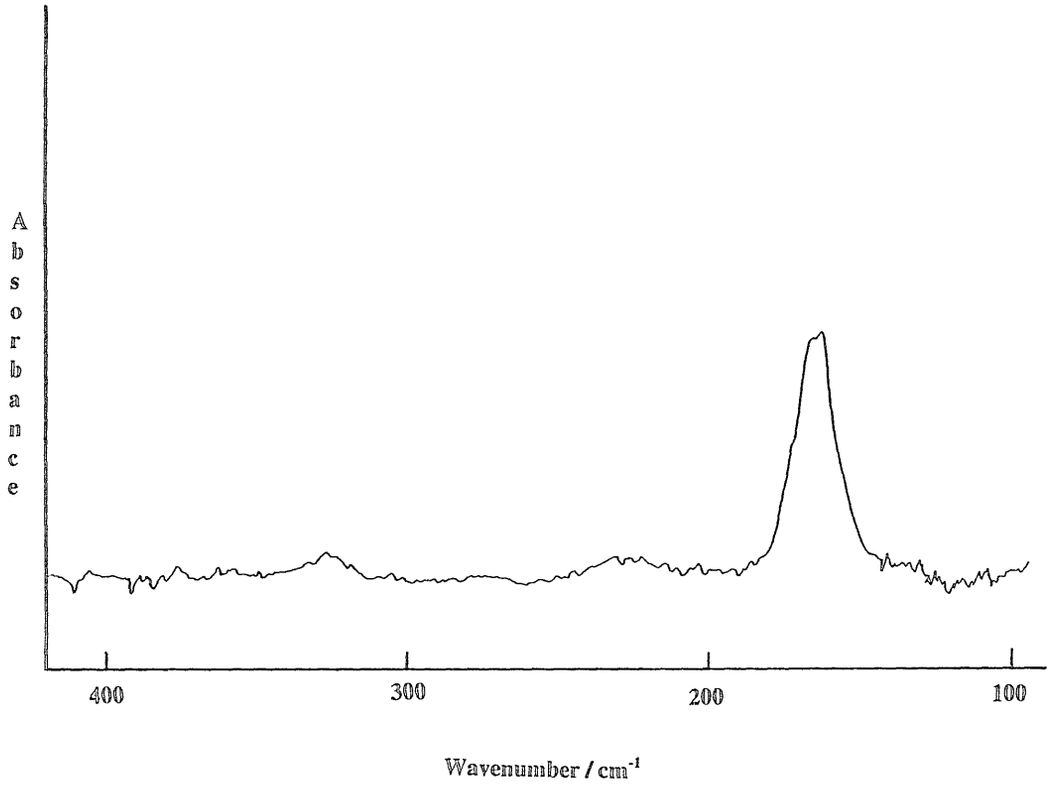

Figure 3.11: Far-infrared spectrum of $(CH_3)_2AlH$

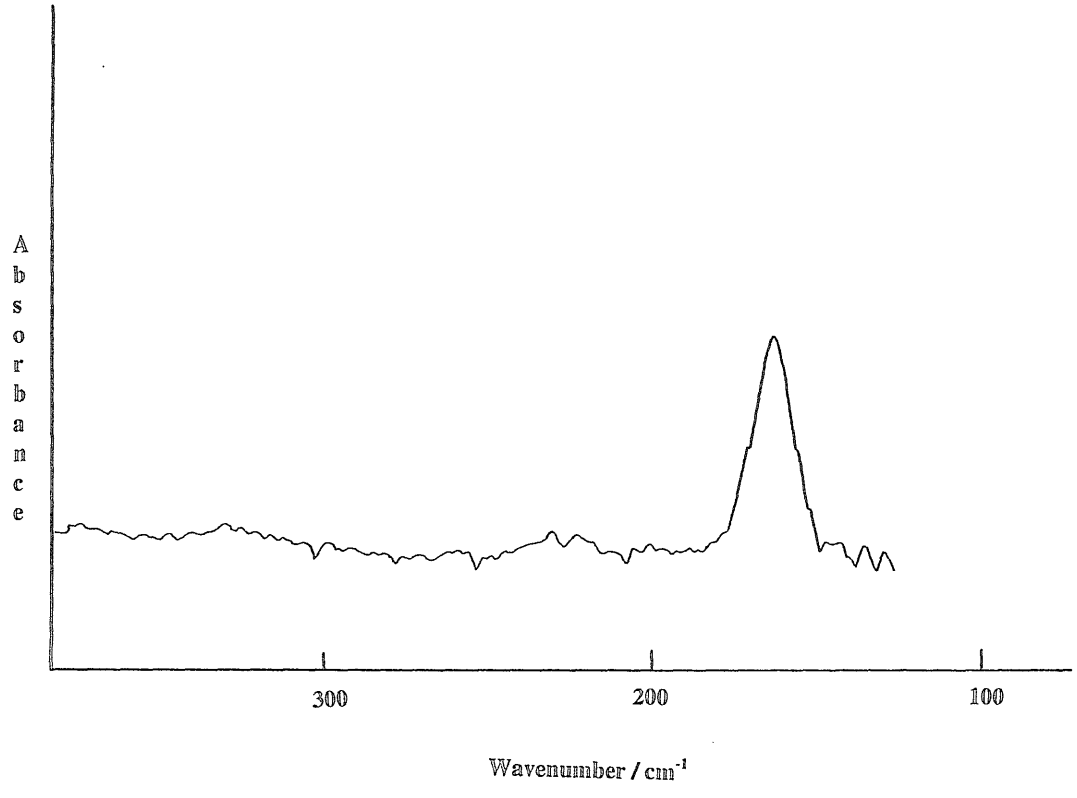

Figure 3.12: Far-infrared spectrum of $(CH_3)_2AlD$

group, namely a methyl group, gives a signal in the far-infrared region and in the mixed-bridged dimer two bridging vibrations due to the Al-H bonds (one due to a symmetric bending vibration and the other due to an asymmetric bending vibration), and two bridging vibrations due to the Al-Me bond (one symmetric and the other asymmetric in the dimeric form) are possible.

The bands at 166 and 326 cm^{-1} may be attributed to the symmetric vibrations and that at 367 cm^{-1} to asymmetric vibration in the molecule containing Al-H-Al and Al-Me-Al bridge [14,28,36]. In the case of the TMAl+DMAlH mixture the vibration of the Al-Me-Al bridging bond is shifted to lower frequency, the replacement of one of the bridging H atom in the $Al(\mu H)_2Al$ by a less strongly electron withdrawing Me group leads to a marked strengthening of the remaining Al-H-Al bridge.

To summarise so far, the gas phase studies of trimethylalane, dimethylalane and their mixtures in the far-infrared region provide evidence to support the dimeric mixed bridge structure of these species.

3.6. Liquid Phase IR Spectra of DMAlH+TMAl mixture in cyclopentane.

In dimethylalane itself, the equilibrium position between dimeric and higher oligomeric forms is considerably shifted in solution [13]. In the gas phase at room temperature, the dimeric form predominates, [14] whereas in cyclopentane solution it is a very minor component [33]. As a preliminary to solution NMR studies, we have examined the IR spectrum of a mixture of dimethylalane and trimethylalane in cyclopentane solution; this is shown in Fig 3.15. Although the dimeric form of the hetero-bridge species is present (as indicated by the peak at 808 cm^{-1}), it is considerably less dominant than in the gas phase[14], with significant contributions coming from the trimer of the initial dimethylalane, as shown by a broad peak at 1800 cm^{-1}. Furthermore, there is no evidence for the presence of either the methyl

rocking vibration at 851 cm^{-1} due to dimeric DMAlH or the mixed trimer peak at 1500 cm^{-1}.

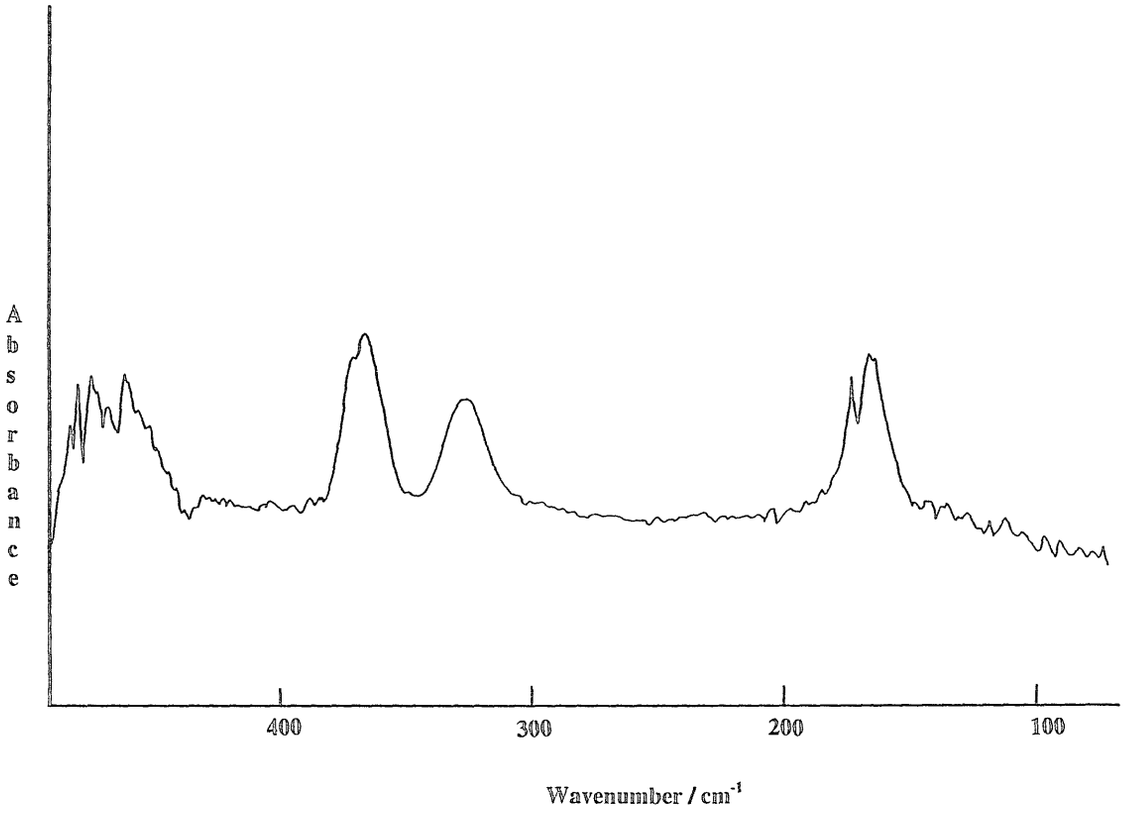

Figure 3.13: Far-infrared spectrum of mixture of $(CH_3)_2AlH$ and $(CH_3)_3Al$

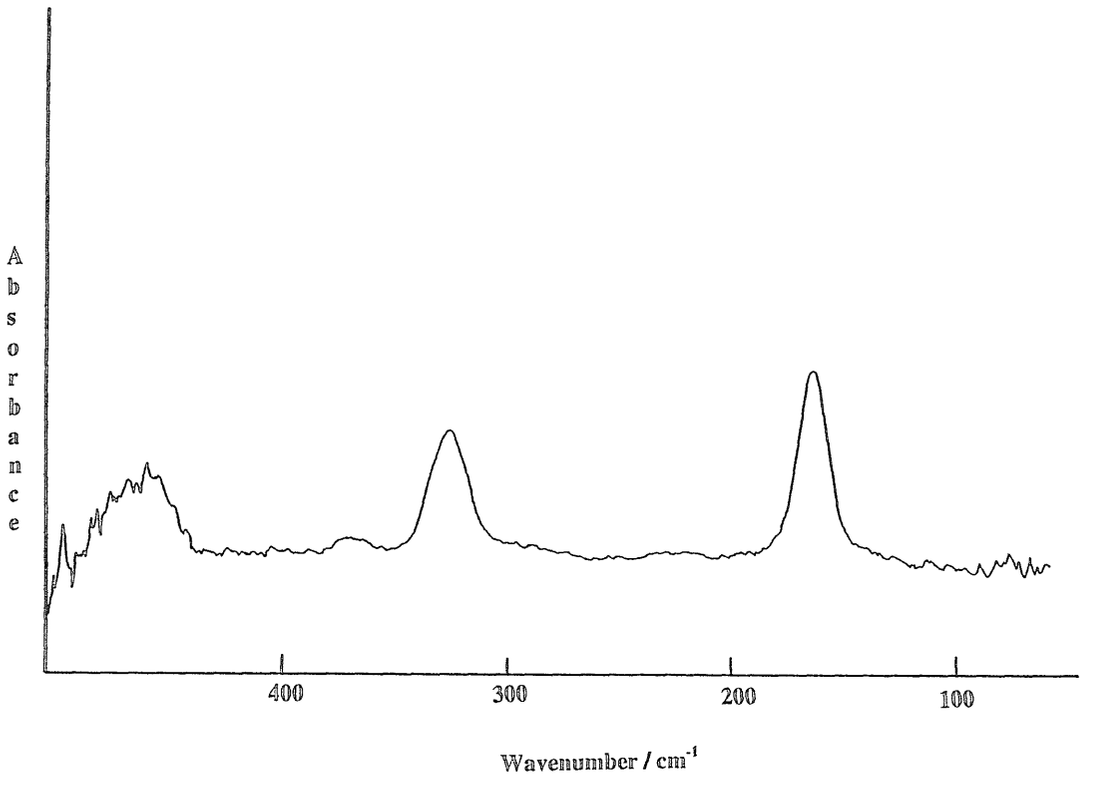

Figure 3.14: Far-infrared spectrum of mixture of $(CH_3)_2AlD$ and $(CH_3)_3Al$

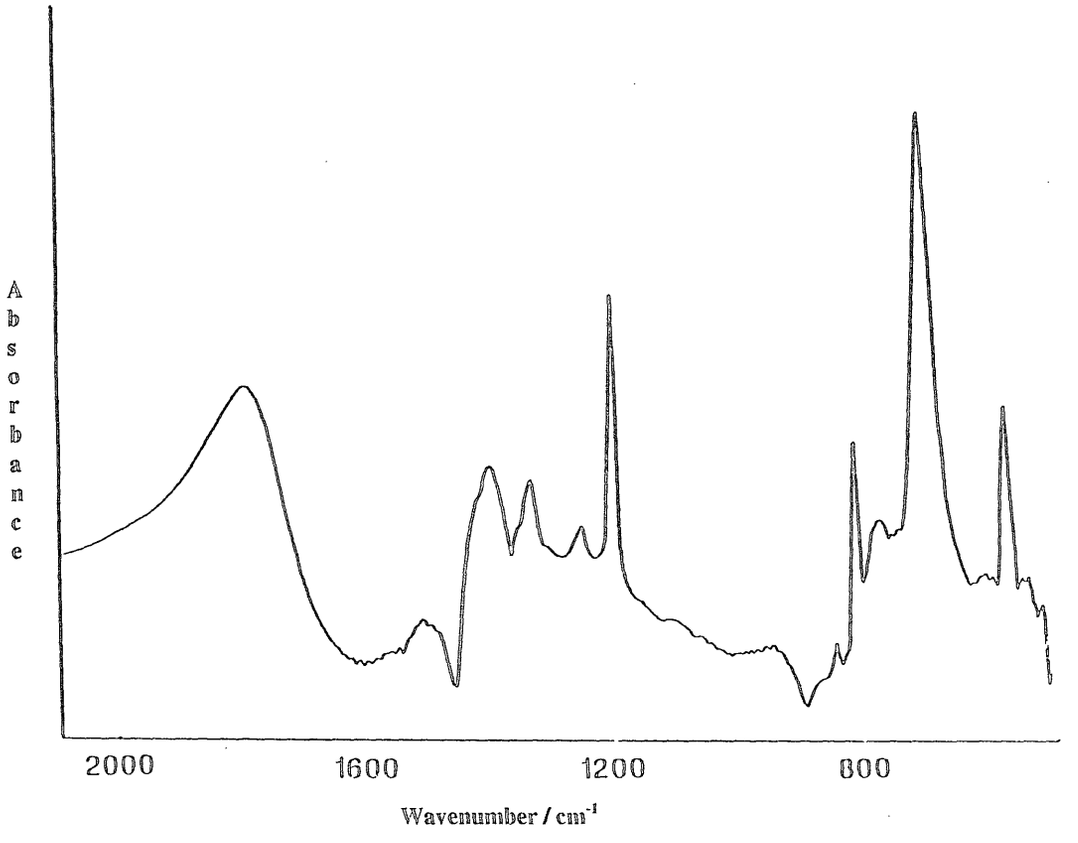

Figure 3.15: FTIR spectrum of mixture of $(CH_3)_2AlH$ and $(CH_3)_3Al$ in cyclopentane solution

Table 3.5 Far- infrared spectral data (cm^{-1})

TMAl	d-TMAl	DMAlH	DMAlD	DMAlH+TMAl	DMAlD+TMAl	Assignment
163	143	163	163	166	163	ρ(Al-Me_2)
				173		ν(Al-Me-Al)
328	318	230	229	326	327	ρ(Al-Me_2)
367	383	327	330	367		ν(Al-H-Al)
475				472	461	ν(Al-Me-Al)

ρ = Rocking, ν = Stretching

3.7. ^{1}H NMR Spectra of DMAlH+TMAl mixture in d_8-toluene

Fig 3.16 shows the ^{1}H NMR spectrum of an approximately 1:1 molar ratio of dimethylalane and trimethylalane in d_8-toluene at the lowest attainable temperature of 191 K (at lower temperature, the solution becomes a glass). In the region where Al-H resonance normally occurs, two strong broad peaks at δ_H 2.65 ppm (C) and δ_H 3.64 ppm (A) are observed, in an integrated ratio of 5:1. The first of these is ascribed (on the basis of a comparison with the spectrum of pure dimethylalane) to dimethylalane in its normal trimeric or higher form; the latter we assign to the crossed species in a dimeric state on the basis of the IR and far-IR spectra. These observations closely resemble those of Eisch and Rhee for the ^{i}Bu system [24]. In some spectra, there is in addition a weaker third resonance at δ_H 3.16 ppm (B): this is ascribed to trimeric mixed bridge species. However the region of the CH_3 resonance is more complicated. In addition to resonance due to the terminal (δ_H -0.52 ppm, G) and bridging (δ_H 0.03 ppm, D) Me groups of trimethylalane, and the Me group of dimethylalane (δ_H -0.41 ppm, E), there is an additional broader peak in the terminal Me region at δ_H -0.48 ppm (F), and some further weak but sharp features. The new broad feature (F) can be assigned to the terminal Me group of the crossed-bridge species; the origin of sharper features is not clear, but investigation of the spectra of solutions of dimethylalane alone at low temperatures suggests that they originate from either impurities or higher oligomeric units in this species (DMAlH) [35].

At higher trimethylalane:dimethylalane ratios, the intensities of both the Al-H and Me features assigned to the mixed bridged species increase relative to those of dimethylalane. Figure 3.17 illustrates the spectra recorded for the ratio 1:1 mixture of DMAlH and TMAl as the temperature is gradually raised. In the methyl region (A), as the temperature is raised above 200 K, the peak assigned to the mixed bridge species broadens and disappears. Around 220 K, the bridging and terminal peaks of TMAl broaden and coalesce, and reappear in the fast exchange regime around 250 K

this is very similar to the classic observations of this species alone reported as long ago as the 1950s [15]. Finally, the dimethylalane (DMAlH) resonance broadens above 270 K, and by 300 K all Me groups are apparently in rapid exchange. The dramatic variation in linewidths over this range of temperature, coupled with the overlap of many of the features, prevented any analysis of the change in the relative proportions of the species present.

The situation in the region of the Al-H resonance is quite different. Here, between 191 and 290 K broadening is relatively modest: on the other hand, the relative integrated intensities of the two peaks shift in favour of the crossed bridge species, so that at temperatures above 280 K, it is the greater of the two. Above 300 K, the two species evidently undergo exchange, with coalescence of the two peaks around 325 K. The greater chemical shift range afforded by ^{13}C NMR might have been expected to reveal clear evidence for mixed bridge species, but unfortunately only resonances assignable to the starting material could be unambiguously detected.

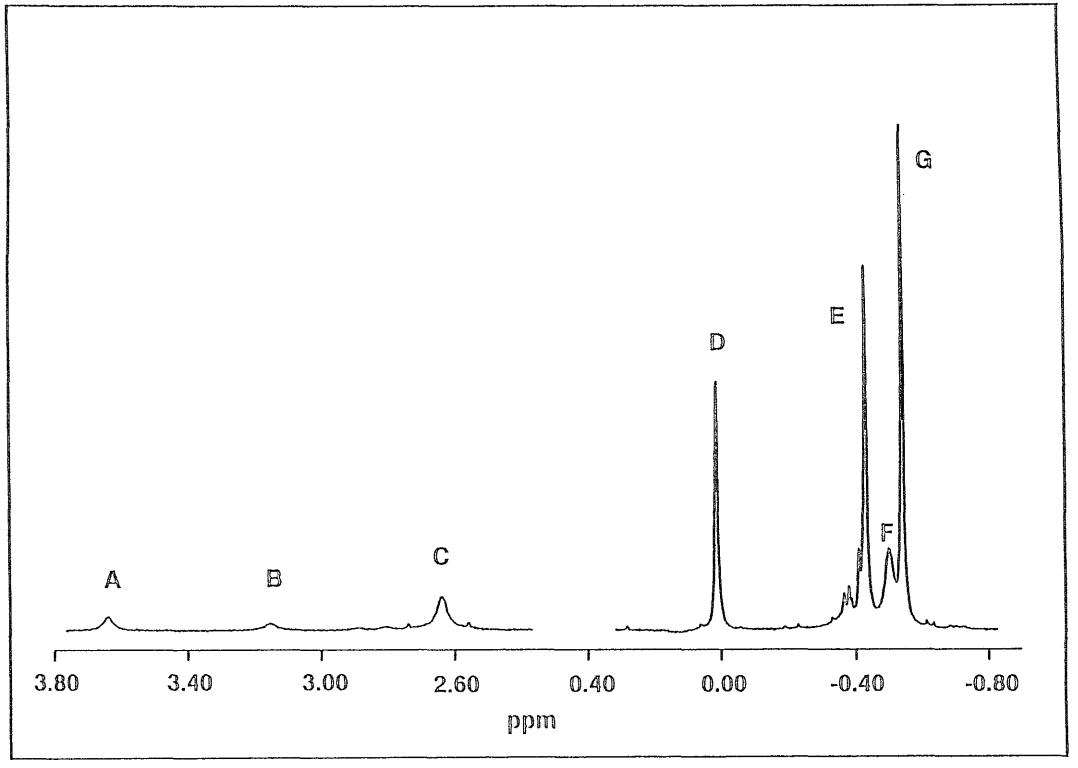

Figure 3.16: ^{1}H NMR spectrum of a 1:1 mixture of $(CH_3)_2AlH$ and $(CH_3)Al$ in d_8-toluene at 191 K. Only the regions of Al-H and CH_3 resonances are shown.

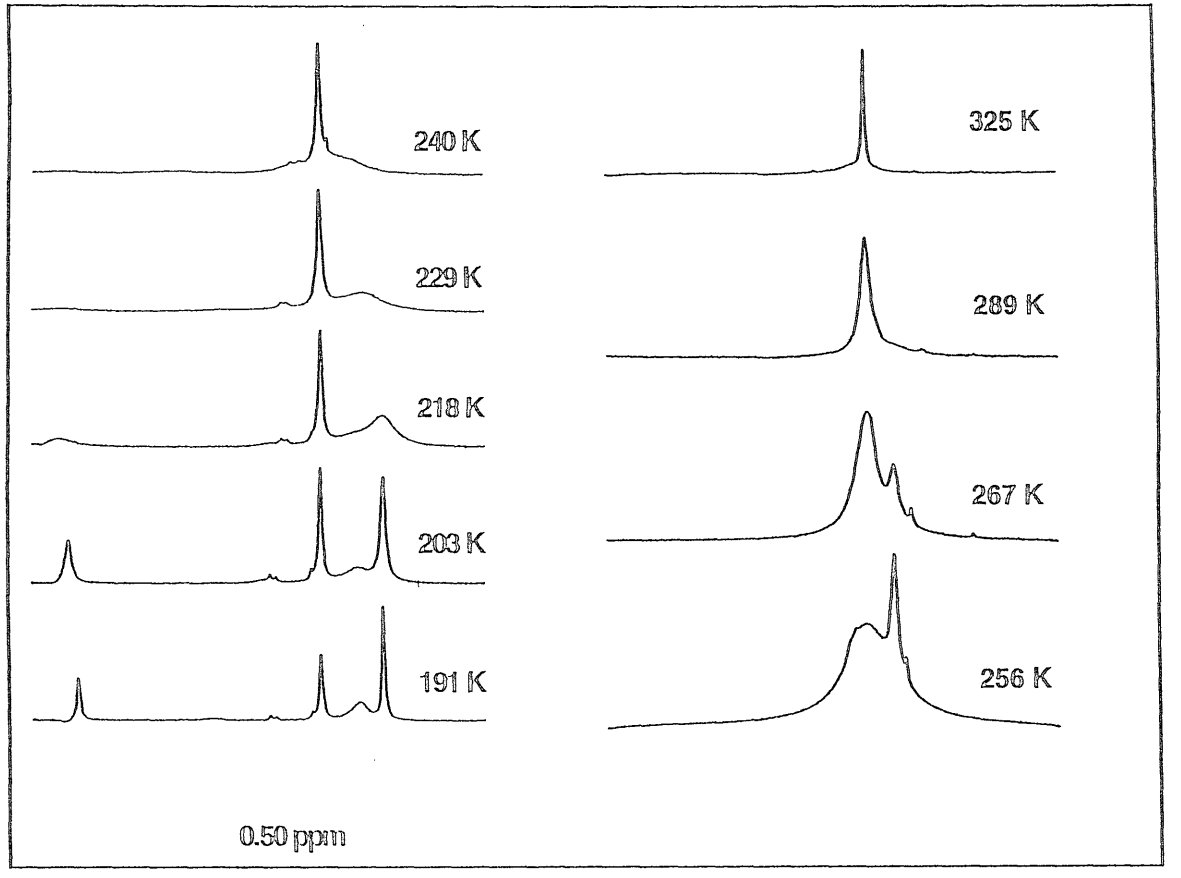

Figure 3.17: Temperature variation of the Me resonances (D-G) of figure 3.16.

3.8. Discussion and Conclusions.

The gas phase IR and far-IR observations leave little doubt that the predominant species in the gas phase is the crossed bridge dimeric species $Me_2Al(\mu H)(\mu Me)AlMe_2$, with smaller contribution from trimeric or higher species with both H and Me bridge units. Although the presence of these species is not surprising, the extent of the dominance of the mixed dimer is somewhat unexpected, and it is of interest to enquire into its origin. In the exchange equilibria

$$TMA_2 + DMA_2 \rightarrow 2X_2 \qquad (3.6)$$

$$3\,TMA_2 + 2DMA_2 \rightarrow 6X_2 \qquad (3.7)$$

with the degree of association of trimethylalane (TMA) and dimethylalane (DMA) indicated by subscripts, and X_2 representing the mixed-bridge dimer, formation of X is entropically slightly favored in (3.7), and is approximately neutral in (3.6). It follows that formation of X_2 in (3.6) must be energetically strongly favorable, and hence that the Al-H-Al bridging bond in the mixed dimer is stronger than that in the homo-bridged dimer.

This suggestion may be verified via a normal coordinate analysis (NCA; carried out by D.K.Russell) [36] of the vibrations of mixed bridge species. This revealed that the force constant of the Al-H-Al bridging bond is stronger in the mixed bridge species; while the force constant of the Al-Me-Al bond is weaker in the mixed bridge species; the resultant force constants are reported in table 3.6. Gas phase far-IR spectra of a mixtures of trimethylalane and dimethylalane showed that the Al-Me-Al bridging bond is shifted to lower frequency, thus providing further evidence to support the conclusion drawn from other experimental observations. Table 3.4 lists observed and calculated wavenumbers of selected vibrations based on this analysis.

The ^1H NMR results provide strong support for the above conclusions. The observation of two major Al-H resonances, readily ascribed to the dominant dimeric mixed bridge and trimeric dimethylalane units, is similar to that of Eisch and Rhee in

the isobutyl case [24]. However, the combined weight of our observations supports the contention that the chemical shift of this resonance is more a measure of variation in the angle subtended at the Al-H-Al centre than of the nature of the other bridging or terminal moieties, with a decrease in this angle resulting in a shift of the resonance to lower field. The ab initio calculations (carried out by Claxton) [36] confirm this contention. Indeed, this hypothesis is further supported by the observation of a weaker resonance at intermediate field in this region (most notably that at δ_H 3.16 ppm), which may well be due to a mixed bridged trimer. In the gas phase IR spectra, the weak broad peaks near 1500 cm^{-1} in the Al-H-Al system compare with those in trimeric trimethylalane near 1800 cm^{-1}; the latter is consistent with an angle near 120^o, and it would appear that this angle is closed down considerably in the mixed trimers. The observed increase in mixed dimer concentration with temperature is a consequence of the usual entropic favoring of (3.7) to the right.

The temperature variation studies also support the above conclusion. The weakest Al-Me-Al bridge is probably that in the mixed dimer, with the result that even at the lowest temperature attainable, bridge-terminal Me exchange on the NMR timescale occurs in this species. This would certainly account for the non-observation of a distinct bridge Me resonance, and it strongly supports the conjecture that bridge-terminal Me exchanges may occur through a single bridging bond rupture;

$$Me_2\,Al(\mu H)(\mu Me^*)AlMe_2 \rightarrow Me_2Me^*Al(\mu H)AlMe_2 \rightarrow MeMe^*Al(\mu H)(\mu Me)AlMe_2 \quad (3.8)$$

Evidence for similar single Me-bridge species has been presented by Kvisle and Rytter in their study of matrix isolated trimethylalane [29]. Rupture of the somewhat stronger Al-Me-Al bridge in trimethylalane requires a slightly greater activation energy, and is hence not significant until a higher temperature is reached.

Exchange of Me groups in dimethylalane cannot occur until a temperature sufficient to effect Al-H-Al rupture in this species is attained, and therefore at this temperature broadening of the Al-H-Al resonance of dimethylalane also occurs. Finally, rupture of the mixed bridge Al-H-Al system requires the highest energy of all, by which time exchange of all bridging Al-H is clearly in evidence. These qualitative observations are all supported by relaxation rate measurements [35]. The interpretation of the vibrational spectra of monomeric trimethylalane showed that ab initio calculations of organoaluminium species can provide crucial insight into the origin of spectroscopic features [31]. There is some experimental evidence to support this: in both the corresponding boron [39] and gallium [40] systems, bridging M-H-M vibrations are very similar in $H_2M(\mu H)_2MH_2$ and $Me_2M(\mu H)_2MMe_2$ (M= B or Ga)

The results of ab initio calculations, which are shown in table 3.7, fully support the NCA results. It can be seen from this table that the Al-H-Al bridging bond in the mixed dimer is indeed calculated to be appreciably shorter than that in dimethylalane (173.0 nm as opposed to 174.8 nm), suggesting a marked strengthening. On the other hand, the angle subtended at the bridge H is not markedly different. This suggestion is born out by the vibrational wavenumber calculated: just as in the experimental observations, both the symmetric and antisymmetric Al-H-Al frequencies are increased, with a marked decrease in separation between the two in the hetero-bridge system. The charge densities on the bridging H atoms (which may be employed for the purpose of rationalising relative NMR chemical shift in the two systems) are very similar in the two dimeric systems. On the other hand, the corresponding charge density in trimeric Al_3H_9 is much larger (-0.323 as opposed to -0.254), leading to an expectation of increased shielding here. This again accords with the marked upfield shift found for the trimeric dimethylalane in comparison with the dimeric crossed-bridge system. In all respects, the ab initio calculations support the conclusion drawn from the experimental observations.

In summary, both experimental and theoretical evidence points to the same conclusion, namely that the species $Me_2Al(\mu H)(\mu Me)AlMe_2$ is formed as the major component in mixture of TMA and DMA, and that this results from a substantial increase in strength of the Al-H-Al bridge bond. NMR results interpreted on this basis strongly support the contention that bridge-terminal group exchange can result from a single bridge bond dissociation and reassociation.

Table 3.6 Force constants in H-Bridged Alanes.

Force constant[a]	In mixed bridge	In DMAlH
Al-H_b stretch	1.07 [b]	0.96 [c]
Al-H_b /Al-H_b stretch/stretch	0.16 [b]	0.09 [c]
Me_t -Al- H_b bend	0.28 [d]	0.26 [c]

a. b=bridge, t = terminal b. mdyn $Å^{-1}$ c. From ref [14]. d. mdyn Å rad^{-2}

Table 3.7: Results from ab Initio Calculations for H-bridge Alanes.

	Al_2H_6	Al_3H_9	Al_2H_5Me [a]
Al-H_b /nm	174.8	170.5	173.0
Al-H_b-Al angle	98°	146°	99°
ν_{as}(Al-H_b-Al)/cm^{-1}	1445	-	1566
ν_s(Al-H_b-Al)/cm^{-1}	1321	-	1478
H_b atomic charge	-0.264	-0.323	-0.254

[a] $H_2Al(\mu H)(\mu Me)AlH_2$

REFERENCES.

[1]. Proc. 4th Intern. Conf. on MOVPE, H akone, 1988, Eds. N. Watanabe, T. Nakanisi and P.D. Dapkus [J. Cryst. Growth, 1988, 93]

[2]. G.B. stringfellow, Organometallic Vapour-phase Epitaxy: Theory and Practice, Ch. 7, Academic Press, San Diego, 1989.

[3]. R. Bhat, M.A.Koza, C.C.Chang, S.A.Schwarz and T.D.Harris, J. Cryst. Growth, 1986, 77, 7.

[4]. A.C.Jones, J.S.Roberts, P.J.Wright, P.E.Oliver and B.Cockayne, Chemtronics, 1988, 3, 152.

[5]. A.C.Jones, P.R. Jacobs, S.A.Rushworth, J.S.Roberts, C.C.Button, P.J.Wright, P.E.Oliver and B. Cockayne, J. Cryst. Growth, 1989, 96, 769.

[6]. A.C.Jones, P.J.Wright, P.E.Oliver, B.Cockayne and J.S.Roberts, J. Cryst. Growth, 1990, 100, 395.

[7]. T.F.Keuch, E.Veuhoff, T.SKuan, V.Deline and R.Potemski, J. Cryst. Growth, 1986, 77, 257.

[8]. A.C.Jones, S.A.Rushworth, J.S.Roberts, C.C.Button and J.P.R.David, Chemtronics, 1989,4,235.

[9]. J.S.Roberts. C.C.Button, J.P.R.David, A.C. Jones and S.A.Rushworth, J. Cryst. Growth, 1990, 104, 857.

[10]. A.C.Jones, S.A.Rushworth, D.A.Bohling and G.J. Muhr, J. Cryst. Growth, 1990, 106, 246.

[11] A.C. Jones and S.A.Rushworth, J. Cryst. Growth, 1990, 106, 253.

[12]. A.S.Grady, Ph.D. Thesis (University of Leicester) 1991.

[13]. R.E.Linney, Ph.D. Thesis (University of Leicester) 1994.

[14]. A.S.Grady, S.G.Puntambekar and D.K.Russell, Spectrochim. Acta, 1991, 47A, 47.

[15]. E.G.Hoffmann, Trans. Far. Soc., 1962.58, 642. and references therein.

[16]. K.C.Willams and T.L.Brown, J.Am. Chem. Soc, 1966, 88, 5460.

[17]. N.Muller and D.E.Pritchard, J. Am. Chem. Soc., 1960, 82, 248.

[18]. E.A.Jeffrey and T.Mole, Aust. J. Chem., 1969, 22,1129.

[19]. E.A.Jeffrey and T.Mole, Aust. J. Chem., 1973, 26,739.

[20]. C.A.Smith and M.G.H.Wallbridge, in Abstract of the Third Symposium on Organometallic Chemistry, 1967, 346.

[21]. M. Fishwick, C.A.Smith and M.G.H.Wallbridge, J. Organomet. Chem., 1970, 21, P9.

[22]. E.A.Jeffrey, T.Mole and J.K.Saunders, Aust. J. Chem., 1968, 21, 649.

[23]. J.J.Eisch and S.G.Rhee, J.Organomet. Chem., 1972, 38, C25.

[24]. J.J.Eisch and S.G.Rhee, J. Organomet. Chem., 1972, 42, C73.

[25]. R.D.W.Kemmitt and S.G.Puntambekar, unpublished results.

[26[. J.R.Surtes, Aust. J. Chem. 1965, 18, 14.

[27]. T.Onishi and T.Shimanouchi, Spectrochim. Acta, 1964, 20, 325.

[28]. T.Ogawa, Spectrochim. Acta, 1968, 24A, 15.

[29]. S.Kvisle and E. Rytter, Spectrochim. Acta, 1984, 40A, 939.

[30]. C.H.Henrickson and D.P.Eyman, Inorg. Chem., 1967, 6, 1461.

[31]. G.A.Atiya, A.S.Grady, D.K.Russell and T.A.Claxton, Spectrochim. Acta, 1991, 47A, 467.

[32]. E.G.Hoffmann and G.Schomburg, Z. Elektrochem., 1957, 61, 1101; ibid., 1957, 61, 1110.

[33]. H.W.Schrotter and E.G.Hoffmann, Bur.Bunsenges. Phys. Chem., 1964. 68, 627.

[34]. A.Almenning, G.A.Anderson, F.R.Forgaard and A.Haarland, Acta.Chem. Scand., 1972, 26, 2315.

[35]. R.D.Markwell and D.K.Russell, unpublished results.

[36]. A.S.Grady, R.E.Linney, Z.Mahmood, R.D.Markwell, D.K.Russell and T.A.Claxton, to be published.

[37]. A.Amenningen, S.Halvorsen, A.Haaland, Acta. Chem. Scand. 1971. 25, 1937.

[38]. W.M.Howard, A.U.Jayasooriya, A.F.S.Kettle, B.D.Powell, N.J.Sheppard, Chem. Soc, Chem. Commun. 1979, 18.

[39]. J.W.Lehmann, I.Shapiro. Spectrochim. Acta. 1961, 17,396.

[40]. R.C.Pulham, A.J.Downs, J.M.Goode, D.W.H.Rankin, H.R.Robertson, J.Am. Chem. Soc. 1991, 113, 5149.

Chapter 4

4.1. Introduction.

The trialkyls of group III elements have been extensively used in the growth of III-V semiconductor devices by metal organic vapour phase epitaxy (MOVPE) [1] and molecular beam epitaxy (MBE) [2]. There are however, several disadvantages associated with these simple precursors, principally being that trimethyl compounds, such as TMAl [3], lead to unwanted carbon incorporation in the deposited film, while triethyl compounds often have low volatility, which requires the heating of the reactor gas-inlet lines, causing premature decomposition and poor growth rates. A possible solution to these problems was thought to be the use of mixed alkyl group precursors, such as $EtMe_2In$, which could combine the high volatility of the methyl compounds with the reduced carbon incorporation of the ethyl compounds.

The indium precursor, $EtMe_2In$, which is liquid at room temperature, was first used to grow GaInAs film in an atmospheric pressure MOVPE reactor. In that work [4,5], the formation of extremly poor quality layers was reported. An alternative aluminium precursor, $^tBuMe_2Al$, was used by Jones et al. [6] to grow AlGaAs in an atmospheric pressure MOVPE reactor. It was thought that the presence of a bulky tertiary butyl group would inhibit the formation of oligomers, through which alkyl exchange occurs. However, the results obtained were somewhat disappointing in that the $^tBuMe_2Al$ may decompose in the reactor prior to growth, yielding dimethylalane, DMAlH, and that although deposited layers of AlGaAs of good optical quality were grown, the level of the carbon contamination was approximately equal to that using TMAl. On the positive side, however, it was concluded that $^tBuMe_2Al$ did show potential for high quality aluminium growth at low substrate temperatures.

On the other hand ethyl-based materials are subject to the facile elimination of ethyl groups by the β-elimination process on pyrolysis [7] which leads to a much cleaner deposition of the desired metal. As a result, Al and AlAs films with no

detectable carbon have been grown using TEAl and Et_2AlH as aluminium precursors [8,9,10,11]. However only limited success has been achieved in the growth of AlGaAs in combination with TMGa. By replacing TMGa with TEGa, AlGaAs layers with no detectable carbon can be grown using TEAl [8]. However, TEAl is thermally less stable than TEGa, with the result that the Al content of the alloy decreases in the downstream direction. The extremely low vapour pressure of TEAl requires the heating of reactor lines and sources, which often leads to the decomposition of the compounds in the reactor lines and poor growth rates [12].

Even a compound that contains no bonds to carbon *i e.* TMAA, has shown no advantage over TMAl when used in combination with TMGa. Again, this is despite the use of TMAA as a precursor to high purity aluminium by chemical vapour deposition [13]. However, on replacement with TEGa, AlGaAs layers with no detectable carbon can be grown at all compositions. TMAA also has a much higher vapour pressure than TEAl and thus, of the alternative materials studied, this compound appears to be most promising.

Clearly, the source of carbon in AlGaAs layer grown using ethyl and hydride based (*i.e.* TMAA) Al-precursors, must be TMGa, yet low carbon-content GaAs layers can be grown with this compound. Furthermore, the thickness uniformity of the AlGaAs layers were generally poor, with the direction of increasing Al content in the alloys being in the opposite direction to that expected from the thermal stabilities of the precursors used, *i e.* the aluminium content of the alloy often increased in the downstream direction. It would seem probable, therefore, that gas-phase reactions transfering ligand groups, and thus forming new molecules with differing thermal stabilties, are responsible, a hypothesis born out by evidence of deposition on the reactor inlet.

Ligand exchange reactions between Al and Ga alkyls have been widely studied in solution [14] but very little is known about the extent of these reaction in the gas-phase. To date, only mixtures of TMAl and TEGa and TMAA and TMGa have

been studied and the methyl-ethyl exchange products formed in gas phase have been identified [15].

The main objective of this work was to investigate the alkyl group exchange reactions for trialkylgallium compounds (TMAA / TMGa, and TMGa / TEGa) at room temperature and low temperatures using FTIR, ^1H NMR and mass spectroscopies. Also, the IR LPHP of triethylgallium (TEGa) and trimethylgallium (TMGa) mixture was investigated. This work showed that the technique of IR LPHP not only give unambiguous evidence for the β-elimination pathway, but also provides a route to diethyl and monoethylgallanes. The aim of this was to selectively β-eliminate the ethyl groups, thus providing a synthetic route to dialkylgallane and the novel monoalkylgallane.

4.2. Synthesis and properties of mixed alkyl group compounds.

Bradley and co-workers have recently reported the synthesis of the compounds Me_2EtM and $Me_2EtM.NMe_3$ where M=Al or In [16]. These heteroleptic alkyls were prepared by reacting Me_2MCl with EtMgBr in diethylether, followed by the formation of adducts with diphos $(Ph_2PCH_2)_2$. The white crystalline solids produced were then heated to 353 K, whereupon colourless distillates of Me_2EtAl and Me_2EtIn formed. Variable temperature ^1H NMR spectra for both compounds revealed that rapid alkyl group exchange occurs and for Me_2EtIn this ligand exchange was so facile that it could not be frozen out at 193 K. Re-distillation of this compound resulted initially in the formation of crystalline Me_3In, which is in agreement with the proposed disproportionation reaction in solution:

$$3Me_2EtIn \rightarrow 3/2\ Me_3In + 3/2\ MeEt_2In \rightarrow Me_3In + Et_3In \qquad (4.1)$$

It was the opinion of these workers [16] that the compounds formulated as Me_2EtAl and Me_2EtIn are not suitable precursors for MOVPE / MBE of III-V materials as the alkyl groups are too labile.

Barron and Cleaver [17] have prepared hybrid organometallic compounds of gallium like $^tBu_2MeGa$ and $^tBuMe_2Ga$ by the reaction of alkylating agents methyl lithium with a halogenated organogallium compounds in hexane. These compounds are colourless pyrophoric liquids, which show little tendency to disproportionate in solution. A mass spectrometry study of these compounds revealed strong evidence to suggest they exist as monomeric three-coordinated gallium compounds. These workers are currently investigating the potential of these hybrid organogallium compounds for the MOVPE of GaAs films [18].

Agnello and Ghandhi have studied the room temperature gas phase exchange reaction between TMGa and TEIn [19]. The experiments were carried out in a conventional low pressure MOVPE reactor and the reaction was monitored using mass spectrometry. From this work Agnello *et al.* conclude that TMGa and TMIn not only form an adduct compound, but some alkyl group exchange occurs also. The evidence for exchange comes from the observation of Me-In and Et-Ga peaks due to Me_2In^+ and Et_2Ga^+, coupled with a reduction in the Me-Ga and Et-In peaks. Signals attributed to $EtMe_2Ga^+$, $MeEt_2Ga^+$ and $EtMe_2In^+$ species were also recorded. A dynamic structure was proposed for TMGa-TEIn addition compound based on the data recorded: $Et_2In(\mu Me)(\mu Et)GaMe_2$. Repeated formation and dissociation of this structure could eventually lead to the formation of TMIn and TEGa.

A similar experiment was used to study a mixture of TEGa and TMAl using H_2 as a carrier gas by Mashita *et al.* [20]. New species were found in this system as a consequence of alkyl group exchange; these were clearly indentified as Me_2EtGa and $MeEt_2Ga$. These workers postulated that carbon incorporation would increase as a result of using mixed alkyl precursors, as the ethyl groups are easily lost at high temperatures leaving MeGa on the surface.

Early studies of the pyrolysis of R_3M (R=Me, Et, M=Al, Ga, In) were dominated by the identification of hydrocarbon products and the determination of

kinetic parameters for the disappearance of starting materials. For example, for the widely-used Ga precursor triethylgallium, Et_3Ga, extensive analysis of the hydrocarbons produced (largely ethene, ethane and butane) by pyrolysis between 450 and 750 K have been carried out, [21,22,23] and Paputa and Price have determined the activation energy for the process using a toluene carrier system [24]. Opinion seems to have been fairly evenly divided over the predominant mechanism, with argument for both a Ga-Et radical homolysis pathway and an intramolecular β-elimination of ethene. Similar studies have been devoted to the alternative Ga source trimethylgallane, Me_3Ga: here of course the β- elimination route is not available, and the major reaction pathway undoubtedly involves Me radicals [25,26]. Radical species have recently been identified as the likely culprit in the contamination of Ga (and Al) by unwanted carbon reducing the usefulness of trimethylgallane as a Ga deposition precursor. On the other hand, the vapour pressure of trimethylgallane is considerably higher than that of triethylgallane, making it a more convenient source in high pressure processes. For these reasons, alluded to briefly in the previous section, there has been some interest in mixed alkyl species, hoping that they would combine the advantages of the greater volatility of the methyl compounds with the molecular decomposition route available for higher alkyl groups. More recently, experiments have been conducted under condition closely resembling those of Metal Organic Chemical Vapour Deposition (MOCVD) or Metal Organic Molecular Beam Epitaxy (MOMBE), with a shift in the focus of attention to the nature of the deposited material [27,28].

4.3. Experimental Details

Trimethylgallium and triethylgallium (high purity grade (99.99 %)) were generously donated by Epichem Ltd. These, and indeed all other compounds employed, notably trimethylamine alane, d_8-toluene, and sulphur hexafluoride, were purified by appropriate trap-to-trap distillation and repeated freeze-pump-thaw cycles. All materials were handled on a rigorously pre-conditioned pyrex vacuum line fitted with greaseless Youngs taps. Infrared spectra were recorded using a Digilab FTS40 FTIR spectrometer at 2 cm^{-1} resolution; all spectra were recorded (either as vapours or as liquid condensed on the windows) using a 10 cm long pyrex cell fitted with ZnSe windows. Although ZnSe does have a rather high cutoff at the low wavenumber end (ca. 500 cm^{-1}), for our laser pyrolysis work it has advantages not possessed by other materials (see chapter 2). ^1H NMR spectra were recorded at 300.15 MHz using a Bruker AM300 NMR spectrometer while mass spectra were recorded using a Kratos Concept 1H double focussing mass spectrometer (electron impact energy ~70 eV). Samples for NMR and mass spectroscopy were distilled directly from a modified laser pyrolysis cell (shown in Chapter 2) into sample tubes fitted with Youngs taps, and the d_8-toluene solvent was added by distillation. All NMR spectra were referenced to the residual CD_3-protonated solvent at δ_H 2.10 ppm.

All pyrolysis studies were carried using the method of IR LPHP [32,33]. This technique has been described in detailed in chapter 2, and thus only a brief description of the important features are provided here. Pyrolysis was carried out in a pyrex cylinder (length 10 cm, diameter 3.8 cm) fitted with ZnSe windows. The cell was filled with a few torr (1 torr = 133 N m^{-2}) of a mixture of the vapour under study and sulphur hexafluoride. The contents of the cell were then exposed to the output of a free-running CO_2 IR laser at power levels of a few Watts. The SF_6 strongly absorbs the laser radiation, which is then very rapidly converted to heat. This produce a strongly inhomogeneous temperature distribution in which the

centre of the cell may be heated as high 1500 K, but where the cell walls remains at room temperature. This technique has a number of advantages. The first of these is that pyrolysis is initiated directly in the gas phase, eliminating the complications frequently caused by competing heterogeneous reactions. The second is that primary products of the pyrolysis are rapidly ejected into cool regions of the cell, where they are not directly subjected to further reaction. In favourable cases, these products may be less volatile than the starting materials, and thus accumulated for further investigation. These advantages have already been amply demonstrated in the successful application of the IR LPHP technique to the study of a number of reactions of importance in MOCVD and MOMBE [34].

4.4. Exchange studies in mixtures of TMGa and TMAA.

4.4.1. Synthesis of Me_2GaH.

Dimethylgalliumhydride was prepared from reaction between trimethylgallium (TMGa) and trimethylaminealane (TMAA). Evidence from FT IR and NMR spectra of products showed that this procedure in accordance with the following equation.

$$Me_3Ga + AlH_3.NMe_3 \rightarrow Me_2GaH + AlX_3.NMe_3 \qquad X=H \text{ or } Me$$

Hence the reaction is analogous to that used for the synthesis of dimethylalane $[Me_2AlH]_n$ from lithium aluminium hydride and trimethylaluminium [35].

The procedure employed was as follows. TMAA was introduced into the sample tube at -196 °C, an excess of TMGa was condensed in the same tube and the reaction mixture was allowed to warm up to room temperature. The reaction vessel was allowed to stand for 15 minutes at room temperature before all the volatile materials were pumped through traps maintained at -40 °C and -196 °C. This led to collection of little material at -196 °C but yielded about 100 mg of a solid in the trap held at -40 °C. The unchanged trimethylgallium passed through the

trap at -40 °C to be retained by that at -196 °C. Typically, the fraction collected at -40 °C was a white waxy solid which melted at 3-5 °C, at this temperature a small quantity of other volatile materials were also condensed which were pumped out by warming the sample to room temperature leaving nearly pure dimethylgalliumhydride.

4.4.2. FTIR Spectra of TMAA:TMGa Mixtures.

Mixtures of TMAA and TMGa in the ratio 1:1 to 1:3 have been studied, at room temperature, by FTIR spectroscopy. Figure 4.1 shows spectra (500-2000 cm^1) for these two ratios. The region of the CH_3 stretches near 3000 cm^{-1} has been omitted as it was heavily overlapped by the vibration of the NMe_3 moiety and provided no additional information. Clearly, these mixtures contain species other than the two starting constituents: indeed, over the range of compositions studied, no trace of TMAA was observed, and absorption due to TMGa was only observed at ratios 1:3 (Al:Ga) and greater. The reactions leading to the formation of these new species were completed within the time scale of mixing and spectrum acquisition (1-2 min). These new species may readily be attributed to the products of gas phase exchange reactions between the two starting materials.

It is very evident from figure 4.1(A) and 4.1(B) that the composition of the mixture was strongly dependent on the initial component ratio. In the mixture rich in TMGa, figure 4.1(A), the most prominent infrared lines are readily attributed to free dimethylgallane, Me_2GaH: this species has recently been shown to exist in the gas phase as a mixture of a hydrogen-bridged trimer (with broad infrared absorption at 1700 cm^{-1}) and a dimer (stronger, narrow bands at 1290 and 1185 cm^{-1}) [36]. Other bands closely matching those of the trimethylamine adduct of TMAl, $Me_3Al.NMe_3$ [37], may also be discerned from the spectrum, although they are much weaker and overlapped in many places by the dimethylgallane features

Infrared spectra of a purified sample of Me_2GaH in the vapour phase have also been recorded. The results are illustrated in figure 4.2 and the band positions and their assignment are summarised in table 4.1. The instability and reactivity of dimethylgallane made it impossible in practice to eliminate all impurities. In spite of these impurities the spectra can be interpreted satisfactorily and most of the bands can be identified with fundamentals which approximate to internal motion of the Me_2Ga group [38,39]. The absorptions at 765 and 720 cm^{-1} correspond to $GaH_3.NMe_3$, reported by Green *et al.* [40], and the features near 2980, 2919 and 1396 cm^{-1} are ascribed to $Me_2GaH.NMe_3$ in light of the similar features found in IR spectra of dimethylgallium tetrahydroborate [39] and found by Grady *et al.* in mixture of TMAA and TEGa [41]. Impurities apart, the spectra gave no sign of significant absorption in the region 1800-2000 cm^{-1}, which is characteristic of the stretching vibrations of terminal Ga-H bonds [42]. On the other hand, the spectra of Me_2GaH vapour contains two prominant absorptions at 1288 and 1183 cm^{-1}. The most suitable interpretation is that these represent antisymmetric and symmetric stretching vibrations of a Ga-H-Ga bridge structure [43]. Such an assignment receives strong support from the IR spectrum reported by Downs and co-workers for dimethylgallane [36,44]. In addition, samples of dimethylgallane vapour show broad and very weak absorption at 1706 cm^{-1} which arises from a trimeric form of this species [36]. Hence, it appears that the dimer $[Me_2GaH]_2$ is the predominant species in the vapour phase under our experimental conditions.

4.4.3. ^1H NMR Spectrum of Me_2GaH.

The ^1H NMR spectrum of dimethylgallane in a solution of d_8-toluene was recorded at room temperature and the spectrum of the solution is depicted in figure 4.3. This shows two resonances; one at δ_H =3.06 is broad, whereas the other at δ_H = 0.01 is sharp. The positions and relative intensities leave no doubt that the broad resonance arises from protons attached to gallium and that the sharper

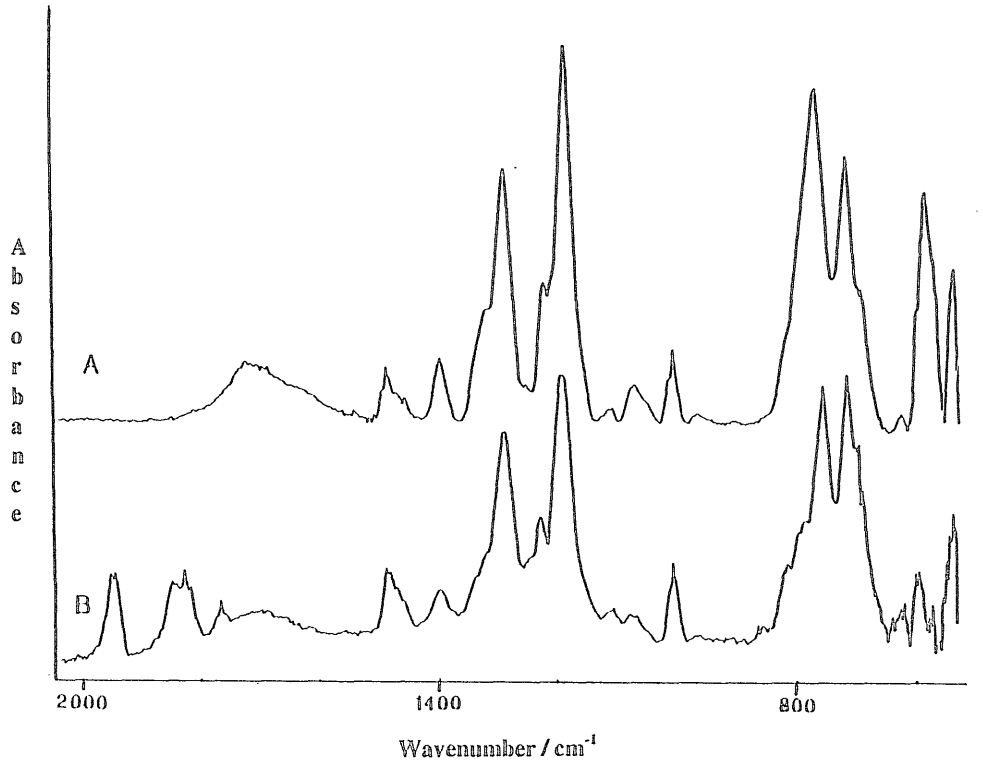

Figure 4.1: FTIR spectrum of mixture of TMAA and TMGa in the ratio 1:3 (A) and 1:1 (B).

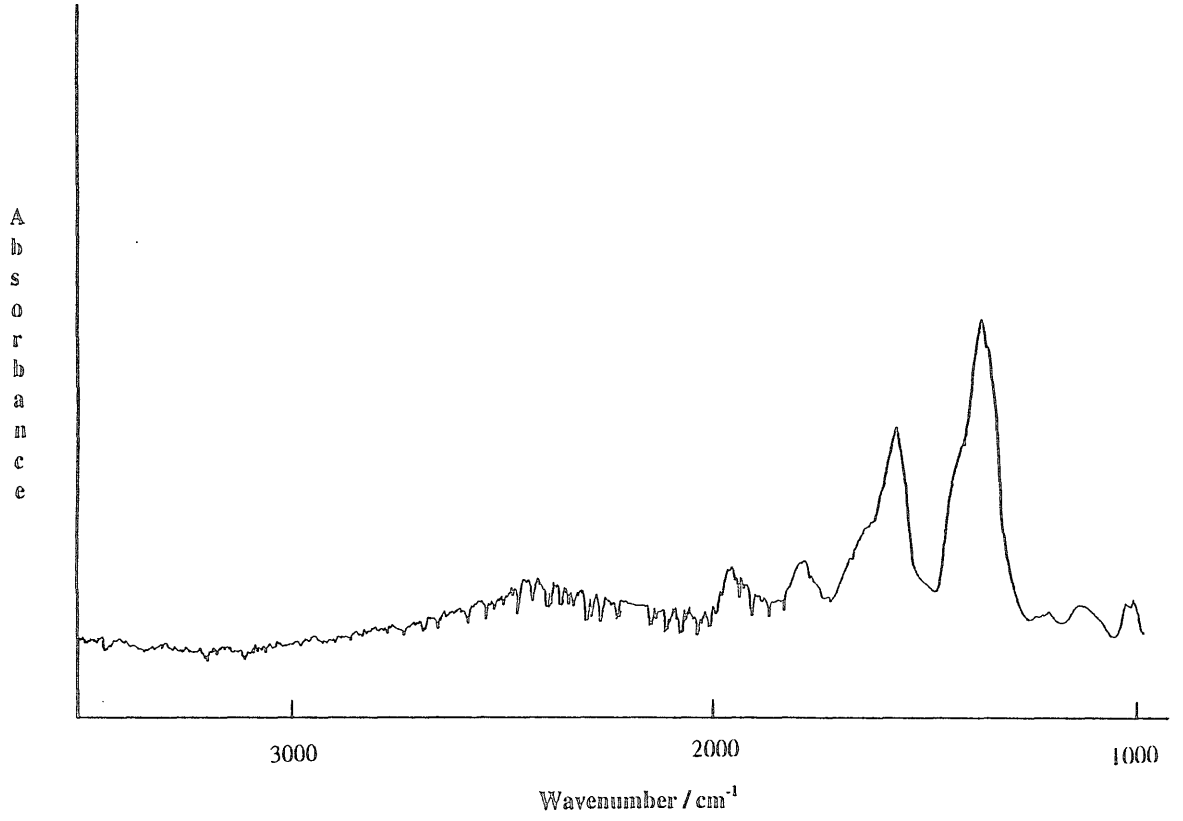

Figure 4.2: FTIR spectrum of DMGaH produced by mixture of TMAA and TMGa in the ratio 1:3

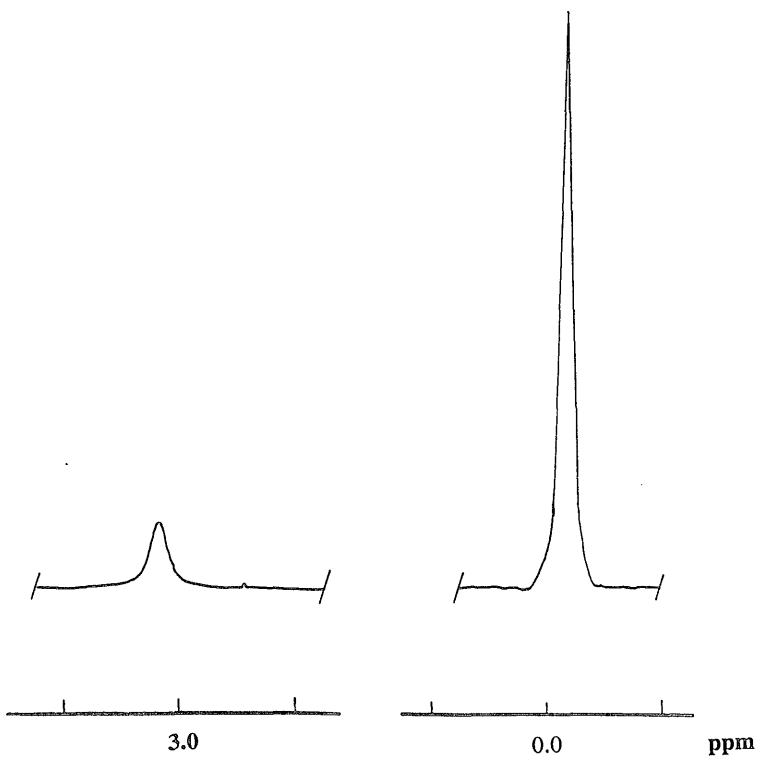

4.3. ^{1}H NMR spectrum of DMGaH in d_8-toluene solution.

resonance arises from a methyl proton [36]. Other peaks in the spectrum come from impurities *i.e.* unreacted materials. The instability and reactivity of dimethylgallane make it impossible in practice to eliminate all impurities.

The fact that the spectrum is so simple means that, if more than one species is present in solution, *e.g.* a mixture of $[Me_2GaH]_2$ and $[Me_2GaH]_3$, rapid exchange must be occurring between these species. It seems more likely, that the predominant species is dimethylgallane.

4.5. Synthesis of Diethylgalliumhydride by IR LPHP

IR LPHP experiments on a TEGa/SF_6 mixture were carried out at laser powers ranging from 1.35 to 1.50 W. Because of the inhomogeneous temperature profile, the precise temperature cannot be defined. However, a comparison with pyrolysis in systems with known kinetic parameters [45] suggest that these powers correspond to maximum temperatures in the range 500 to 750 K. The partial pressure of SF_6 in all cases was 10 torr, and the TEGa was condensed in the cell as required.

An FTIR spectrum obtained after exposure of 1.45 W of CO_2 laser radition (after removing all the volatile materials) is shown in figure 4.4. Exposure to laser radiation at powers as low 1.25 W resulted in change but at a much reduced rate; TEGa appeared to be thermally stable at powers below 1.25 W. Further exposure to laser radiation led to the gradual disappearance of TEGa and the production of significant quanties of viscous liquid product and ethene. The contents of the cell were rapidly condensed into a sample tube for further analysis at 77 K (-196 °C) and then pumping at 197 K in order to remove C_2H_4 and SF_6.

FT IR spectra of a mixture of TEGa and SF_6 before and after brief IR LPHP at 1.45 W are shown in figure 4.5 of reference [46]. The most prominent feature of the product spectrum is the appearance of a strong broad absorption near 1640 cm^{-1} together with sharp peaks readily ascribed to C_2H_4. Examination of the pyrolysis

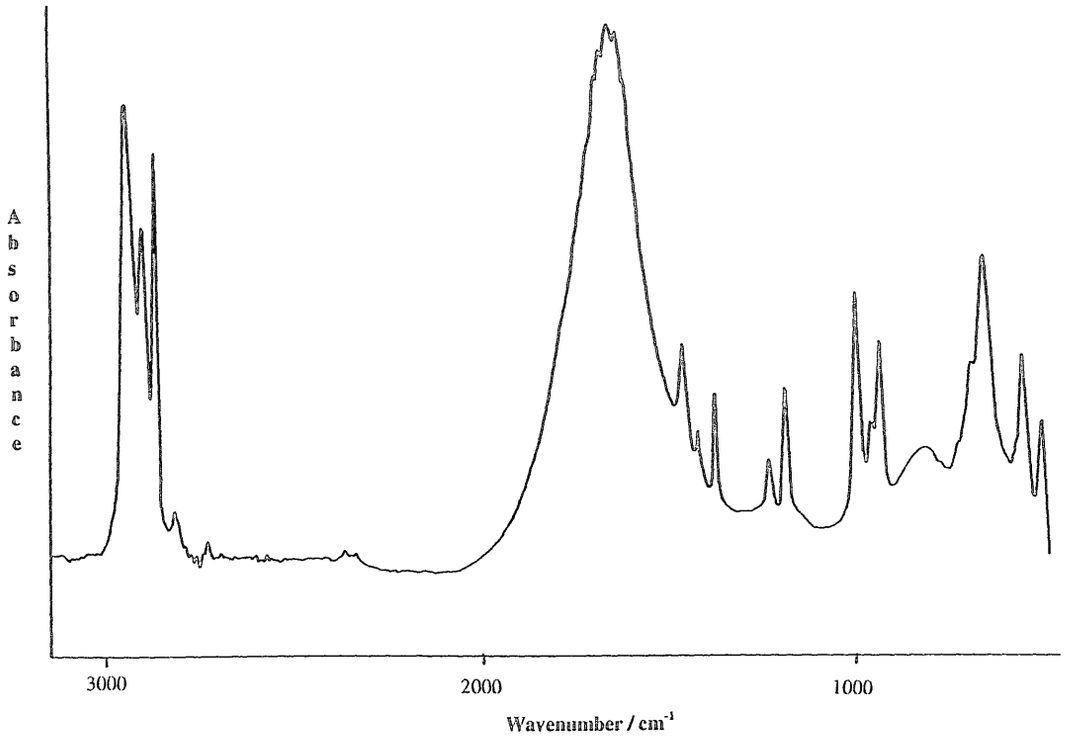

Figure 4.4: FTIR spectrum of DEGaH produced by IR LPHP of TEGa.

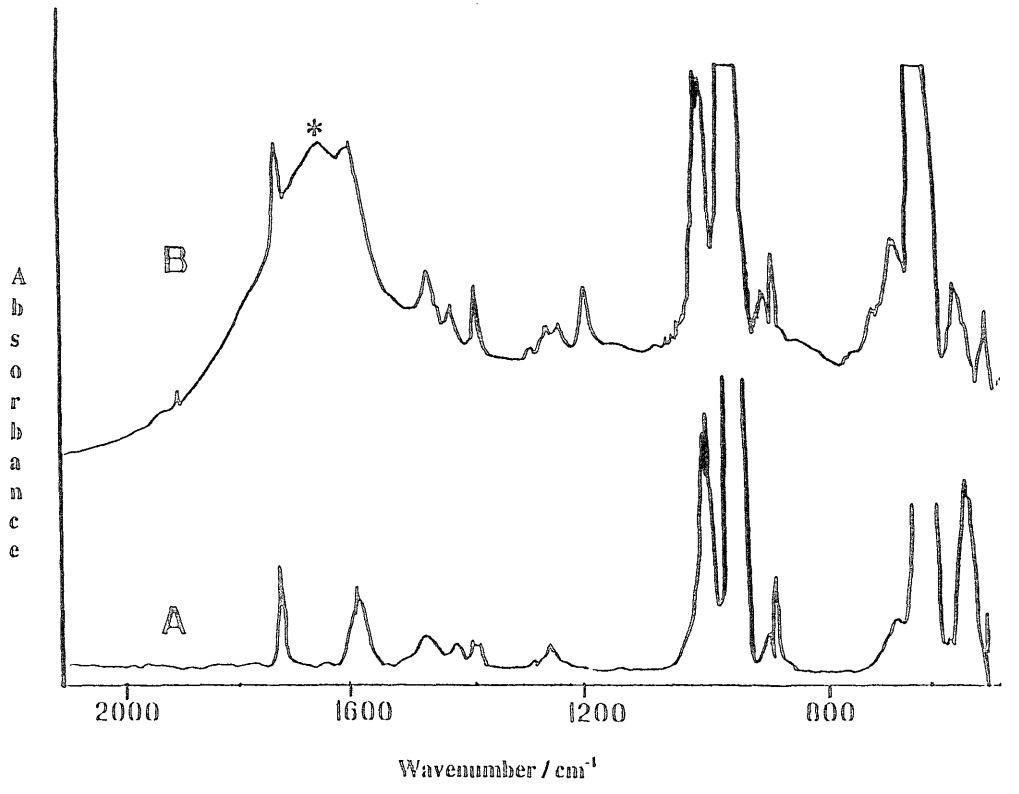

4.5. FTIR spectrum of a mixture of SF_6 and TEGa before (A) and after (B) irridiation at 2 W of laser power for 45 seconds. Feature assigned to Et_2GaH is indicated

cell revealed the presence of a liquid, and distillation from cell walls to window confirmed this liquid to be the origin of the broad absorption. The liquid product has a relatively low vapour pressure *i.e.* 0.5 torr at room temperature. The FTIR spectrum of this product, isolated by rapidly pumping away the volatile SF_6 and the C_2H_4 product is shown in figure 4.4, it is readly identified as that of diethylgallium hydride, DEGaH, in comparison with spectra of the similar DMGaH [36] and ^{i}BuGaH [47]. The broad absorption near 1640 cm^{-1} is very characteristic of a Ga-H-Ga bridging bond in a trimeric ring system. Very recently, Pulham *et al.* [48] have synthesised DEGaH by the reaction of Ga_2H_6 with C_2H_4 at high pressure and the IR spectrum reported by them is identical with that of figure 4.4.

In an earlier study of TEGa pyrolysis [29], the product contained a proportion of unreacted TEGa, with which Et_2GaH apparently undergoes rapid Et group exchange in solution at room temperature. Although this exchange is slowed sufficiently to permit resolution of the NMR spectra of individual components at low temperature, it does lead to some uncertainty in identification of species present. On the other hand, the pyrolysis products isolated have ^{1}H NMR spectra which showed a broad resonance at 3.07 at room temperature in d_8-toluene typical of Ga-H. This is in complete accord with that of Et_2GaH by Pulham *et al.* with no evidence of other organometallic species. Although it proved possible to produce a sample of pure Et_2GaH by means of IR LPHP, the product often contained a proportion of unreacted TEGa or further products and this complicates the interpretation of the NMR spectrum.

4.6: ^{1}H NMR Spectrum of Me_2GaH and Et_2GaH Mixture.

The ^{1}H NMR spectra of dimethylgalliumhydride and diethylgalliumhydride mixtures in a solution of d_8-toluene were recorded at room temperature and also at lower temperatures. At room temperature all hydride, methyl and ethyl resonances collapse into single feature (at δ_H 3.15 ppm) while at 203 K, at least five distinct

Ga-H environments are identifiable in varying proportions, as indicated by the complex group of broad absorptions between δ_H 2.70 and 3.00 ppm shown in figure 4.6(a). Ga-CH_3 resonances fall into two sets, a broad singlet at δ_H -0.17 ppm and a complex group at between δ_H 0.00 ppm and 0.25 ppm attributed to methylgallium hydrides (see figure 4.6(b)) and a complex overlapped cluster near δ_H 0.70 ppm arising from ethylgallium hydride. Also, some resonances in the spectra may be clearly identified with homoalkylated gallanes on comparison with those identified in $AlH_3.NMe_3$ mixtures with Me_3Ga [49].

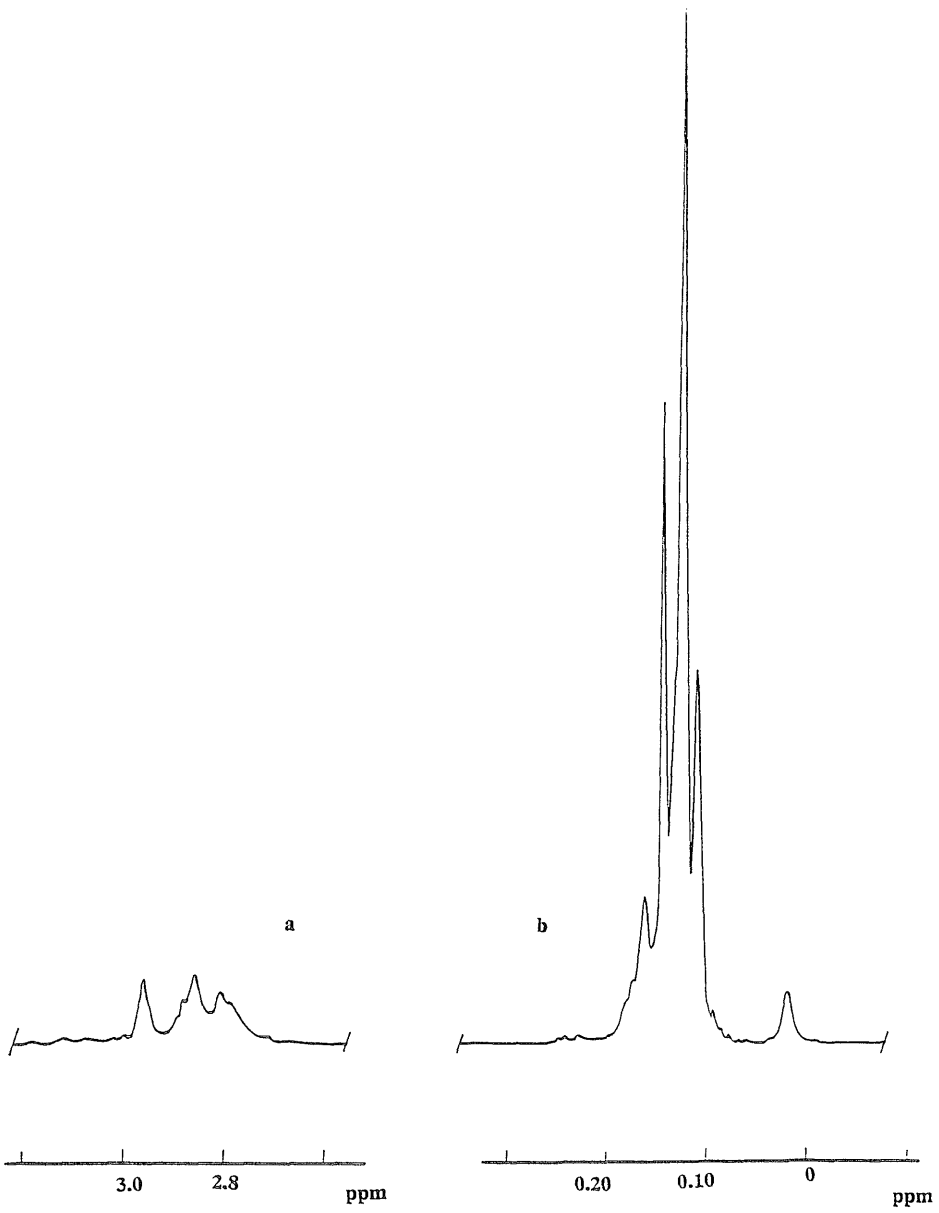

4.6. ^{1}H NMR spectrum of mixture of DMGaH and DEGaH at 203 K. Only the region of Ga-H (a) and Ga-CH_3 (b) resonances are shown.

Table 4.1

FTIR spectral data for Et_2GaH (cm^{-1})

Et_2GaH(liquid).	**Et_2GaH(solid)***	**Assignment.**
2942 (s)	2944(s)	$\nu_{as,s}(CH)$
2900(s)	2902(s)	$\nu_{as,s}(CH)$
2865(s)	2867(s)	$\nu_{as,s}(CH)$
2813(w)	2813(w)	Overtone
2728(w)	2730	Overtone
1642(vs,b)	1657(vs,b)	$\nu_{as}(GaH)$
1462(m)	1462(m)	$\delta_{as}(CH_3)$
1418((w)	1417(w)	$\delta(CH_2)$
1375(m,s)	1375(w)	$\delta_s(CH_3)$
1231(m)	1231(w)	$\omega(CH_2)$
1188(s)	1191(m)	$\omega(CH_2)$
997(s)	999(m)	$\rho(CH_3)$
950(w)	961(m)	$\nu(CC)$
937(m,s)	838(m)	$\nu(CC)$
810(w,br)		$\nu_s(GaH)$
697(sh)	698(m,sh)	$\rho(CH_2)$
660(s)	663(m)	$\rho(CH_2)$
	563(m)	$\nu_{as}(GaC_2)$
	513(m)	$\nu_s(GaC_2)$

s = strong m = medium, w = weak, v = very, br = broad, sh = shoulder.

* = from reference 46.

4.7. IR LPHP of TMGa+TEGa Mixtures.

Laser pyrolysis of an equimolar mixtures of Et_3Ga and Me_3Ga was carried out at a laser power of 2 W. This laser power, corresponding very approximately to a maximum temperature of 500 K, is sufficient to lead to β-elimination in Et_3Ga but not to bring about decomposition of Me_3Ga alone [45].

4.7.1. FT IR study of the Pyrolysis Products.

Figure 4.7 shows the FTIR spectrum of a mixture of TMGa (5 torr), TEGa (5 torr) and SF_6 (10 torr), both before (A) and after (B) extended exposure to 2 W of CO_2 laser radiation for 300 seconds. In the initial stage of pyrolysis, a viscous condensate formed on the cell walls and this was accompanied by a strong absorption at around 1650 cm^{-1} in the IR spectrum. This was identified from earlier work [31] as the asymmetric Ga-H-Ga stretch in dimethylgallane. Sharp features due to ethene were also observed at 2989, 1889 and 949 cm^{-1}. As the reaction proceeded further increases in the ethene signals were observed, and the diethylgallane features decreased to be replaced by new peaks at 1288 and 1182 cm^{-1}. These are assigned to the stable dimeric form of dimethylgallane, $Me_2Ga(\mu\text{-}H)_2GaMe_2$ [36]. At no stage during the reaction was any methane formed or gallium metal deposited. It did not prove possible to eliminate all of the Ga-bound ethyl groups in one single pyrolysis step; this was only achieved after a rapid pumping away of ethene and SF_6, followed by addition of fresh SF_6 and further pyrolysis, thus driving the system towards dimethylgallanes and monoalkylgallanes. Figure 4.8 shows the infrared spectrum of DMGaH in the vapour phase after pumping away all volatile materials, notably ethene and SF_6. Evidently, in this system β-elimination is reversible; this phenomenon is well known in the corresponding aluminium-based systems, and the ease of insertion of ethene into Ga-H bonds was demonstrated by Pulham *et al.* in their synthesis of Et_2GaH[48].

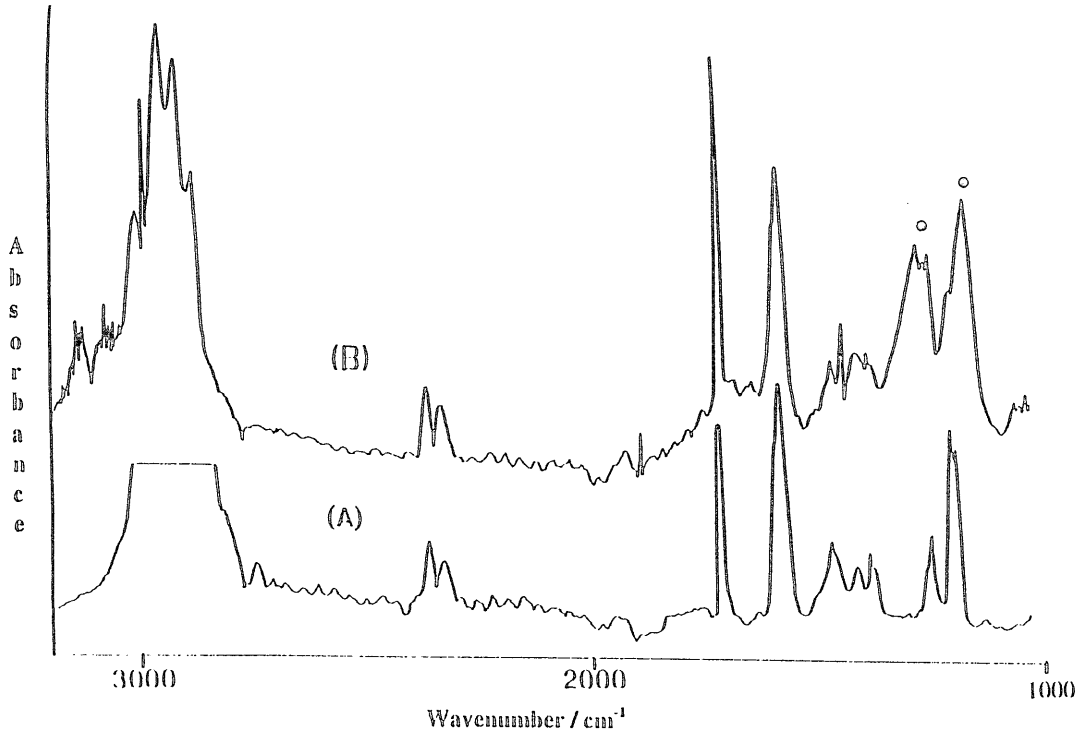

Figure 4.7: FTIR spectrum of the products of the IR LPHP of mixture of SF_6, TMGa and TEGa before (A) and after (B) exposure to 2 W of laser power for 300 s. Features assigned to Me_2GaH (©) are indicated.

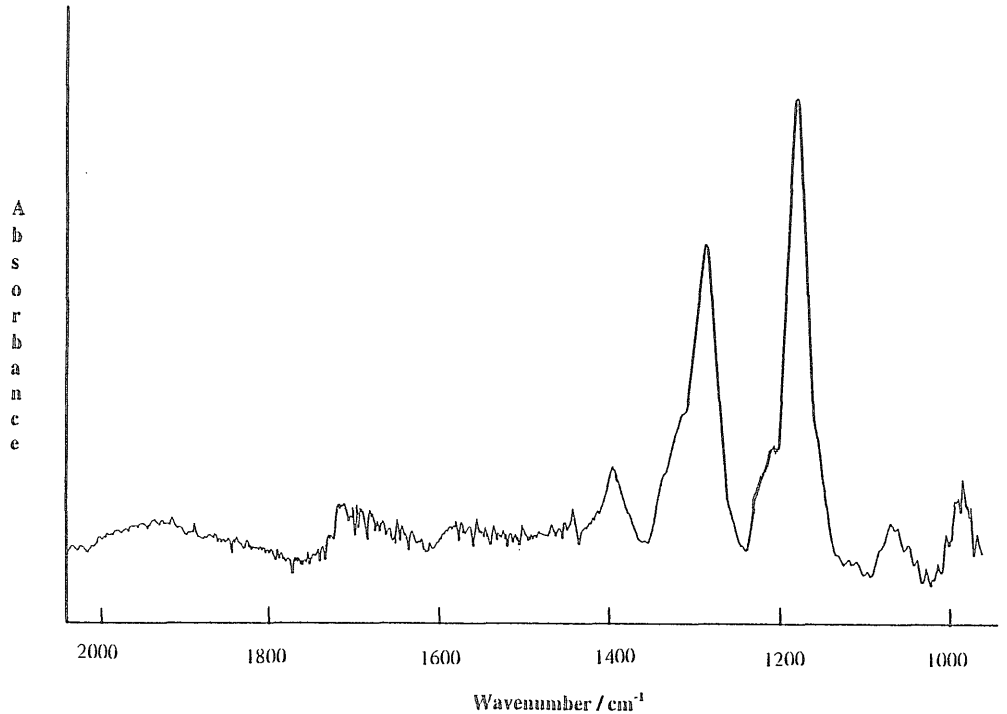

Figure 4.8: FTIR spectrum of the product of IR LPHP of TMGa and TEGa mixture

4.7.2. ^{1}H NMR Study

Following irradiation for approximately 45 minutes at 1.5 to 2.0 W of laser power, the reaction cell was cooled to 77 K and pumped to remove ethene and SF_6. The remaining contents of the cell were then rapidly condensed into an NMR tube at the same temperature.

The ^{1}H NMR spectrum of the pyrolysis cell was rather complex, as can be seen in figure 4.9(A) which shows the presence of at least five broad Ga-H peaks (between δ_H2.70 and 3.00 ppm) at 2.77, 2.79, 2.84, 2.86 and 2.95 ppm at 207 K. The methyl group resonances fall into two sets, a broad singlet at δ_H -0.17 ppm, similar to that observed for the pre-pyrolysis mixture and assigned to the trialkylgallanes, and a complex set between δ_H 0.00 ppm and δ_H 0.20 ppm attributed to methyl gallium hydrides, shown in figure 4.9(B). Similarly, the ethyl CH_2 resonance appears as an isolated quartet at δ_H 0.30 ppm arising from trialkylgallane, and a complex overlapped cluster near δ_H 0.70 ppm arising from ethyl gallium hydrides. The CH_3 substituent of the ethyl groups yields bands that are overlapped (δ_H 1.24-1.33 ppm). Simultaneous high power homonuclear decoupling of all hydride resonances resulted in a pronounced sharpening of the Ga-CH_3 and the ethyl CH_2 features, confirming the origin of these peaks and indicating a ^{3}J(H-Ga-C-H) coupling constant smaller than the line width (0.5 Hz). Examination of these patterns revealed at least ten methyl resonances and broad unresolved ethyl CH_2 peaks. The most intense of the methyl resonances corresponds to dimethylgallane [35] (δ_H 0.06 ppm) and can be matched to the strong isolated hydride peak at 2.95 ppm. The origin of the rest of the species relies on the fact that dialkylgallanes exist in solution as trimers or larger units, $R_{2n}Ga_nH_n$. Exchange of Me and Et group is very rapid, and due to the higher ratio of Me to Et groups, the dominant species will therefore be $Me_{2n}Ga_nH_n$, followed by $Me_{2n-1}EtGa_nH_n$ and $Me_{2n-2}Et_2Ga_nH_n$, with negligible contribution from more highly ethylated species. Figure 4.10 shows the resulting stereochemical consequence when n=3. The

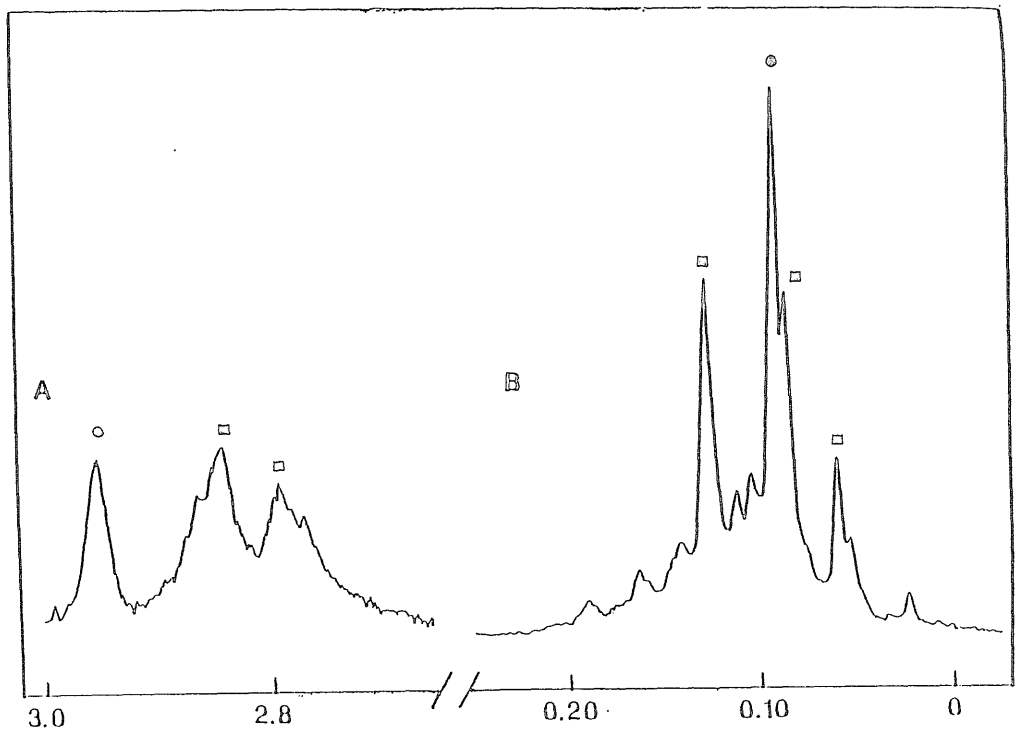

Figure 4.9. ^{1}H NMR spectrum of the pyrolysis products of the IR LPHP of TMGa and TEGa at 203 K. Only the region of Ga-H (A) and Ga-CH_3 (B) resonances are shown, with features arising from $Me_6Ga_3H_3$ (o) and $Me_5EtGa_3H_3$ (□) identified

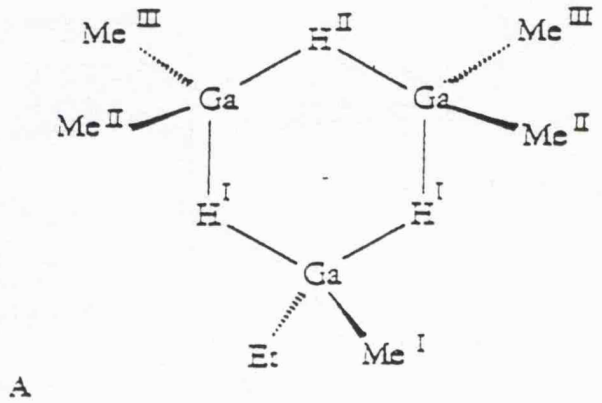

A

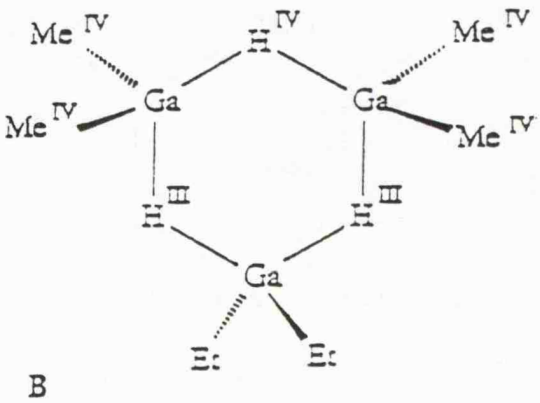

B

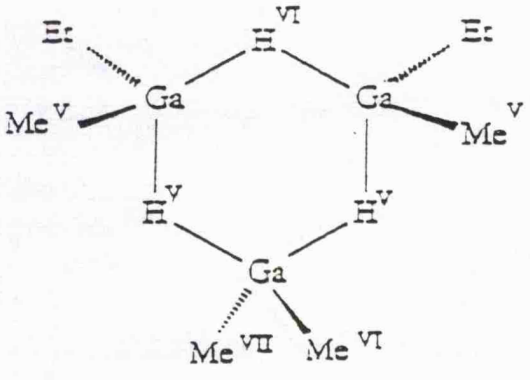

C

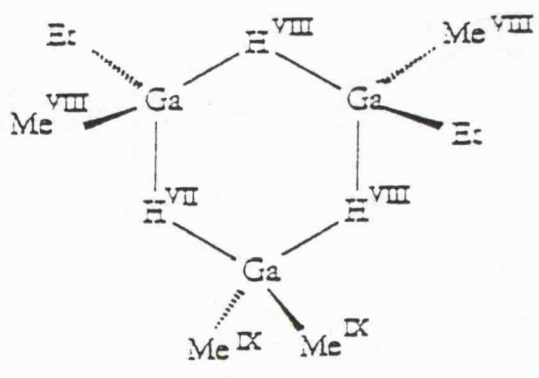

D

Figure 4.10. Ga-Me and Ga-H environments in $Me_5EtGa_3H_3$ (A) and $Me_4Et_2Ga_3H_3$ (B = gem diethyl, C = cis diethyl, and D = trans diethyl). The Ga_3-H_3 ring is assumed to be planer in each case.

dominant species (A) exhibits three Me resonances in the ratio 1:2:2 (1) in figure 4.10. The remaining weaker resonances arise from the disubstituted species B, C and D. Association into forms other than trimers would lead to different patterns being observed. Perhaps the most interesting aspect of the mixed system is the structural information revealed by the spectroscopic observations. From the NMR spectrum of pyrolysis products, it is very evident from figure 4.10 that several enironments are available to Ga-Me groups in the dialkylgallane mixture. The most intense peak, at 0.05 ppm, is easily assigned to $[Me_2GaH]_2$. The origin of the remainder becomes clear when we consider the nature of the dialkylgallanes in solution, where there is abundant evidence that species such as trimeric or higher units exit, but the dominant species is Me_2GaH.

At room temperature all hydride, methyl and ethyl resonances collapse into single features. Integration of this spectrum provided an estimate of relative Me:hydride:Et proportions of 5:1.5:1 in the products, suggesting a substantial loss of ethyl and/or hydride units at some stage (H_2, a sharp singlet at δ_H 4.50 ppm was observed in this spectrum, similar to that produced by the disproportionation of monoethylgallane in the work of triethylgallane [31]).

4.7.3. Mass Spectrum.

Mass spectra of organogallanes are known to be complex as is found to be the case here (see figure 4.11). This spectrum is dominated by peaks characteristic of methylgallane system, namely gallium atoms (m/z = 69 and 71), and Me_2Ga^+ (m/z = 99 and 71); [50] these features are not shown in in figure 4.11. Of more significance here are the two series of clusters which can be attributed to dimeric Ga_2 species (starting near m/z = 200) and trimeric species (starting near m/z = 300). These can be ascribed to ions arising from the two series $Me_{4-n}Et_nGa_2H_2$ (n = 0 - 4) and Me_{6-n} $Et_nGa_3H_3$ (n = 0 - 6). Each cluster contains peaks arising from the Ga_n units ($^{69}Ga_2$, ^{69}Ga $^{71}Ga_2$ and $^{71}Ga_2$ in the ratio 0.36:0.48:0.16; $^{71}Ga_3$, $^{69}Ga_2{}^{71}Ga$,

$^{69}Ga\ ^{71}Ga_2$, and $^{71}Ga_3$ in the ratio 0.22:0.43:0.29:0.06), and is dominated by the ions formed by loss of a proton. Thus, in the cluster near 200, the major peaks arise from $Me_4Ga_2H^+$ (m/z = 199, 201 and 203); the most abundant ion in the trimeric cluster near 300 is $Me_6Ga_3H_2^+$ (m/z = 299, 301, 303, and 305). Heavier clusters in each series arise from successive replacement of Me by Et; in these, the patterns are more complex, reflecting the well-known additional fragmentation pathways available to methyl-ethyl groups. Cluster below 200 or 300 arise from loss of alkyl groups. Significantly, there are no subtantial peaks ascribable to tetrameric or heavier oligomers (the strongest group, near m/z = 433, is less than 2% of that near 200). We conclude from this that the toluene solution contains significant amounts of dimer and trimers, but no higher oligomers. This contrasts with the finding of Baxter et al, [36] who showed conclusively that the vapour of Me_2GaH contains only dimers.

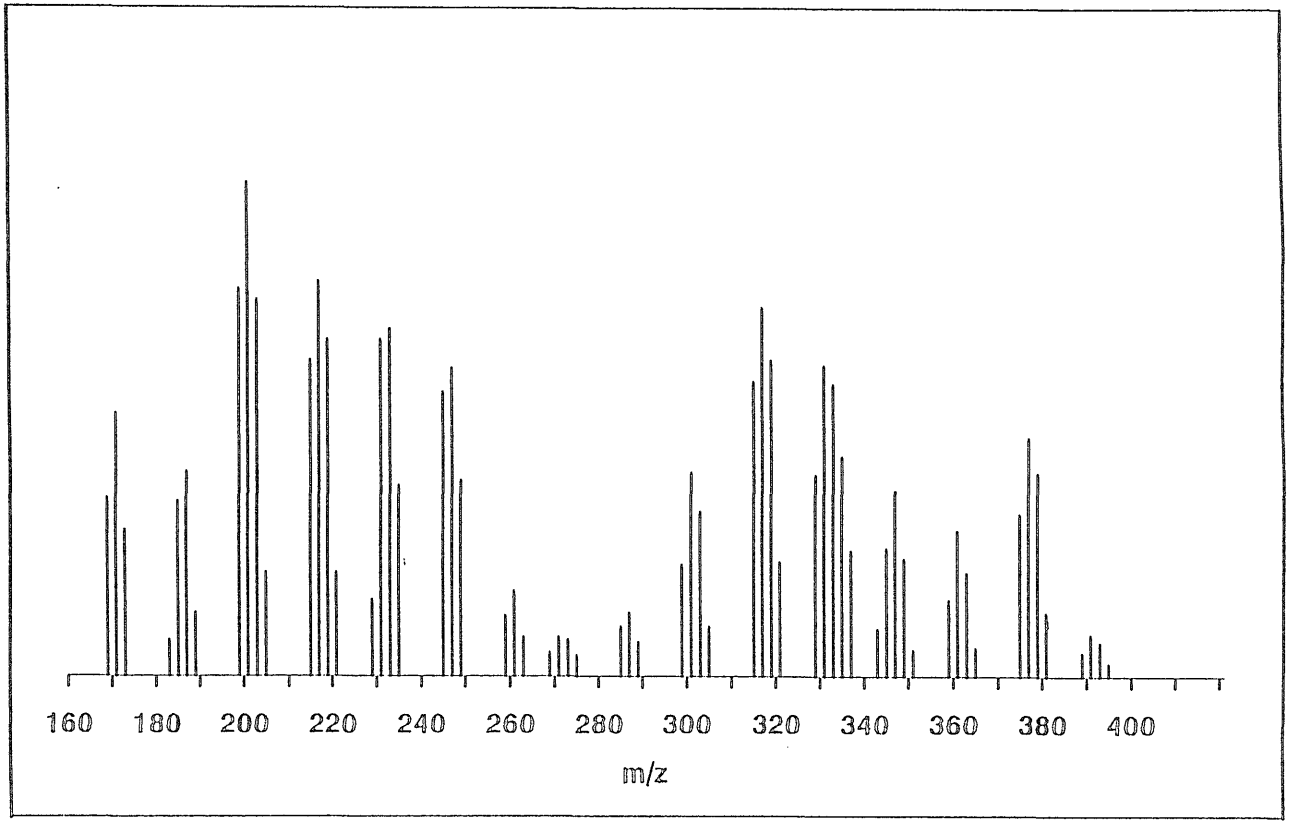

Figure 4.11. Mass spectrum (m/z from 160 to 400) of a solution in d_8-toluene of a mixture of Me_2GaH and Et_2GaH (Me:Et approximately 2:1).

Table 4.2.

Spectral data of Me_2GaH (cm^{-1})

[a][$Me_2GaH]_n$ (vapour)	[$Me_2GaH]_n$ ✱	[b][$Me_2GaH]_n$	Assignment
2982	2981		
2919	2921		ν(C-H)
2864			
1706	1705		ν(Ga-H_b)of[$MeGaH_b]_n$
1478			with n = ≥ 3
1396	1397		(CH) + ν_{sym}(Ga-C)
1288	1290	1288	ν(Ga-H_b)
	1223	1222	sym(CH_3)
1185	1185	1183	ν(Ga-H_b)
1110	1115		ν_{sym}(Ga-C)or ν_{sym}(Ga-C)
1071	1071		+ ν_{sym}(Ga-C)
1008			
	965		
	790		
765	769		$\rho(CH_3)$
720			
	590		
	538		

H_b= Bridging H atom, ✱= From reference [36]

a = IR spectral data of DMGaH synthesis from TMGa and TMAA mixture.

b = IR spectral data of DMGaH after eliminating all the volatile materials

synthesis from pyrolysis of TEGa and TMGa mixture.

4.8. **Discussion and Conclusion.**

The FTIR and NMR observations show clearly that exchange of Me groups with Et or NH_3 occurs rapidly in the gas phase, whereas exchange of Me groups with ^{i}Bu (or ^{t}Bu) [17] does not occur. The most likely gas phase mechanism for exchange is metathesis via transient bridge dimers or higher oligomers, for example

$$R_3\,Ga + R'_3\,Ga \leftrightarrow R_2\,Ga\{\mu R\}\{\mu R'\}GaR_2 \leftrightarrow R_2\,R'\,Ga + R'_2\,RGa \quad (4.2)$$

Exchange is only thought to be favourable for alkyl groups which have a tendency towards bridge formation, which in turn is directly related to size in that the exchange rate is in the order Me>Et>^{i}Pr>^{i}Bu>^{t}Bu, and also due to the fact that the corresponding trialkylalanes dimerize; it is therefore expected that trialkylgallane will undergo exchange reactions.

The IR LPHP studies of TMGa+TEGa mixtures are very revealing, both in their own right and in the additional light they shed on the TEGa system. The first conclusion is that at moderate temperatures the products observed are consistent with the almost complete removal of Ga-bound ethyl groups and retention of methyl groups. This confirms the contention that β-elimination is strongly preferred to Ga-R bond homolysis. The products identified are entirely consistent with exchange of alkyl groups, coupled with the loss of Ga-Et groups via β-hydride elimination, the overall chemistry is summarised in figure 4.12. The laser pyrolysis of TMGa+TEGa has provided a novel route to the production of dialkylgallanes [49], in particular dimethylgallane in previous work [36]. These workers reduced trimethylgallane using sodium tetrahydridogallate, which is itself prepared from gallium(III) chloride and sodium hydride in diethylether at room temperature, to produce dimethylgallane. This was shown to be dimeric in the vapour phase from spectroscopic evidence, and is consistent with our observations.

The TEGa+TMGa mixture study presented does, however, cast doubt on the viability of mixed alkyl group systems as precursors for MOVPE, since the change in constitution as the reaction proceeds is likely to result not only in a non-

uniform layer thickness, but also a graduation in carbon content. These factors are additional to any preferential volatilisation of lighter components. However, growth studies using mixtures of TMGa and TEGa have yet to be carried out. It is important that the differences in conditions between the gas phase homogeneous pyrolysis of TEGa and TMGa mixtures described in this chapter and those in an MOVPE growth reactor are taken into account, as surface reactions play a significant role in the latter system with the possible consequence that the β-hydride elimination mechanism may be less predominant.

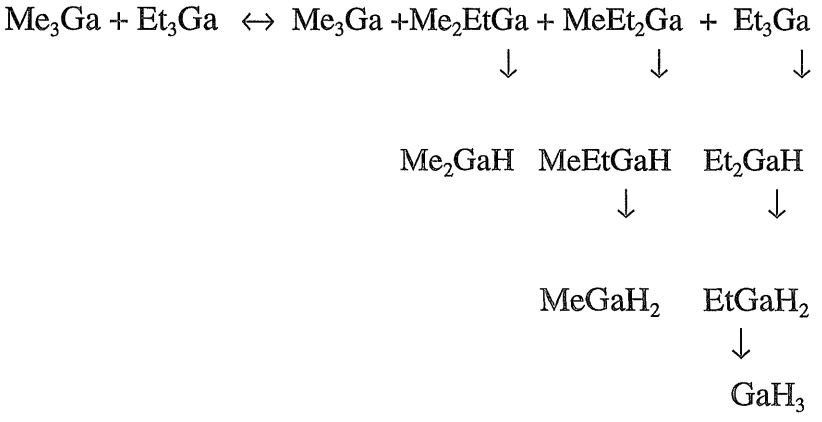

Figure 4.12: Reaction scheme to show the production of the observed products in the pyrolysis mixture of TEGa and TMGa.

References.

[1]. G.B.Stringfellow, Organometallic Vapour-Phase Epitaxy: Theory and Practice, Acadmic Press, Sandiego, 1989.

[2]. S.J.Moss and A. Ledwith Eds. The Chemistry of the Semiconductor Industry, Blackie, Glasgow, 1987.

[3] A.C.Jones, J.S.Roberts, P.J.Wright, P.E.Oliver and B. Cockayne, Chemtronics, 1988, 3, 152.

[4]. J.Knauf, D. Schmitz, G.Strauch, H.Jurgensen, M.Heyen and A.Melas, J. Cryst. Growth, 1988, 93, 34.

[5]. K.L.Fry, C.P.Kuo, C.A.Larsen, R.M.Cohen, G.B.Stringfellow and A.Melas, J. Electron. Mater., 1986, 15,91.

[6]. A.C.Jones, P.R.Jacobs, S.A.Rushworth, J.S.Roberts, C.Button, P.J.Wright, P.E.Oliver and B.Cockayne, J. Cryst. Growth, 1989, 96, 768.

[7]. W.L.Smith and T.Wartik, J. Inorg. Chem., 1967, 29,629.

[8]. T.F.Kuech, E. Veuhoff, T.S.Kuan, V.Deline and R.Potemski, J. Cryst. Growth,. 1986, 77,257.

[9]. N.Kobayashi and T. Makimoto, Jap. J. Appl. Phys., 1985, 24, 1824.

[10]. N.N.Korneev, N.N.Govorev, E.P.Besuch, I.V.Shevnenko and N.G.Gudkova, Zh. Obs. Khim., 1985, 55,1762.

[11]. H. O.Pierson, Thin Solid Films, 1977, 45, 257.

[12] A.C.Jones, S.A.Rushworth, J.S.Roberts, C.C.Button and J.P.R.David Chemtronics, 1989, 4, 235.

[13]. W.L.Gladfelter, D.C.Boyd and K.F.Jensen, Chemistry of Materials, 1989,1, 339.

[14]. J.P.Oliver, Adv. Organomet. Chem., 1977,15,235.

[15]. M.Mashita, S.Horiguchi, M. Kamon, M.Mihara and M.Ishii, J. Cryst. Growth, 1986, 77, 194.

[16]. D.C.Bradley, H.Chudzynska and D.M.Frigo, Chemtronics,1988, 3, 159.

[17]. W.M.Cleaver, A.R.Barron, Chemtronics, 1989, 4, 146.

[18]. W.M.Cleaver, A.R.Barron, Y.Zhang and M.Stuke, Appl. Surf. Sci., 1992, 54, 8.

[19]. P.D.Agnello and S.K.Ghandhi, J. Cryst. Growth, 1989, 94, 311.

[20]. M.Mashita, S.Hoiguchi, M.Shimazu, K.Kamon, M.Mihara and M.Ishii, J. Cryst. Growth, 1986, 77,194.

[21]. G.G. Petukhov, N.N.Shabanova, V.I.Shcherbakov, and L.A.Faminskaya, Tr. Khim, Tekhnol., 1973, 2, 115.

[22]. N.N.Travkin, B.G.Gribov, V.P.Rumyantseva, I.G.Tonoyan, and E.N.Zorina, Zh. Obshch. Khim., 1975, 45,316.

[23]. M.Yoshida, H.Watanabe, and F.Uesugi, J. Electrochem. Soc., 1985, 132, 667.

[24] M.C.Paputa and S.W.G.Price, Can. J. Chem., 1979, 57,3178.

[25]. M.G.Jacko and S.W.G.Price, Can, J. Chem., 1963, 41, 1560.

[26]. J.E.Butler, N.Bottka, R.S.Sillmon, and D.K.Gaskill, J. Cryst. Growth, 1986, 77, 163.

[27]. M. Mashita, S.Horihuchi, M.Shimazu, K.Kamon, M.Mihara, and M.Ishii, J. Cryst, Growth, 1986,77,194.

[28] J. O . Williams, R.Hoare, N.Hunt, and M.J.Parrot, Nato ASI. Ser. B, 1989, 198, 131.

[29] A.S.Grady, A.LMapplebeck, D.K.Russell, and M.G.Taylorson, J. Chem., Soc., Chem. Commun., 1990, 929.

[30] A.S.Grady, R.D.Markwell, D.K.Russell, J. Chem. Soc., Chem. Commun., 1991, 14.

[31]. A.S.Grady, PhD Thesis, Leicester University 1991.

[32]. G.A.Atiya, A.S.Grady, S.A.Jackson, N.Parker, and D.K.Russell, J.Organomet Chem., 1989, 378, 307.

[33]. D.K.Russell, Chem. Soc. Rev., 1990, 19, 407.

[34]. D.K.Russell, Coord. Chem. Rev., 1992, 112, 131.

[35]. J.R.Surtes, Aust. J. Chem, 1965, 18, 14.

[36]. P.L.Baxter, A.J.Down, M.J.Good, D.W.H.Rankin and H.E.Robertson, J. Chem Soc., Chem. Commun.,1986, 805; J. Chem.Soc., Dalton Trans., 1990, 2873.

[37]. R.D.Markwell and D.K.Russell unpublished results.

[38]. R.S.Tobias, M.J.Sprague, and G.E.Gass, Inorg. Chem., 1968, 7, 1714.

[39]. A.J.Downs and P.D.P.Thamas, J. Chem. Soc., Dalton Trans., 1978, 809.

[40]. N.N.Greenwood, A. Storr and M.G.H. Wallbridge, Inorganic Chemistry, 1963, 2, 1036.

[41]. A.S.Grady, R.D.Markwell, D.K.Russell and A.C.Jones, J. Cryst. Growth, 1991, 110,739.

[42]. P.L.Baxter, A.J.Downs and D.W.H.Rankin, J. Chem. Soc Dalton Trans 1984, 1755., b). P.L.Baxter, A.J.Downs, D.W.H.Rankin, and H.E.Robertson, ibid., 1985, 807.

[43]. S.F.A.Kettle, D.B.Powell and N.Sheppard, J. Chem., Chem Commun., 1979, 18; J.S.Anderson and J.S.Ogden, J.Chem Phys., 1969, 51, 4193.

[44]. A.J.Downs, M.J.Goode, and C.R.Pulham, J. Am. Chem. Soc 1989,111, 1936.

[45]. G.A.Atiya, D.A.Pape, and D.K.Russell, unpublished results; G.A.Atiya, Ph.D. Thesis, Leicester University.

[46]. A.S.Grady, A.L.Mapplebeck, D.K.Russell, and M.G.Taylorson, J. Chem, Soc., Chem, Commun., 1990, 929.

[47]. V.V.Marakova, V.A.Kormer and A.A.Petrov, J. Gen. Chem. USSR (Eng Transl), 37 (1967) 1662.

[48]. C.R.Pulham, A.J.Downs, M.J.Goode, D.W.H.Rankin, and H.E.Robertson, J. Am. Chem. Soc., 1991, 113, 5149.

[49]. A.S.Grady, R,D.Markwell, D.K.Russell, and A.C.Jones, J. Cryst. Growth, 1990, 106, 239

[50]. M.Yoshida, H.Watanabe, and F.Vesugi, J. Electrochem. Soc., 1985, 132, 677.

Chapter 5

5.1: Introduction:

The structure and reactivity of alkene-transition metal complexes is of considerable interest in view of their likely role in the heterogeneous catalysis of hydrocarbon transformation [1]. In addition, the unusual η-bonding in polyene complexes has prompted many experimental and theoretical investigations of their structure (see for example reference [2] and references therein).

Many investigations have been carried out on the vibrational spectra of (hydrocarbon)$M(CO)_n$ systems, where the hydrocarbon fragment is η-bonded to a transition metal. Such compounds are, almost without exception, coloured and therefore most of the work has been concerned with mid -infrared data. Several systems have now been examined, e.g. (cyclooctatetraene)$Fe(CO)_3$ [3], (cyclopentadienyl)$Mn(CO)_3$ [4], (cyclopentadienyl)$V(CO)_4$, (mesitylene)$Cr(CO)_3$ and (mesitylene)$Mo(CO)_3$ [5,6] in the CO stretching frequency region. Where other assignments have been made there is disagreement on the normal modes assignments.

All the above complexes involve a cyclic hydrocarbon but very many non-cyclic alkenes (conjugated and non-conjugated) can also form η-bonded complexes with transition metal carbonyl systems. Among the simplest of these is 1,3-butadiene, and perhaps the earliest compound of this class to be characterized was η^4-buta-1,3-diene iron tricarbonyl (BdFe$(CO)_3$), $C_4H_6Fe(CO)_3$, first prepared by Reihlen *et al.*[7] in 1930. The η^4-bonded structure proposed by Hallam and Pauson [8] has been abundantly confirmed both by X-ray investigations of the crystal and by gas-phase electron diffraction. The crystal structure [9] clearly shows that the

butadiene fragment is cis, planar and situated almost parallel to the plane defined by the three carbonyls. The iron atom is approximately equidistant from the four butadiene carbon atoms, and all the C-C distances are equal within experimental error.

Hallam and Pauson [8] reported C-O stretching frequencies of liquid $BdFe(CO)_3$ (from the IR spectrum) of 2051 cm^{-1} and 1978 cm^{-1}, and a band (assigned as the C=C stretch) at 1464 cm^{-1}. Reckziegel and Bigorgne [10], on the other hand, resolved three C-O stretches for $BdFe(CO)_3$ in an alkane solvent indicating an effective symmetry of C_S for the $Fe(CO)_3$ fragment. Subsequently, a more detailed investigation of the IR spectrum was carried out by Grogan and Nakamoto [11], but assignments were proposed for the C_4H_6 vibrations only. Recently, rotationally-resolved infrared absorption spectra of jet-cooled butadiene iron tricarbonyl in the C-O stretching region near 2000 cm^{-1} have been obtained and assigned by Gang *et al.* [2] using a diode laser and confirm the effective symmetry of the $Fe(CO)_3$ unit in the molecule.

IR and Raman data are available for a closely analogous system, (cyclooctatetraene)$Fe(CO)_3$, in which the cyclic polyene is acting as a conjugated (1,3)-diene towards the $Fe(CO)_3$ [3]. However, the complexity of the spectrum due to the C_8H_8 made a detailed assignment of the observed frequencies difficult. In view of the above discussion concerning the bonding in $BdFe(CO)_3$ [12], a study of its complete vibrational spectrum, with a view to obtaining as complete an assignment as possible, would be a worthwhile exercise.

Tricarbonyl cyclopentadienylmanganese (η^5-$C_5H_5Mn(CO)_3$), $CpMn(CO)_3$ and its methyl derivative η^5-$MeC_5H_5Mn(CO)_3$, $MeCpMn(CO)_3$ serve as archetypal η^5-bonded compounds. Indeed, cyclopentadienylmanganese tricarbonyl is the earliest known and best characterised η-bonded system [13]. Both compounds are thermally stable, relatively volatile, low melting point solids and liquids respectively. The physical properties and chemistry of these compounds have been extensively investigated [14] with major emphasis on the bonding and reactions of the cyclopentadienyl ring system. Tricarbonyl(η-cyclopentadienyl)manganese, $CpMn(CO)_3$ (Cp =η^5- C_5H_5) and its methyl derivative has been fully characterised by numerous physical techniques including vibrational (IR and Raman) spectroscopy [15], microwave spectroscopy [16] as well as by X-ray diffraction [17], molecular orbital and photoelectron studies. However no far-infrared spectra of these compounds in the vapour phase have been reported.

Cotton *et al.* [6] have studied the infrared absorption spectra of metal carbonyls $CpMn(CO)_3$ in the C-O stretching region (1700-2200 cm^1), but do not report the complete spectrum. Fischer has also studied this compound in the CO stretching region [18]. In a general study of metal carbonyls substituted by an aromatic group, Fritz and Paulus [19] contend that within a homologous series, e.g cyclopentadienyl M-carbonyl (where M=Mn, Tc, Re), the sum of the MC and CO bonds orders should be constant and hence so should the sum of the corresponding frequencies for $CpMn(CO)_3$.

Extensive vibrational spectra of these compounds should provide useful information on both the normal modes of the $Mn(CO)_n$ group and the ring

frequencies for η-bonded cyclopentadienyl compounds. Ring fundamentals should fall between 3000 and 700 cm^{-1}, apart from the out of plane ring deformation which is expected near 500 cm^{-1}. The $Mn(CO)_3$ fundamentals should, in the main, lie below 700 cm^{-1} and because the CO stretching frequencies will be near 2000 cm^{-1}, they will not be strongly coupled to other modes in the molecule. The modes pertaining to the vibration of the ring against the $Mn(CO)_3$ group are also expected below 700 cm^{-1}. Consequently, for more complete comparison of these compounds, we have examined their far-infrared spectra in the vapour phase.

5.2: Experimental

Commercial samples of 1,3-butadiene irontricarbonyl were used in this work and were purchased from Aldrich Chemical Company Ltd. Purification by repeated trap-to-trap distillation was always employed before each experiment. ^1H NMR spectroscopy at 300 MHz of the purified sample revealed no significant impurities.

Samples of cyclopentadienylmanganese tricarbonyl and methylcyclo-pentadienylmanganese tricarbonyl were also purchased from Aldrich and purified by vacuum distillation. Because of the very low vapour pressures of these two compounds at room temperature, the samples were heated in some experiments in a cell specially constructed for low vapour pressure compounds (see Chapter 2 for details).

The far-infrared spectra of all the above compounds were examined down to wavenumbers as low as 10 cm^{-1}. Vapour phase IR spectra were recorded with a Digilab FTS 40V Fourier-transform spectrometer, normally at 2 cm^1 resolution.

5.3 Results and Discussion.

5.3.1 Butadiene irontricarbonyl

Figures 5.1 and 5.2 show mid-infrared and far-infrared spectra of butadiene irontricarbonyl, while table 5.1 shows possible band assignments.

The vibrational spectrum of 1,3-butadiene has been extensively studied [21,22] and the work has shown that the molecule exists almost exclusively in the trans form. However, when butadiene is complexed to $Fe(CO)_3$ it is known to be in the cis configuration [9]. In addition, it has been assumed in previous work that the frequency order observed for the modes of free (trans) butadiene also holds for the $BdFe(CO)_3$ complex. A calculation of the expected normal vibrational frequencies of the trans- and cis-isomers has been performed by Sverdlov and Tarasova [23], and this has been of considerable help in the assignment made in this work. There have been previous investigations of C_4H_6 vibrations in $BdFe(CO)_3$ in the far-infrared in both a crystalline sample and in solution [11]. A complete assignment of the observed frequencies was proposed by those workers on the basis of the IR spectrum alone, but no discussion was given. As the infrared data in the vapour phase reported here are new, it seems worthwhile to discuss the assignment of the butadiene frequencies including those in the mid-IR.

The overall symmetry of $BdFe(CO)_3$, is presumably C_S, which has also been assumed in the solution phase spectrum of $BdFe(CO)_3$ [24]. Our assignment will begin with C_4H_6 vibrations, followed by consideration of other vibrations including skeletal modes in particular.

By analogy with free butadiene [11] and calculations for the cis-isomer [23], the region 700-1100 cm^{-1} may contain the following modes; CH_2 (in-plane) rock, CH_2 (out-of-plane) twist and CH_2 (out-of-plane) wag. From the limited amount of data available from analogous molecules, the most likely assignment for the observed frequencies in the vapour phase spectra of $BDFe(CO)_3$ are as follows; 1048 cm^{-1} (A'' CH_2 twist), 977 cm^{-1} (A'' CH_2 rock), 953 cm^{-1} (A' CH_2 twist), 925 cm^{-1} (A' CH_2 rock), 899 cm^{-1} (A'' CH_2 wag), 790 cm^{-1} (A'' CH wag). The band observed at 415 cm^{-1} in the far-infrared probably corresponds to an out of plane C-C=C bending (A'') mode by analogy with Sverdlov and Tarasova's calculation for cis-butadiene [23] and the assignment of Davidson for the $BdFe(CO)_3$ spectrum in the solution phase [24]. Some of the wavenumbers of these modes differ slightly from those of Davidson [24] and Grogan and Nakamoto [11] presumably due to the fact that our work is in the vapour phase rather than liquid or solid state.

The frequencies for the skeleton modes are all expected to lie below 700 cm^{-1}. A considerable amount of accumulated evidence for other metal carbonyl systems, especially those of the general type (hydrocarbon)$M(CO)_n$, can be used to assist the assignment [25,26]. The A' symmetric Fe-CO stretching vibration is assigned to the strong absorption band observed at 376 cm^{-1} in figure 5.1, since a strong, polarised Raman band at 380 cm^{-1} and an IR absorption at 378 cm^{-1} have been observed by Davidson [24] in spectra of butadieneiron tricarbonyl in solution and were assigned to this mode. The band observed at 351 cm^{-1} is assigned to the Fe-(C_4H_6) stretch (A') mode by analogy with the Davidson assignment. In all previous cases where analogous molecules has been studied, the relative position of these two bands has been as suggested here [3,4]. Evidence from a variety of

complexes [4,27] shows that the Fe-CO stretches vary in frequency over 300-500 cm^1. The bands at 449 and 462 cm^{-1} observed in the vapour phase spectrum of $BdFe(CO)_3$ probably arise from the $A' + A''$ combination of Fe-CO stretches, which under a C_{3V} environment would be a degenerate pair.

M-C-O deformations (bend) tend to be found at higher frequencies than M-C stretches, and are more intense in IR spectra, but less intense in Raman spectra [5,25]. For $BdFe(CO)_3$ a strong band is found in the vapour phase IR spectrum at 506 cm^{-1}, and from the position and intensity the assignment of that to an Fe-C-O deformation seems quite reasonable by analogy with an assignment by Davidson for the liquid phase spectrum of $BdFe(CO)_3$ [24].

The only remaining vibration associated with the $Fe(CO)_3$ unit alone is the C-Fe-C deformation and this has been assigned to features between 100 and 150 cm^{-1} in solution and solid state spectra [3,4,26]. Grogan and Nakamoto assign an IR band at 135 cm^{-1} as the C_4 torsion of the C_4H_6 group [11]. In the vapour phase spectrum we did not find any observable bands at such low frequencies, which indicates that either they lie at higher frequencies and overlap with stronger bands or, more likely, they are too weak to observe.

Finally we must consider the metal-butadiene tilt. The tilt frequency is usually higher than that of the M-C_4H_6 stretch in C_4H_6M-$(CO)_n$ systems [3] and in the vapour phase spectrum of butadiene irontricarbonyl it is assigned to the band observed at 361 cm^{-1} by analogy with the liquid phase spectrum of $BdFe(CO)_3$.

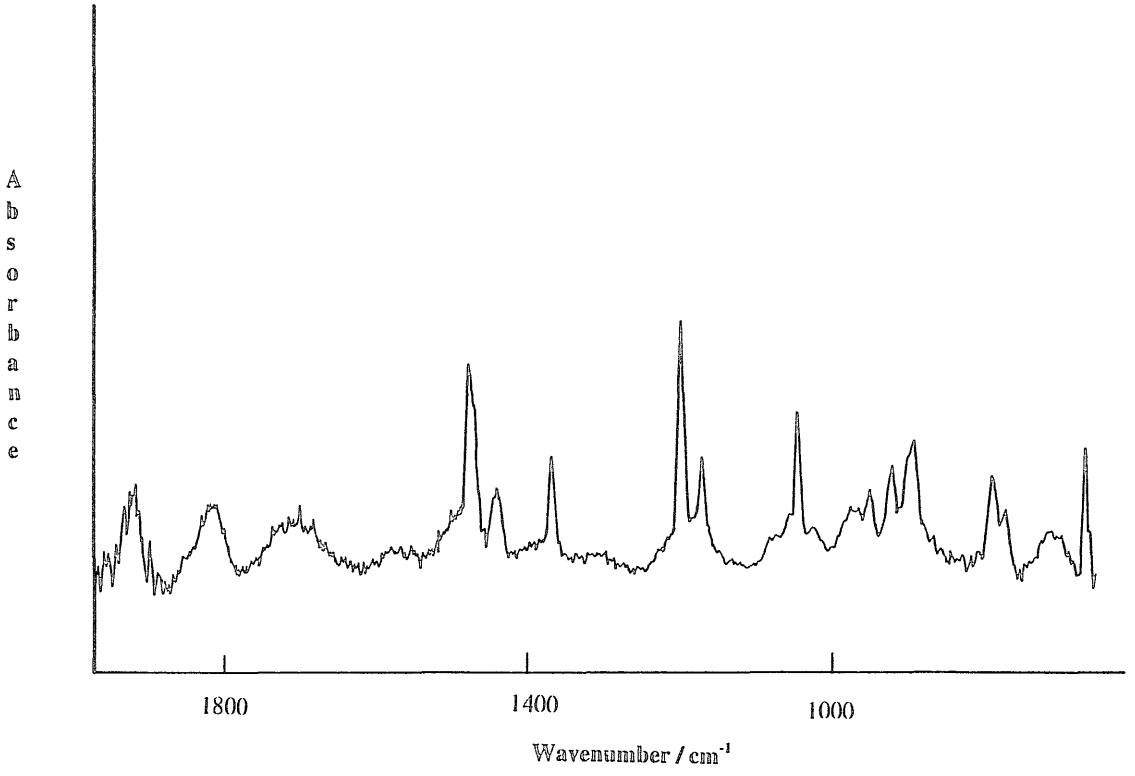

Figure 5.1. FT IR spectrum of $C_4H_6Fe(CO)_3$

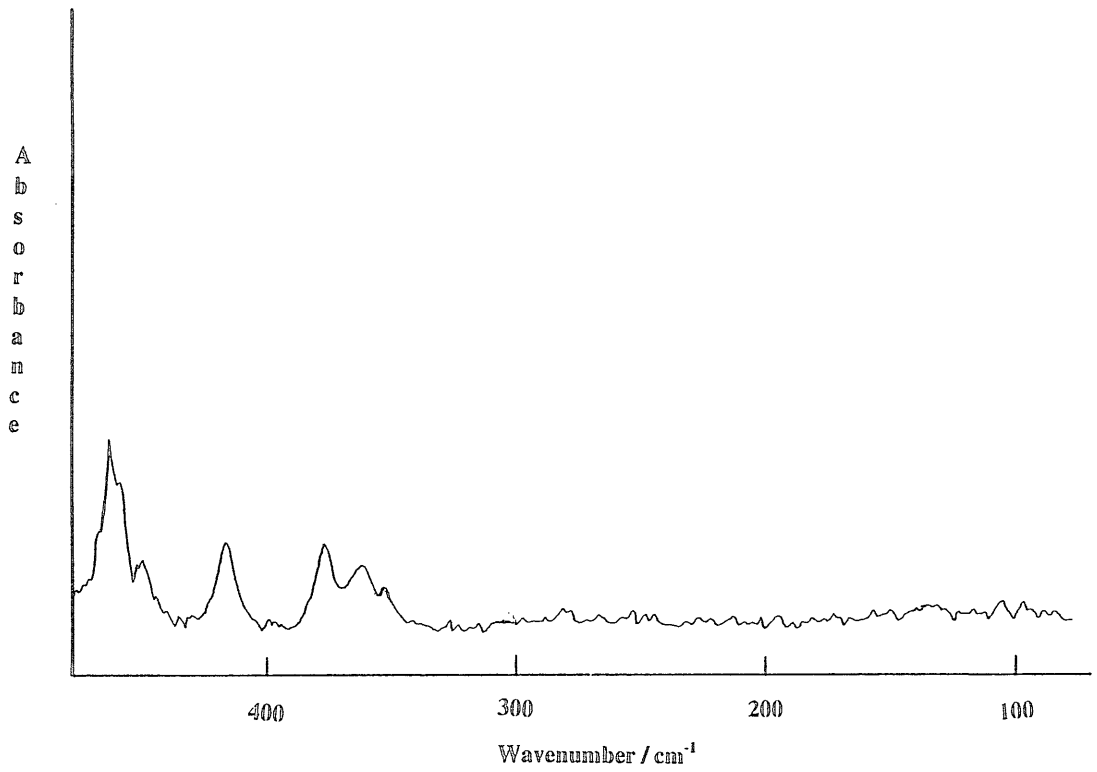

Figure 5.2. Far-infrared spectrum of $C_4H_6Fe(CO)_3$

Table 5.1: Frequencies and assignment of vapour phase spectrum of $BdFe(CO)_3$

Wavenumber/cm^{-1} Vapour phase (present work)	Wavenumber/cm^{-1} Liquid phase [ref 24]	Assignment
351	351	(C_4H_6)-Fe stretch
361	362	(C_4H_6)-Fe tilt
376	378	Fe-CO stretch
415	416	C-C=C bend
449	452	Fe-CO stretch
462	463	Fe-CO stretch
506	510	Fe-C-O def

5.3.2. Cyclopentadienylmanganese Tricarbonyl and Methylcyclopentadienylmanganese Tricarbonyl.

From microwave spectroscopy and X-ray diffraction studies [16,17] of $C_5H_5Mn(CO)_3$ ($CpMn(CO)_3$) it is reasonable to assume that the C_5H_5 ring is symmetrical and lies parallel to the plane formed by the three oxygen atoms. It is clear that the highest possible molecular symmetry of the compound is C_S and under the selection rules of this point-group all vibrations should be IR active. However, IR spectra in the CO stretching region [6,13] suggest that there is little interaction between the ring and the CO groups, and therefore the use of local symmetry is applicable, i.e. the ring will behave approximately as though it had C_{5V} symmetry and the $Mn(CO)_3$ moiety as though it had C_{3V} symmetry, and the IR activity of vibrational modes localised primarily in these groups will follow the local symmetry selection rules. Further, the close similarity between the IR spectrum of η-$CpMn(CO)_3$ and those of other compounds containing the η-Cp group suggest that η-Cp vibrations may be assigned, at least initially, on this basis. A similar approach has been applied to the spectra of η-$CpV(CO)_4$ [5].

The $Mn(CO)_3$ moiety will have fifteen vibrations which under assumed C_{3V} symmetry will transform as $4A_1+A_2+5E$. When the ring is taken into consideration, many new modes will appear, including the following skeletal modes; ring-metal-$(CO)_3$ stretches (A_1), an A_2 twist of the ring with respect to the (CO) groups, an E ring tilt and an E ring-metal-$(CO)_3$ bend. Of course the modes which have nominal E symmetry will split into A' and A'' modes under C_S symmetry. For cyclopentadienyl with C_{5V} symmetry the normal modes of vibration transform as

$3A_1$ (IR,R active)+ A_2 + $4E_1$ (IR active) + $6E_2$ (R active) (once again it is assumed, for convenience, that the higher (C_{5V}) symmetry representations can be used).

This investigation, which involved the measurement of IR spectra of $CpMn(CO)_3$ and $MeCpMn(CO)_3$ in the vapour phase in the range 500-10 cm^{-1}, was carried out in order to characterise low frequency vibrations in these complexes. Only five bands in the case of $CpMn(CO)_3$ and six bands in the spectrum of $MeCpMn(CO)_3$ are observed which are shown in figure 5.3 and 5.4 respectively. The observed bands have therefore have been assigned by comparison with the spectra of related compounds, i.e. metal cyclopentadienyl and metal carbonyl complexes.

The first cyclopentadienyl compound to be studied in detail by IR and Raman spectroscopy was ferrocene, $Fe(Cp)_2$ [28]. The observed vapour phase spectrum associated with the ring vibrations of cyclopentadienyl metal carbonyls should be closely related to that of ferrocene, and possibly also similar to the well-studied compound, benzenechromium tricarbonyl [29,30]. Observed ring frequencies of the complexes studied were indeed found to be very close to those observed for equivalent modes in ferrocene and $C_6H_6Cr(CO)_3$. It is therefore useful to examine the detailed assignment of the vibrational spectrum of these compounds and then make a correlation with the observed spectra of the cyclopentadienyl metal carbonyls.

In table 5.2 the assignment of the observed modes is summarised. This assignment has been reached largely through comparisons with the sandwich compounds ferrocene and benzenchromium tricarbonyl [27,28]. Since the $M(CO)_3$ groups in $CpMn(CO)_3$ and $C_6H_6Cr(CO)_3$ are isoelectronic, their spectra in the

region of the δ(MCO), and ν(M-CO) modes are very similar [29], with bands at the following positions:

$CpMn(CO)_3$	668, 663, 634, 609, 541, 499, 487	cm^{-1}
$C_6H_6Cr(CO)_3$	667, 654, 635, 612, 533, 488, 483	cm^{-1}

According to Adams [25], the following generalisations are possible: C-M-C angle deformations occur near 100 cm^{-1}, -M-C stretching vibrations are rarely above 500 cm^{-1}, while M-C-O angle deformations are sensitive to their environment and can be anywhere between 735 and 275 cm^{-1}.

In the vapour phase spectrum of $CpMn(CO)_3$ a band observed at 375 cm^{-1} seems to arise from the Mn-Cp stretching vibration, since Hyams [4] assigned a band at 357 cm^{-1} to the same vibration in the solid-state spectrum of this compounds. This assignment is also in accord with Adams' [29] assignment of a spectrum of $C_6H_6Cr(CO)_3$, who assigned a band at 358 cm^{-1} to the Cr-C_6H_6 stretch. The band observed in the vapour phase spectrum at 302 cm^{-1} is tentatively assigned to a Mn-CO stretching vibration (degenerate in C_{3V} symmetry) by analogy with Adams [29] assignment for the solid-state spectrum of $C_6H_6Cr(CO)_3$, where the Cr-CO stretch was assigned to a band at 306 cm^{-1}. The band observed at 215 cm^{-1} corresponds to a ring deformation (it is associated with out-of-plane bending vibration of C-H bond of the ring) by analogy with the Parker assignment of a spectrum of $CpMn(CO)_3$ in solution [30]. The second lowest frequency band in the vapour phase spectrum of $CpMn(CO)_3$, the band observed at 111 cm^{-1}, most likely corresponds to the totally symmetric CMnC bending vibration (umbrella mode) since it ties in with Hyams assignment of the solid-state spectrum of $CpMn(CO)_3$

(band at 107 cm^{-1}). The lowest frequency band observed in the $CpMn(CO)_3$ spectrum at 55 cm^{-1} corresponds to ring-Mn-C bending vibration; the same type of band is found at a similar frequency for analogous complexes such as $C_6H_6Cr(CO)_3$ [27,29].

Infrared spectra of complexes where cyclopentadienyl is substituted by methylcyclopentadienyl are usually assigned by comparison with the spectra of the equivalent complexes containing an unsubstituted ring. Bands associated with the metal-carbonyl moiety are unlikely to be significantly affected by ring substitution [31]. In the following assignment the spectrum of $MeCpMn(CO)_3$ has, therefore been compared with that of $CpMn(CO)_3$ in a way similar to the comparison of the spectra of toluene with benzene [31] and dimethylferrocene with ferrocene [32]. Assignment of bands resulting from vibration associated with the methyl group of $MeCpMn(CO)_3$ have been made by comparison with those of $Cr(CO)_3\eta$-toluene and dimethylferrocene [31,32]. The band observed at 495 cm^{-1} in the vapour phase spectrum of $MeCpMn(CO)_3$ in figure 5.4 is assigned to the totally symmetric Mn-CO stretching vibration by analogy with the spectrum obtained by Adams [34] for $MeCpMn(CO)_3$ in Nujol mull. We expect a similar band at nearly the same position in the spectrum of $CpMn(CO)_3$ but the signal to noise ratio is not good and this band is not observed. The band observed at 391 cm^{-1} is tentatively assigned to the Mn-Cp stretching vibration; this assignment is in accord with Parker's assignment of solution spectra of the same compound who assigned this band at 388 cm^{-1}, and is at a similar position to the band assigned to the Mn-Cp stretch of $CpMn(CO)_3$ spectra (see table 5.2). The band observed at 316 cm^{-1} in the vapour phase spectra of $MeCpMn(CO)_3$ is tentatively assigned to Mn-CO stretching vibration by analogy

with Adams [29] assignment on spectra of $Cr(CO)_3$(η-toluene) and the assignment of dimethylferrocene [30] and this is in accord with the assignment of vapour phase spectra of $CpMn(CO)_3$ in the present work. The ring deformation of the $MeCpMn(CO)_3$ is expected to be at a similar frequency to the analogous mode in $Cr(CO)_3$η-toluene and in the vapour phase spectrum of $MeCpMn(CO)_3$ this is observed at 218 cm^{-1}, in the solid-state spectrum of $Cr(CO)_3$η-toluene this band observed at 205 cm^{-1} [29]. This assignment is also in accord with Parker's assignment [30] on solution spectra of $MeCpMn(CO)_3$ and the vapour phase spectra of $CpMn(CO)_3$ in the present work. The lowest frequency bands observed at 108 and 41 cm^{-1} are tentatively assigned to the totally symmetric CMnC bending vibration (umbrella) and a MeCp-Mn-C bending vibration, respectively, by analogy with Adams assignment on solution spectra of $MeCpMn(CO)_3$ [29] and by comparison with the vapour phase spectrum of $CpMn(CO)_3$ obtained in the present work.

Below 500 cm^{-1} both complexes show bands assigned to skeletal vibrations of the $Mn(CO)_3$ group and other bands at similar frequencies. The methyl substituent does not appear to cause substantial splitting of the nominally degenerate modes of the $Mn(CO)_3$ group and the spectral patterns of $CpMn(CO)_3$ and $MeCpMn(CO)_3$ are therefore found to be similar.

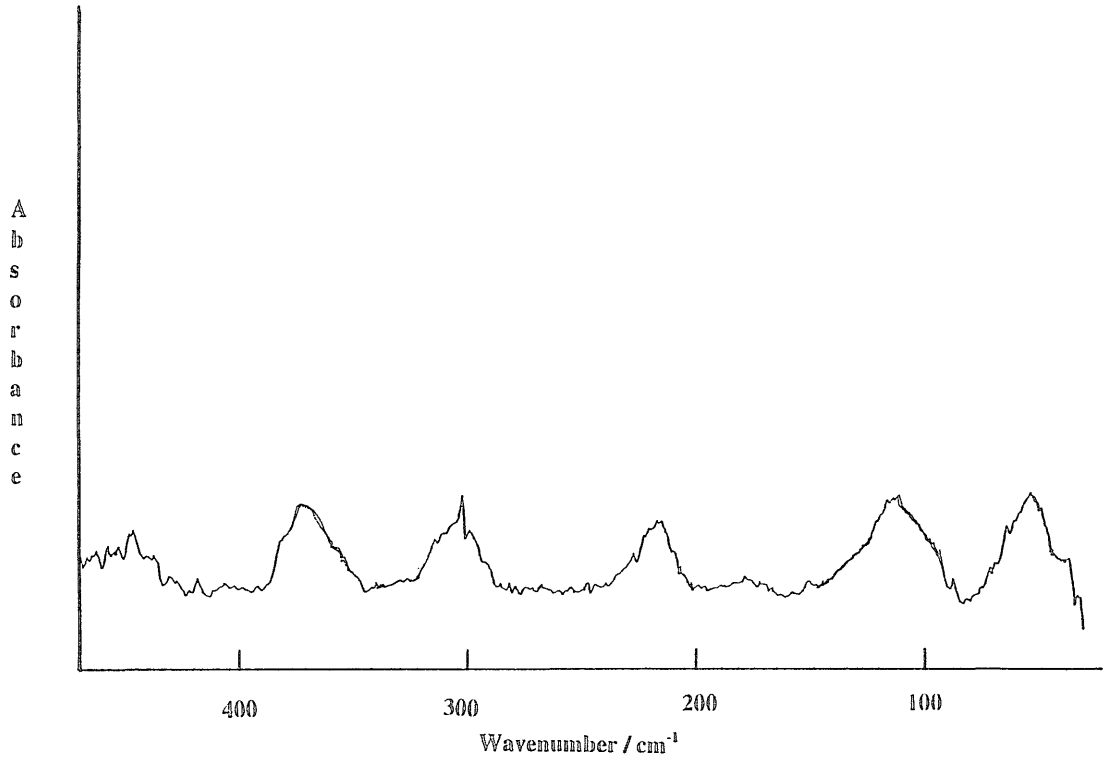

Figure 5.3. Far-infrared spectrum of $CpMn(CO)_3$

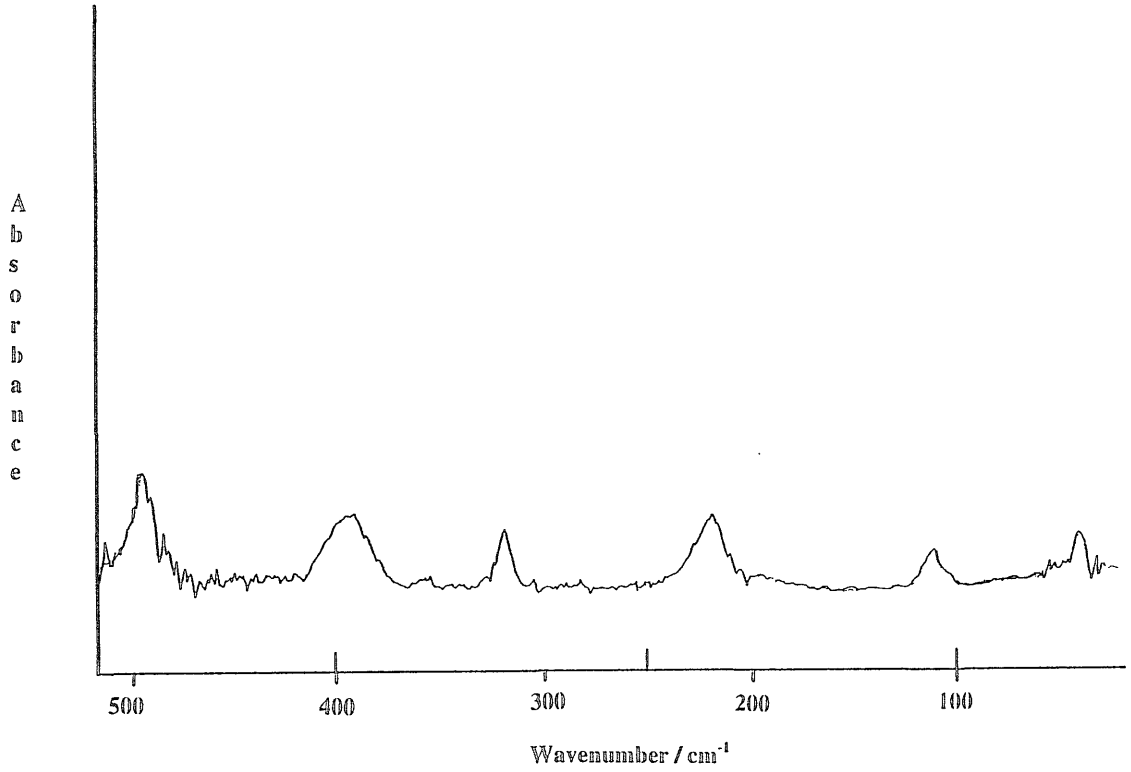

Figure 5.4. Far-infrared spectrum of $MeCpMn(CO)_3$

Table 5.2: Frequencies and assignment of $CpMn(CO)_3$ and $MeCpMn(CO)_3$ spectra in vapour phase (500-10 cm^{-1} region).

$CpMn(CO)_3$		$MeCpMn(CO)_3$	
Wavenumber/cm^{-1}	Assignment	Wavenumber/cm^{-1}	Assignment
55	(Cp-Mn-C) bend	41	(MeCp-Mn-C) bend
111	(C-Mn-C) bend	108	(C-Mn-C) bend
215	Ring-deform	218	Ring deform
302	(Mn-CO) stre	316	(Mn-CO) stre
375	(Mn-C_5H_5) stre	391	(Mn-C_5H_5) stre
		495	(Mn-CO) stre

Conclusion

The vibrational spectra of $BdFe(CO)_3$, $CpMn(CO)_3$ and $MeCpMn(CO)_3$ have been studied for the first time in the vapour phase in the far-infrared region. For $BdFe(CO)_3$ some vibrational wavenumbers show small or modest shifts relative to condensed phase work, but the vibrational pattern remains essentially the same. Only one band due to localised butadiene vibration, namely the C=C (bend) at 416 cm, is observed below 500 cm^{-1}. Butadiene frequencies would be expected to be decreased by complex formation, as has been found for the benzene moiety in $C_6H_6Cr(CO)_3$. This is indeed found to be the case, with average downward shift being about 10 cm^{-1}.

For $CpMn(CO)_3$ and $MeCpMn(CO)_3$ both complexes show bands assigned to skeletal vibrations at nearly identical positions in their vapour phase spectra. The methyl substituent does not appear to cause substantial splitting of the nominally degenerate modes of the $Mn(CO)_3$ group when moving from $CpMn(CO)_3$ to $MeCpMn(CO)_3$. Each vibrational mode of $CpMn(CO)_3$ is in turn related to the equivalent mode of $MeCpMn(CO)_3$. The ring-metal modes are shifted to higher frequency in the spectrum of $MeCpMn(CO)_3$ in agreement with trends previously noted in the spectrum of ferrocene and dimethylferrocene [34]. The MeCp-Mn-C bending mode is observed at lower frequency than Cp-Mn-C due to the increased reduced mass on methyl substitution and its electron donating effect.

References.

[1]. G. Wilkinson, F. G. A Stone, and E. W. Abel eds. "Comprehensive Organometallic Chemistry" (Pergamon Press, Oxford, 1982), Vol . 8, Chapter 58;

[2]. J.Gang, M.Pennington, D.K.Russell, F.J.Basterrechea, P.B.Davies and G.M.Hansford. Opt. Soc. Am. B, 11, 184, 1994.

[3]. R. T. Bailley, E. R. Lippincott and D. Steele, J. Am. Chem. Soc; 87, 5346. 1965.

[4]. I. J. Hyams, R. T. Bailey and E. R. Lippincott, Spectrochim. Acta, 23 A, 273. 1967

[5]. J. R. During, R. B. King, L. W. Houk and A. L. Marston, J. Organometallic Chem; 16, 425, 1969.

[6]. F.A.Cotton, A.D.Liehr and G.Wilkinson, J. Inorg. Nucl. Chem. 1, 175, 1955.

[7]. H. Reihlem, A. Gruhl, G Von Hessling and O. Pfrengle, Lieligs. Ann 482, 161. 1930.

[8]. B. J. Hallam and P.L. Pauson, J. Chem. Soc; 642. 1958.

[9]. O. S. Mills and G. Robinson, Proc. Chem. Soc., 421. 1960.

[10]. A. Reckziegel and M. Bigorgne, J. Organometallic Chem., 3. 341. 1965.

[11]. M. J. Grogan and K. Nakamoto, Inorg. Chim Acta, 1, 228. 1967.

[12]. G. E. Coats, M. L. H. Green and K. Wade, Organometallic Compounds, (Methuen and Co. Ltd., London 1968) Vol. 11 P. 70.

[13]. T. S. Piper, F. A. Cotton, G. Wilkinson. Inorg. Nuc. Chem. 1966, 1, 165.

[14]. G. Wilkinson, F. G. A. Stone, E. W. Abel, Pergamon Press: Oxford, 1982; Chapter 29.

[15]. D. J. Parker and M.H. B. Stiddard, J. Chem Soc. A, 480. 1970.

[16]. J. K. Tyler, A. P. Co, and J. Sheridan, Nature (London), 183, 1182. 1959.

[17]. A. F. Berndt and R. E. Marsh, Acta Crystallogr., 16, 118. 1963.

[18]. R. D. Fischer, Chem. Ber. 93, 165. 1960.

[19]. H.P.Fritz and E.F.Pauls, Z. Naturforsch, 18b, 435, 1963.

[20]. R. K. Harris, Spectrochim. Acta. 20, 1129, 1964.

[21]. L. M. Sverdlov and E. N. Boltina, J. Russ. Phys. Chem. Soc. 36, 1502. 1962.

[2]. P. A. Bazhulin, Yu. A. Lazarev and N. V. Desyatova, Opt. and Spectroscopy, 13, 41. 1962

[23]. L. M. Sverdlov and N. V. Tarasova, Opt. and Spectroscopy, 9, 159, 1960.

[24]. G. Davidson, Inorganica. Chimica. Acta, 3, 596. 1969.

[25]. D. M. Adams, J. Chem. Soc., 1771. 1964.

[26]. D. M. Adams, Metal-Ligand and Related Vibrations, (E. Arnold Ltd., London, 1967) Chapters 3 and 4.

[27]. H. P. Fritz and J. Manchot, Spectrochim, Acta, 18, 171, 1962.

[28]. E. R. Lippincott and R. D. N. Nelson, Spectrochim, Acta, 10, 307, 1958.

[29]. D.M.Adams and A.Squire, J. Chem. Soc. 814. 1970

[30]. D. J. Parker and M. H. B. Stiddard, J. Chem. Soc, 1040, 1970.

[31]. J.K.Wilmshurst and H.J.Bernstein, Canad. J. Chem., 35, 911, 1957.

[32]. R. T. Bailey and E. R. Lippincott, Spectrochim. Acta, 21, 389, 1965.

[33]. D.M.Adams and A.Saquire, J. Organomet. Chem, 63, 381, 1973.

Chapter 6

6.1 Introduction

The infrared spectra of metal carbonyl compounds below 700 cm^{-1} provide good examples of the use of this region as a supplement to higher-frequency spectra for structural studies. The spectra contain quite a few bands of reasonable intensity and the position of some of these bands may be correlated with the structural details of the molecules. This region thus serves as both a fingerprint region and as a region providing useful molecular information.

The vibrational spectra of metal carbonyls and their derivatives have been extensively studied particularly in the CO stretching region, and the frequencies of vibrations have been correlated with the accepter abilities of the ligands and with the degree of substitution of the carbonyl complex [1,2]. There have also been studies of lower frequency vibrations, such as the metal-carbon stretching [ν(MC)] and metal- carbon-oxygen bending [δ(MCO)] vibrations in some metal carbonyl halides and their derivatives [3].

Subsequent work on the series of $XMn(CO)_5$ compounds dealt with the application of the IR spectroscopic method of assigning and analysing the CO stretching modes to a variety of octahedral molecules derived from the carbonyls of the group VIA and group VIIA [4,5] metals and to $M_2(CO)_{10}$ (M=Mn, Re) molecules [6]. Other authors [7] have used this method in varying degrees, and often in association with the kind of intensity arguments suggested by Orgel [8] in order to analyze and assign the CO stretching spectra of numerous $M(CO)_xL_{6-x}$ molecules, where L_{6-x} represent a collection of donor molecules or univalent groups which are not necessarily all the same. Lewis and co-workers [9,10] made detailed studies of the spectra of $M_2(CO)_{10}$ and $M_2(CO)_8L_2$ molecules which lead them to comment on various features of the study by Cotton and Wings [6] on $Mn_2(CO)_{10}$ and $Re_2(CO)_{10}$ in particular and on the Cotton-Kraihanzel force field in general.

However, there has been no unified study in the far-infrared region and so we have performed a comparative series of far-infrared spectroscopic investigations of manganese carbonyl derivatives of the type $XMn(CO)_5$, where X = CH_3, CD_3, H, D, CF_3, Cl, Br. Following the number of metal-carbon stretching and metal-carbon-oxygen bending vibration active in the far-infrared region, accurate values for the band maxima in the 700-10 cm^{-1} region have been obtained for these complexes

The far-infrared data can potentially reveal the effect of the X (ligand) in $XMn(CO)_5$ on the bonding in the $Mn(CO)_5$ group. No systematic study of the infrared spectra of these molecules in the region 500-10 cm^{-1} in the vapour phase have been previously reported, although some data have been reported in solution and Nujol mull [11]. Vibrational assignments have been made for all these molecules in the present work, partly by comparison with earlier condensed phase work.

This chapter will deal then with two related problems. First procedures for enlarging the body of experimental data pertaining to Mn-C stretching and Mn-C-O bending modes of a particular molecules will be discussed. Second, using these data, the assignment will be reviewed and evaluated where possible in terms of the implication for bonding models of the compounds

6.1.1. Methylmanganesepentacarbonyl.

$CH_3Mn(CO)_5$ is one of the best known examples of a molecule with a σ-bonding interaction between a transition metal and an organic alkyl group [12]. This compound has been the subject of a number of structural studies, involving gas-phase electron diffraction [13], X-ray diffraction, incoherent inelastic neutron scattering [14], and vibrational spectroscopy [15]. These have left uncertain two structural features associated with the methyl group, its geometry and its internal rotational motion. The disordered structure of the Mn crystal meant that no geometric information could be obtained from the X-ray study, while the hydrogen

positions were not located by the electron-diffraction experiment. Vibrational data are more complete, but despite several infrared investigations [14,15] a number of vibrational assignments are still open to question. In particular, the attribution [16] of the Mn-CH_3 stretch to a band 100 cm^{-1} higher in energy than any of the Mn-CO stretches runs counter to expectation based on the longer Mn-CH_3 distance (2.19 Å) vs. Mn-CO distance (1.86 Å) [12a].

Given the incompleteness of previous IR assignments in condensed phase work, we have carried out a study of this compound in the gas phase in the region 500-10 cm^{-1}. $CD_3Mn(CO)_5$ was also prepared and analysed in order to assist in the spectral assignment.

6.1.2. Hydridemanganesepentacarbonyl.

Following the initial reports of $HMn(CO)_5$ preparation [17], the nature of the compound was subjected to number of studies. Investigation of the vapour phase infrared spectrum by Cotton, Down, and Wilkinson [18] and by Wilson [19] led to the conclusion that the molecular symmetry is definitely lower than C_{4v}, although no complete vibrational assignments were made. Subsequently, however, La Placa, Hamilton and Ibers [20] showed that $HMn(CO)_5$ crystalizes such that the $Mn(CO)_5$ moiety does have C_{4v} local symmetry in the solid state and suggested that it is unlikely that it would assume lower symmetry in the vapour phase. This structure determination prompted Huggins and Kaesz [21] to report a prior interpretation of the C-O stretching region of the solution spectrum of $HMn(CO)_5$ based upon C_{4v} symmetry. However these studies do not solve the problem of apparent disparity between the X-Ray results [20] and previous infrared data [18,19]. Since the spectra of both $HMn(CO)_5$ and its deuterated analogue, $DMn(CO)_5$, are identical in the 5μm (1900-2200 cm^{-1}) region, it is only with the remainder of the spectrum that a C_{4v} assignment can be tested by the Teller-Redlich isotope product role. In order to resolve this disparity, we have investigated the infrared spectrum of a gaseous

sample of $HMn(CO)_5$ which was known to be pure, so that bands due to impurities were eliminated. We report the far-infrared spectrum of gaseous samples of $HMn(CO)_5$ and $DMn(CO)_5$ in the region 700-10 cm^{-1} and propose a vibrational assignment of the infrared active modes.

6.1.3. Trifluoromethylmanganesepentacarbonyl.

It has been recognized for some time that, on the basis of chemical behaviour [22], where transition metal atoms are in low formal oxidation states metal to perfluoroalkyl bonds are more stable and thus presumably thermochemically stronger than metal to alkyl bonds. It was observed, more or less simultaneously, by King and Bisnette [23] and by Cotton and McCleverty [24] that in several perfluoromethyl compounds of transition metals the C-F stretching frequencies are lower, by the order of 100 cm^{-1}, than the frequencies found in perfluoromethyl halides. Both group of workers [25] ascribed this to π-interactions involving the filled d_π orbital of the metal and the empty antibonding C-F orbitals. Detailed formulation can be made either in valence bond or molecular orbital terms [23,24,25]. By either interpretation, it is also to be expected that the C-M bond would be strengthened in rough proportion to the weakening of the C-F bonds. Structural data showing that the bonds in perfluoroalkyl compounds are short relative to those in the normal alkyl compounds has been provided in several cases [26,27]. The purpose of the present work was an investigation of the far-infrared spectrum of $CF_3Mn(CO)_5$, to characterise low frequency fundamentals and to ascertain new information on the bonding in this compound.

6.1.4. Halide manganesepentacarbonyl.

The carbonyl halides of manganese have been of interest for some time, partly because of the metal-carbon bonds which involve d_π-p_π bonding, but also because they are quite symmetrical (C_{4v}), making a detailed dicussion of their

vibrational spectrum feasible. Bennett and Clark [3] have studied the infrared spectra of the series $XMn(CO)_5$ where X=Cl, Br, I and assigned the metal-halogen and one of the metal-carbon stretching modes. Other low frequency data has been reported by Valenti *et al.* [28], while Hyams [11] has made a more complete study of this series of compounds between 33-2200 cm^1 in solution and Nujol mull and based his assignment on approximate force constant calculations. while Cotton [29], and Kaesz *et al.* [30,31] have carried out a similar study for all of the halides but extended their work to intensity measurements and ^{13}C isotopic enrichment. The vibrational spectra of $IRe(CO)_5$ have been reported [32] and comparison between the manganese and rhenium analogues has proved useful.

The present work is concerned with the far-infrared spectra of the manganese carbonyl halides in vapour phase. The resulting data in conjuction with infrared data reported earlier [3-30] has permitted a more complete vibrational assignment.

6.2 Experimental Details.

6.2.1: Sample preparations.

Derivatives were prepared according to methods described in the literature. This is briefly summarised below;

(a) $\underline{CH_3Mn(CO)_5}$. This was prepared in a nitrogen atmosphere by treating $Mn_2(CO)_{10}$ with methanolic NaOH solution followed by CH_3I addition and subsequent purification by vacuum sublimation [33]. Purity was checked using low resolution Fourier transform mid-infrared (FTIR) spectroscopy and ^1H NMR spectroscopy. The spectra showed no evidence of any impurties.

(b) $\underline{CD_3Mn(CO)_5}$. This was prepared as above but substituting CD_3I in place of CH_3I. IR and ^1H NMR spectra showed no evidence of any impurities.

(c) $\underline{HMn(CO)_5}$. [34] Under an inert gas atmosphere 0.500 g of freshly sublimed $Mn_2(CO)_{10}$ was dissolved in 25 ml of freshly distilled tetrahydrofuran (THF) and

stirred over a Na/Hg amalgam (0.062 g in 50 ml Hg) for 3 hours. The solution was then filtered and solvent distilled off leaving a greyish residue. After admitting nitrogen to the flask, which now contained $NaMn(CO)_5$, 30 ml of aqueous phosphoric acid was added over a period of one hour. During the addition of phosphoric acid, the $HMn(CO)_5$ and water from the acid were distilled into an external trap containing phosphorus pentoxide where water was removed. The $HMn(CO)_5$ was identified by its infrared spectrum. The infrared spectrum showed no indication of THF and CO_2 and the purity of the sample was verified by recording a mass spectrum.

(d) $\underline{DMn(CO)_5}$. This was prepared as in (c) above except D_3PO_4 was used in place of H_3PO_4. However, care was taken with the vacuum line as deuterium will exchange rapidly with any protonic sites on the glassware. Care was taken to dry all apparatus with which manganese pentacarbonyl deuteride came into contact. Because of the difficulty in preparing $DMn(CO)_5$, there has been disagreement among several workers [18,19] as to just which maxima observed in IR spectra belong to $DMn(CO)_5$ itself and which belong to small amounts of $HMn(CO)_5$ impurity.

(e) $\underline{CF_3Mn(CO)_5}$. Trifluromethylmanganese pentacarbonyl was prepared by a method described by McClellan [35] in which $CF_3COMn(CO)_5$ was heated at 110°C for one hour under a nitrogen atmosphere. The rate of carbon monoxide evolution was monitored by the flow through a gas bubbler. Initially, the carbon monoxide evolution should be very vigorous, but toward the end of reaction no gas evolution should occur. After the reaction period was completed the solid residue was transferred to a sublimer and trifluromethylmanganese pentacarbonyl was isolated by sublimation. The product is a white air stable and an extremely volatile solid and its infrared spectrum exhibited strong metal carbonyl bands at 2155, 2055, and 2015 cm^{-1}. The ^{19}F NMR spectrum exhibited a single sharp resonance at -9.3ϕ due to the

CF_3 group. The spectroscopic data indicated formation of a high purity $CF_3Mn(CO)_5$ sample.

(f) $BrMn(CO)_5$ and $ClMn(CO)_5$. These compounds were prepared by methods described in the literature [36]. The CO stretching region in the products were compared with earlier work [28,30] to check the purity.

6.2.2 Infrared Spectroscopy.

Gaseous samples were examined in a 10 cm long cell equipped with polyethylene windows. The sample pressure was generally of the order of 1-5 Torr except when the intense carbonyl peaks were examined, for which it considerably reduced. Far IR spectra of each compound were recorded using a digilab FTS 40 V far-infrared spectrometer in the region 500-10 cm^1. In the case of the manganesecarbonyl halide samples, these were heated in the gas cell to increase the vapour pressure and therefore enhance weak absorption bands. Several scans of each spectrum were taken, so that the frequencies quoted should be accurate to ± 2 cm^1.

6.3. Results and Discussion.

6.3.1. $BrMn(CO)_5$ and $ClMn(CO)_5$.

Vapour phase IR spectra were obtained for $BrMn(CO)_5$ and $ClMn(CO)_5$ in the region between 500-10 cm^{-1}. To obtain the spectra solid deposits of the compound were condensed in the cell under vacuum. While the spectrum was being recorded the cell was maintained at ca. 40 ^0C to increase the vapour pressure. The signal-to-noise ratios in both spectra shown in figures 6.1 and 6.2, are reasonable but improved spectra would have been desirable to identify weak absorption bands

that may be obscured by noise. Unfortunately the cell could not be heated to temperatures above 40^0C because of compound decomposition.

Based on chemical and infrared evidence [5], the molecular structure of $XMn(CO)_5$ (where X=Br,Cl) is thought to be pseudo-octahedral (C_{4V} symmetry). The irreducible representations for the normal modes of vibration for this symmetry are

$$\Gamma_{vib}{}^{C4v} = 7A_1 + A_2 + 4B_1 + 2B_2 + 8E$$

A_1 and E modes are both infrared and Raman active, B_1 and B_2 are only Raman active; and the A_2 mode is both Raman and infrared inactive.

Eight fundamentals are expected for $XMn(CO)_5$ molecule in the region 700-200 cm^1, four E and four A_1 modes. These consist of Mn-C stretching vibrations, Mn-C-O bending vibration and a Mn-X stretching vibration. Below 200 cm^{-1} four absorption bands are expected and they should approximately correspond to the following motions, A_1 and E out of plane CMnC deformation, E CMnC in plane deformation and E XMnC deformation [11, 28]. Only eight bands are observed in the case of $BrMn(CO)_5$ and seven for $ClMn(CO)_5$. Because the modes of the same symmetry type are known to be extensively mixed in the low frequency region, none of the frequencies in this region will be comprised of the assigned motion alone. This caveat applies particularly to the A_1 and E modes in the Mn-C stretching and Mn-C-O bending regions.

Due to the relatively large mass of Br and the small bond strength of Mn-Br in relation to Mn-CO, it is reasonable to expect that the lowest frequency (E) mode will correspond to CMnBr bending. Thus we have tentatively assigned the band at

53 cm^{-1} in figure 6.1 to the CMnBr bending mode, which is expected to occur below 70 cm^{-1} [2]. This mode is almost certainly the lowest fundamental frequency of the $Mn(CO)_5Br$ molecule and is expected to be extensively mixed with the CMnC bending modes. No clear corroboration of this assignment could be obtained by changing the halogen atom to Cl as the spectra of this compound in the region in question were markedly different from the spectrum of $Mn(CO)_5Br$ [11,37]. It is found that a band observed at 127 cm^{-1} in spectrum of $ClMn(CO)_5$ which is below the usual Mn-C stretching region, is assigned to the ClMnC bending mode. Clearly this assignment is in line with the expected mass effect of the halides i.e the lighter chloride has a higher frequency mode than the bromide. The band observed at 302 cm^{-1} in the spectrum of $ClMn(CO)_5$ is assigned to Mn-Cl stretching mode and the band observed at 224 cm^{-1} in the spectrum of $BrMn(CO)_5$ corresponds to the Mn-Br stretching mode. This is consistent with the assignment of several metal-halogen stretching vibrations reported earlier [3]. The stronger bands observed at 378 cm^{-1} in $BrMn(CO)_5$ and 394 cm^{-1} in $ClMn(CO)_5$ are assigned to the (A_1) Mn-C stretching mode; this mode has been observed at 372 cm^{-1} in $IRe(CO)_5$. Similarly the bands observed at 384 cm^{-1} in $BrMn(CO)_5$ and 392 cm^{-1} in $ClMn(CO)_5$ have been assigned to E Mn-C-O bending modes by analogy with the assignment of Valenti et al. [28] on solid-state spectra of metal halide carbonyls. These bands were previously reported as shoulders but in our experiment they are quite well resolved, especially in the case of $BrMn(CO)_5$. The band observed at 448 cm^{-1} in the spectrum of $BrMn(CO)_5$ corresponds to Mn-C-O bending vibration. This assignment was made by analogy with Adams and Sequre [38] solid-state work in

which the corresponding band was at 470 cm^{-1}. The weak band observed at 220 cm^{-1} in $ClMn(CO)_5$ is unexplained.

There were no major differences between the gas phase spectra in the current work and in previous studies on solutions and the solid-state, apart from modest frequency shifts. Other research groups have investigated the solution and solid-state spectra of $ClMn(CO)_5$ and $BrMn(CO)_5$ in the mid-infrared spectral region and found that differences only occured in the C-O stretching region [3,37]. The present study sheds further light on how condensed phase influence the metal-carbon stretching and metal-carbon-oxygen bending frequencies. The data assembled in tables 6.1 and 6.2 (comparison between gas phase and solution and solid-state spectrum) shows that the frequency shifts for $XMn(CO)_5$ from solution to vapour phase are mostly upward, are all relatively small, but are not equal. If an average shift ± 10 cm^{-1} was applied to all bands no serious error between gas phase and solution would be introduced.

It is difficult to make an unequivocable assignment without observing every possible band. There is no doubt that substantial mode mixing occurs in the fundamental modes in the low frequency region. Thus the Mn-C stretching motion and the Mn-C-O bending motion have a pronounced tendency to mix and one can expect some mixing of the axial and planar stretching motion in the A_1 vibrations. While a detailed discussion of the bonding in the $XMn(CO)_5$ compounds requires a force field calculation, it is possible to make some qualitative comments concerning the observed frequencies. It is interesting to note what happens to the metal carbon stretching and metal-carbon-oxygen bending frequencies if the halides are

substituted in the order Cl and Br. The bromide, being less electronegative, should leave the most negative charge on the metal atom. The carbon-oxygen force constant should change in order $Mn(CO)_5Cl > Mn(CO)_5Br$. This change would be reflected in the correspondingly increasing frequencies to higher modes in $ClMn(CO)_5$ spectrum than $BrMn(CO)_5$. However, these frequencies change very little from halide to halide.

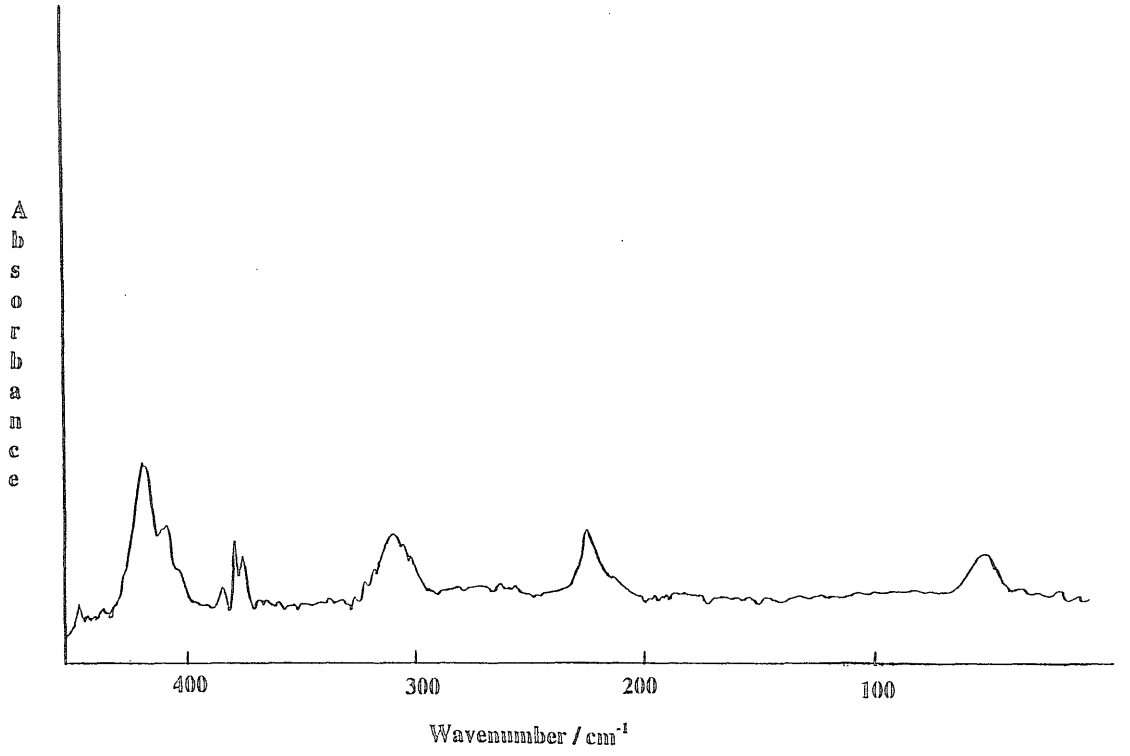

Figure 6.1. Far-infrared spectrum of $BrMn(CO)_5$

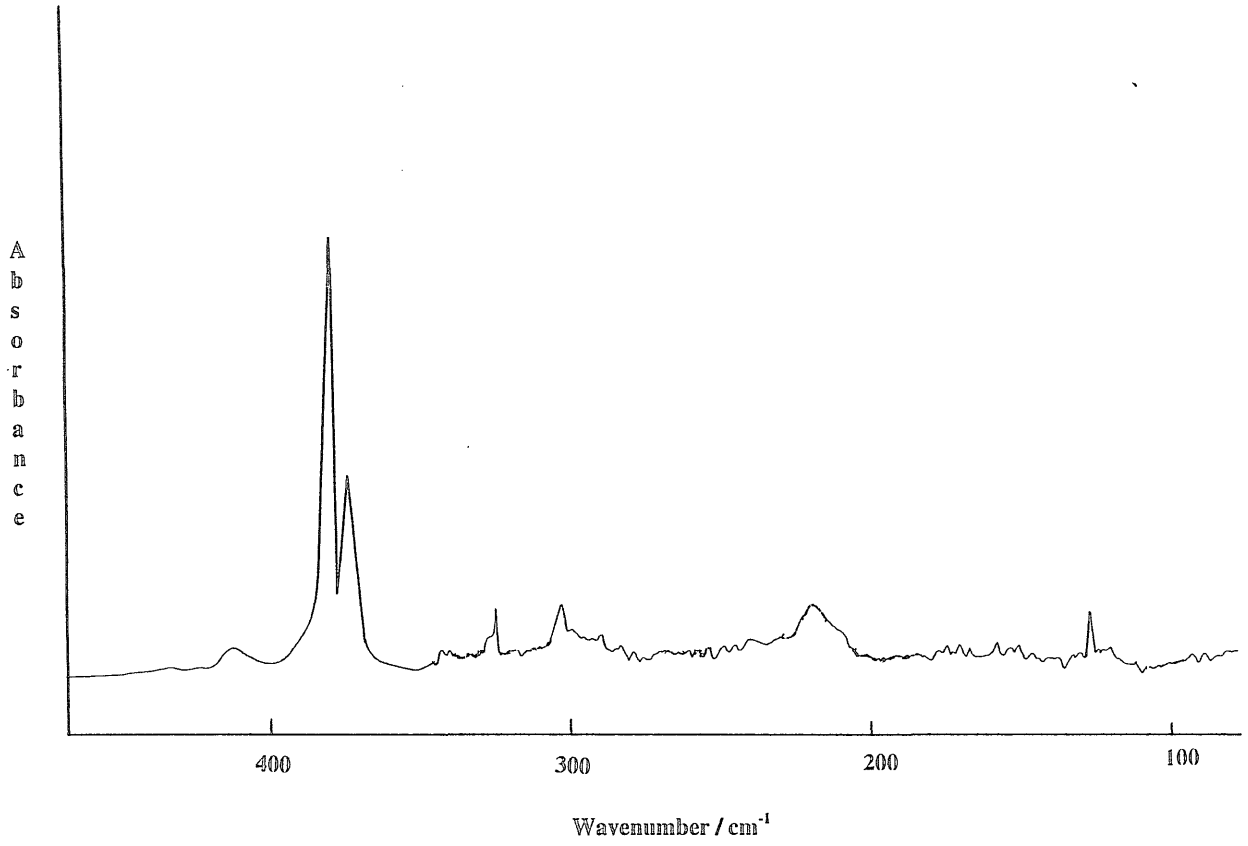

Figure 6.2: Far-infrared spectrum of $ClMn(CO)_5$

Table 6.1

Frequencies and assignment of vapour phase spectrum of $BrMn(CO)_5$

Wavenumbers/cm^{-1}			Assignment[A]
Gas Phase	Solution	Solid	
53	50	50	(E) CMn Br bending
224	219	222	(A_1) Mn-Br stretching
315			(A_1) Mn-C stretching
378			(A_1) Mn-C stretching
384	384		(E) Mn-C-O bending
408	405	405	(E) Mn-C stretching
419	415	415	(E) Mn-C stretching
448	472	471	(E) Mn-C-O bending

A= Assignments made mainly by comparison with work reported in references [11] and [28].

Table 6.2

Frequencies and assignment of the vapour phase spectrum of $ClMn(CO)_5$

Wavenumbers/cm^{-1}			**Assignment[A]**
Gas phase	Solution	Solid	
127	126	126	(E) ClMn-C bending
220			
302	292	295	(A_1) Mn-Cl stretching
325			(A_1) Mn-C stretching
392	384	382	(E) Mn-C-O bending
394	390		(A_1) Mn-C stretching
403	406	409	(E) Mn-C stretching

A= Assignments made mainly by comparison with work reported in references [11] and [28].

7.3.2 $HMn(CO)_5$ and $DMn(CO)_5$.

Manganese pentacarbonyl hydride in C_{4v} symmetry would be an approximately octahedral molecule with the hydrogen located on C_4 axis [18,19]. The irreducible representation of the vibration in this molecule is the same as in $BrMn(CO)_5$ and $ClMn(CO)_5$ and is:

$$\Gamma_{vib}{}^{C4v} = 7A_1 + A_2 + 4B_1 + 2B_2 + 8E$$

Of the modes, only A_1 and E modes are infrared active. Seven modes involving Mn-CO stretching and Mn-C-O bending motions are expected in the region 800-300 cm^{-1}, four E and three A_1 modes [7]. Two E modes and one A_1 mode are expected in the very low frequency region (below 300 cm^{-1}) consisting of O-C-Mn-C-O deformations [7, 39].

We have recorded IR spectra of a pure gaseous sample of $HMn(CO)_5$ in the region between 800-10 cm^{-1} for the first time in an attempt to characterise low frequency vibrations of this molecule. In making the vibrational assignment for $HMn(CO)_5$, reference is made to the work of Hyams and Lippincott [11] on $XMn(CO)_5$ (X=Cl, Br) and Wilson on $HMn(CO)_5$ [19]. Figures 6.3 and 6.4 show the low frequency spectra of $HMn(CO)_5$ and $DMn(CO)_5$.

There are six bands observed in the spectrum of $HMn(CO)_5$ in the region 800-300 cm^{-1}, which are clearly fundamentals and not structural components of other bands while below 300 cm^{-1} three bands are observed. In case of $DMn(CO)_5$ we observe seven bands in the region 800-300 cm^{-1}, Due to the difficulty in preparing $DMn(CO)_5$ free of the hydride isotopomer, there has been disagreement among several investigators [18,19] as to just which maxima observed belong to

$DMn(CO)_5$ itself and which belong to traces of $HMnCO)_5$ impurity. There are considerable number of bands in this region (Below 800 cm^{-1}) which apparently disappeared upon deuteration and also there is sufficient disagreement in the literature about the existance and position of bands in this region. In this portion (between 800-300cm^{-1}) of the hydride spectrum there are four strong bands at 731, 663, 613 and 462 cm^{-1} while strong $DMn(CO)_5$ bands occur at 729, 661,606 and 456 cm^{-1}. It is helpful in assigning these bands to refer to the work on the $XMn(CO)_5$ compounds by Edgell and Cengel [39], who have made middle frequency assignments for these compounds

The strong band in the spectrum of $HMn(CO)_5$ at 462 cm^{-1} is assigned to an A_1 mode of Mn-CO stretching vibration. This is consistant with the same vibration at 460 cm^{-1} in $DMn(CO)_5$ and also accords with the $XMn(CO)_5$ (X=Br, Cl, I) assignment, for the band observed at 471 cm^{-1}. In this series, none of the A_1 modes can shift very much upon deuteration.

Several strong bands still remain to be assigned in these spectra, namely the $HMn(CO)_5$ bands at 731, 663 , and 613 cm^{-1}. The $XMn(CO)_5$ correlation indicates that the 663 cm^{-1} hydride band is an A_1 mode involving Mn-C-O bending motion. The key to understanding the other two hydride bands is provided by the discussion of Edgell *et al.* [39]. These 731 and 613 cm^{-1} bands are E modes and also correspond to Mn-C-O bending vibrations. The analogous bands are found at 729 and 608 cm^{-1} in the $DMn(CO)_5$ spectrum. The band observed at 561 cm^{-1} in the hydride spectrum is due to an E mode analogous to the 542 cm^{-1} deuteride mode which consists largely of Mn-C-O bending motion. There is a band of $DMn(CO)_5$ at 510 cm^{-1}, which is absent in the hydride spectrum, that is assigned to an E mode

of Mn-CO stretching motion. Cotton *et al.*[18] assigned this band at 511 cm^{-1} in the spectrum of $DMn(CO)_5$. The bands observed at 359 cm^{-1} for the hydride and 362 cm^{-1} for the deuteride are assigned to an E mode corresponding to Mn-C-O bending motion; this proposal is based on analogy with the result of Edgell *et al.* on $HMn(CO)_5$.

The assignment for all the modes observed in the spectra of $HMn(CO)_5$ and $DMn(CO)_5$ is given in the table 6.3. In the very low frequency region, weak bands observed at 243 and 47 cm^{-1} and a strong band at 63 cm^{-1} in the spectrum of $HMn(CO)_5$. We refer to the work of Edgell and Hyams [4,5] on the $XMn(CO)_5$ (X=Br, Cl, I) compounds. They observed that there are two far-infrared bands characteristic of the $Mn(CO)_5$ moiety in these compounds at 64 and 88 cm^{-1} in the solution spectra of the series. These modes are C-Mn-C deformation modes. Considering $HMn(CO)_5$ and $DMn(CO)_5$, we may compare their band positions to those in molecules in which the coupling between modes involving the X- and -$Mn(CO)_5$ moieties is small. The band observed at 63 cm^{-1} in the vapour phase spectrum of $HMn(CO)_5$ correspond to an A_1 C-Mn-C bending vibration by analogy with band at 88 cm^{-1} in $BrMn(CO)_5$ and in the same way the band at 47 cm^{-1} correspond to C-Mn-C bending vibration of E symmetry by analogy with the $BrMn(CO)_5$ spectrum.

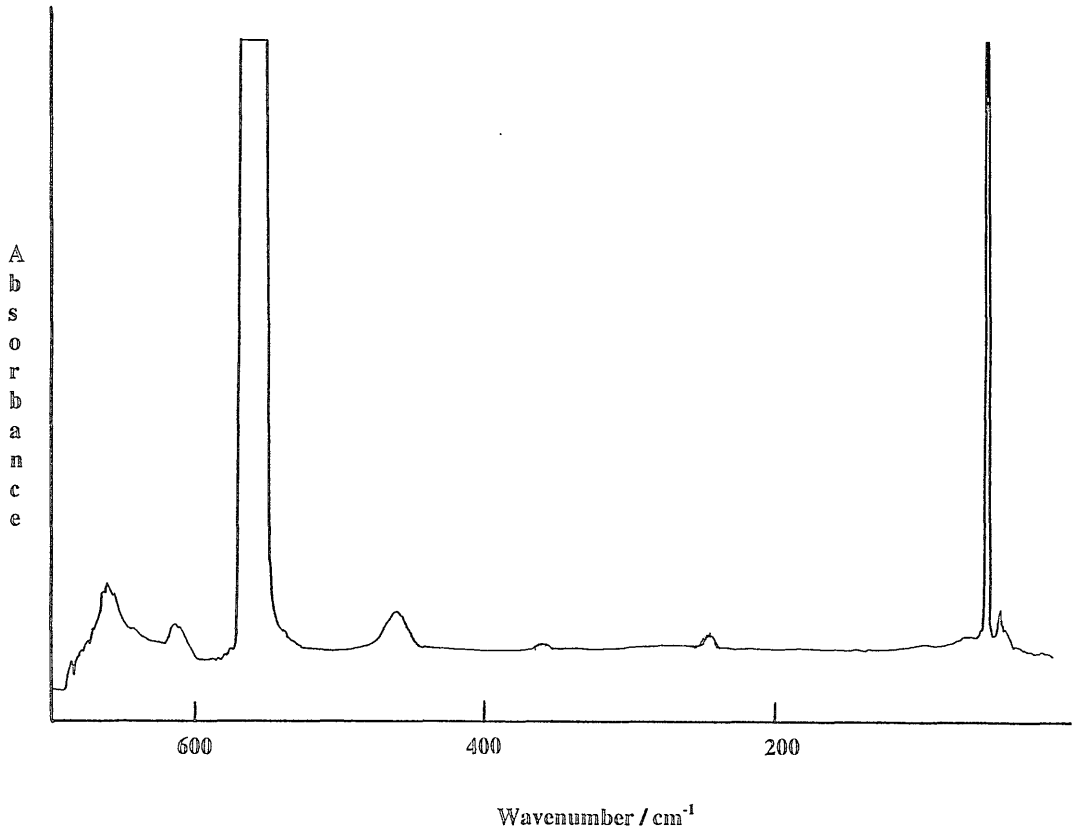

Figure 6.3. Far-infrared spectrum of $HMn(CO)_5$

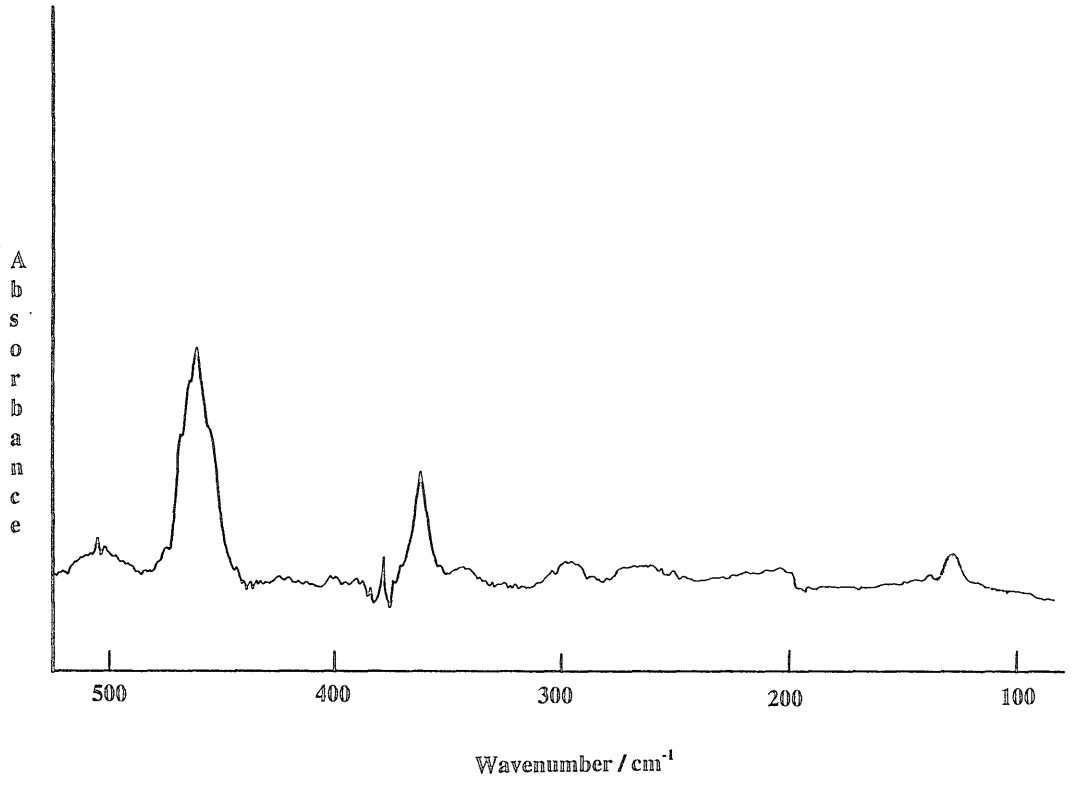

Figure 6.4. Far-infrared spectrum of $DMn(CO)_5$

Table 6.3

Frequencies and assignment of vapour phase spectra of $HMn(CO)_5$ and $DMn(CO)_5$

Wavenumber/cm^{-1}			Assignment
$HMn(CO)_5$ Wilson [Refe 1]	$DMn(CO)_5$ (observed)	$HMn(CO)_5$ (observed)	
731	729	731	(E) Mn-C-O bending
663	661	663	(A_1) Mn-C-O bending
612	608	613	(E) Mn-C-O bending
562	542	561	(E) Mn-C-O bending
	510		(E) Mn-CO stretching
462	460	462	(A_1) Mn-CO stretching
362	362	359	(E) Mn-C-O bending
	131	243	(E) C-Mn-C bending
		63	(A_1) C-Mn-C bending
		47	(E) C-Mn-C bending

Assignments made mainly by comparison with work reported in references [18] and [19].

6.3.3. $CH_3Mn(CO)_5$ and $CD_3Mn(CO)_5$

The vapour phase far-infrared spectra of $CH_3Mn(CO)_5$ and its deuterated analogue $CD_3Mn(CO)_5$ at room temperature are shown in figures 6.5 and 6.6. The δ(MCO) and ν(M-C) region of $CH_3Mn(CO)_5$ has been partially assigned by other workers in the condensed phase studies [11, 40]. Our present analysis in the low frequency region aims to enlarge on these data to find more fundamental vibrations in this region for a vapour phase sample. We observe bands at 657, 610, 559, 457, 376, 149 and 63 cm^1 in the $CH_3Mn(CO)_5$ spectrum and 665, 594, 456, 376, and 63 cm^1 in $CD_3Mn(CO)_5$. Considering previous work on $CH_3Mn(CO)_5$ and similar studies of $BrMn(CO)_5$, we report assignments of the infrared data for $CH_3Mn(CO)_5$ and $CD_3Mn(CO)_5$ by drawing direct analogies [41,42]. Our assignment for this region is also based in part on correlations of the vapour phase and solid-state spectra of $CH_3Mn(CO)_5$ and $CH_3Re(CO)_5$ [14,15]. The assignment are summarised in table 6.4.

The irreducible representations for the normal modes of the vibration for $CH_3Mn(CO)_5$ (if the vibration of CH_3 is not considered) are the same (C_{4V} symmetry) as in $BrMn(CO)_5$ and $HMn(CO)_5$. Eight modes ($4A_1+4E$) consisting of Mn-C-O bending and Mn-CO stretching vibrations are expected in the region 700-300 cm^{-1} and four modes (A_1+3E) are expected below 300 cm^{-1} [7]. In the case of $CH_3Mn(CO)_5$ seven bands are actually observed in the vapour phase spectrum and five bands are observed in the $CD_3Mn(CO)_5$ spectrum. We assign the bands observed at 657 and 559 cm^1 for $CH_3Mn(CO)_5$ as due to E modes corresponding Mn-C-O bending vibrations. Our identification is confirmed as correct by the polarization of the A_1 solution Raman band at 664 cm^{-1} and by the shift to higher

energy of the E mode on deuteration, (in the solution infrared spectra of $CD_3Mn(CO)_5$, this shift result in a single, symmetric band due to concidental overlap of the A_1 and E modes) [41]. In the gas phase spectrum of $CD_3Mn(CO)_5$ this shift results in a symmetric band at 665 cm^1. The band observed at 594 cm^1 in $CD_3Mn(CO)_5$ is also tentatively assigned to an E mode involving Mn-C-O bending motion, and the very weak shoulder at 610 cm^1 in $CH_3Mn(CO)_5$ is tentatively assigned to an A_1 mode correspond to Mn-C-O bending motion by analogy with the solid state spectrum of $CH_3Mn(CO)_5$.

The vapour phase far-infrared spectrum of $CH_3Mn(CO)_5$ is dominated by a peak at 457 cm^{-1}, which can be readily assigned to an A_1 Mn-CO stretching vibration by comparison with the solid-state spectra of $CH_3Mn(CO)_5$ and $CH_3Re(CO)_5$. We note that the same vibration in $CD_3Mn(CO)_5$ is at 456 cm^1. We also observe a very weak band at 376 cm^1 in both $CH_3Mn(CO)_5$ and its deuterated analogue; an obvious assignment for this vibration is the E mode corresponding to a M-CO stretching vibration, since it is close to the frequency observed at 375 cm^{-1} in the solid-state spectrum of $CH_3Re(CO)_5$ [15].

It is generally dificult to make definitive assignments in the very low frequency region (below 300 cm^{-1}) for δ(CMC) modes of metal carbonyl complexes. In the present case we find two bands in $CH_3Mn(CO)_5$, a weak band at 149 cm^1 in $CH_3Mn(CO)_5$ and a very strong band at 63 cm^1 in both $CH_3Mn(CO)_5$ and its deuterated analogue. The vibration at 149 cm^1 can probably be assigned to a C-M-C bending vibration of E symmetry, and that at 63 cm^1 corresponds to an A_1 mode C-M-C bending vibration. The analogous bands in the solid-state spectrum of

$BrMn(CO)_5$ occurs at similar positions [28] i e. 143 and 64 cm^{-1} respectively, and also in the present work these bands are observed at similar positions in the vapour phase spectrum of $HMn(CO)_5$.

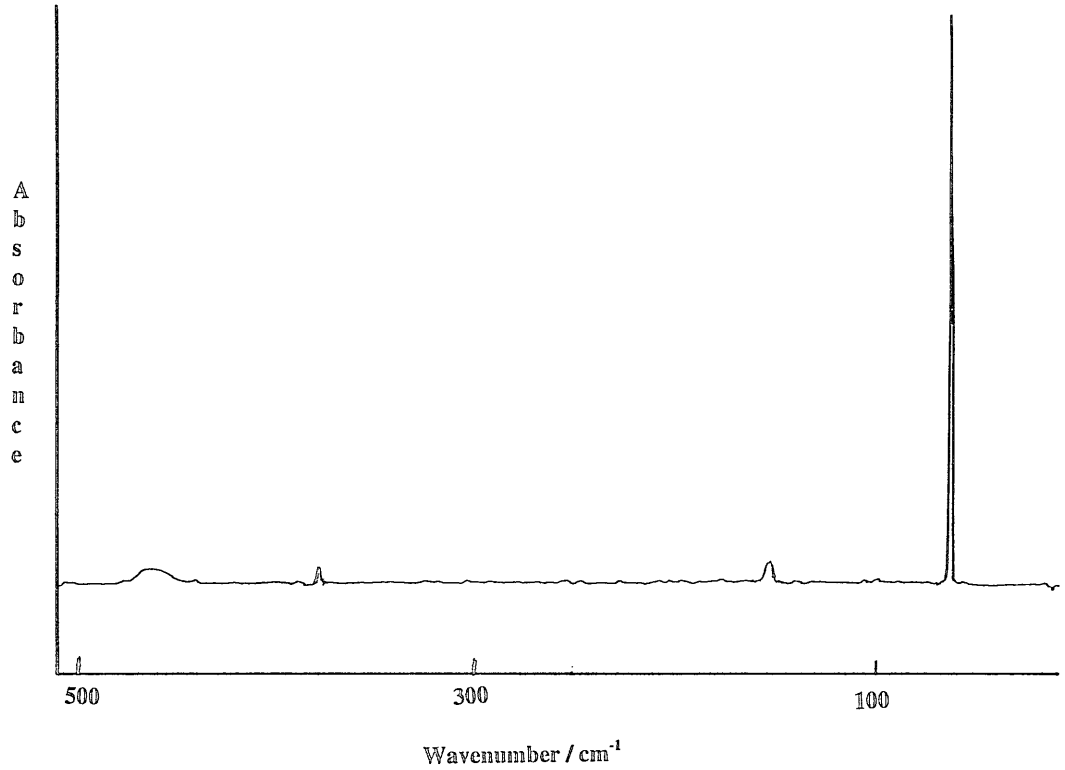

Figure 6.5. Far-infrared spectrum of $CH_3Mn(CO)_5$

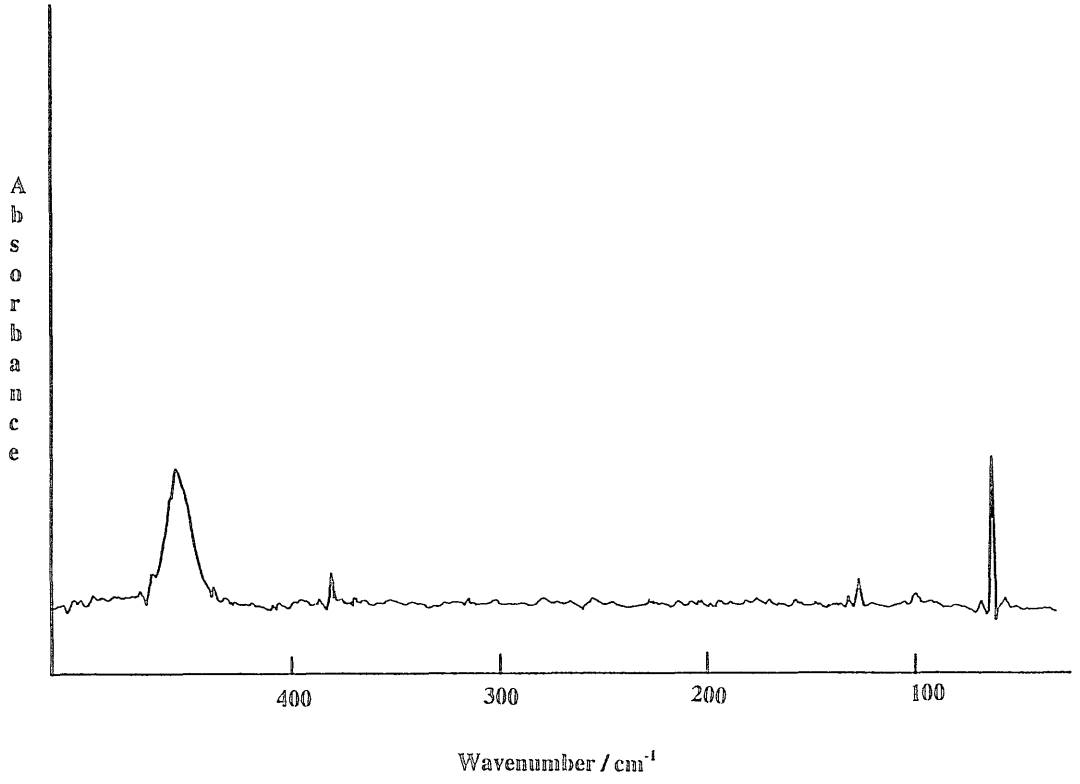

Figure 6.6: Far-infrared spectrum of $CD_3Mn(CO)_5$

Table 6.4

Frequencies and assignment of vapour phase spectra of $CH_3Mn(CO)_5$ and $CD_3Mn(CO)_5$

$CH_3Mn(CO)_5$	$CD_3Mn(CO)_5$	Assignment
657	665	(E) Mn-C-O bending
610	594	(A_1) Mn-C-O bending
559		(E) Mn-C-O bending
457	456	(A_1) Mn-CO stretching
376	376	(E) Mn-CO stretching
149		(E) C-Mn-C bending
63	63	(A_1) C-Mn-C bending

Assignments made mainly by comparison with work reported in refs [14] and [15].

6.3.4. $CF_3Mn(CO)_5$

The IR spectrum of $CF_3Mn(CO)_5$ has been measured and interpreted in the CO stretching region in considerable detail previously [24,43]. The previous studies have all involved solution work. In the present work the infrared spectrum of $CF_3Mn(CO)_5$, has been recorded in the gas phase in the region 700-10 cm^1 for the first time.

The irreducible representations for the normal modes of vibration in $CF_3Mn(CO)_5$ (if the CF_3 vibration is not seriously considered) are the same as in $BrMn(CO)_5$, $HMn(CO)_5$ and $CH_3Mn(CO)_5$ (assuming C_{4v} symmetry). Eight infrared active bands ($4E+4A_1$) are expected in the region below 700 cm^{-1}. These consist of M-C-O bending, Mn-CO stretching and C-F stretching vibrations. Only four bands are observed at 296, 362, 373 and 442 cm^1; the band at 362 cm^{-1} is strong while the other three bands are very weak. The signal-to-noise ratio in the spectrum shown in figure 6.7 is not very good; improved spectra would have been desirable to identify weak absorption bands that may be obscured by noise.

The spectrum of the $CF_3Mn(CO)_5$ is similar to that of $BrMn(CO)_5$, $HMn(CO)_5$ and $CH_3Mn(CO)_5$ in the CO stretching region [44]. The correlation between $CF_3Mn(CO)_5$ and these homologous molecules in the carbon-oxygen stretching region can be easily extended to low frequency region. With reference to the previous work [24,44] on $CF_3M(CO)_5$ we assume that the bands observed in the vapour phase spectrum of $CF_3Mn(CO)_5$ in the present work are due to the $Mn(CO)_5$ group. We can compare $BrMn(CO)_5$ with $CF_3Mn(CO)_5$, which is reasonable based on the similarity of Br and CF_3 in electronegativity and mass. On

this basis and comparison with the vapor phase spectra of $XMn(CO)_5$ (X=Br, H, CH_3) molecules we assign the band observed at 296 cm^{-1} to an E Mn-C-O bending vibration, the analogous band being observed at at 243 cm^{-1} in the spectrum of $HMn(CO)_5$. The band observed at 362 cm^{-1} is assigned to a degenerate Mn-CO stretching vibration , with the corresponding band observed at 359 cm^{-1} in the hydride spectrum. The band observed at 373 cm^{-1} in the gas phase spectrum of $CF_3Mn(CO)_5$ most likely arises from a degenerate Mn-C-O bending vibration. The analogous band observed at 384 cm^{-1} in $BrMn(CO)_5$. The band observed at 442 cm^{-1} is assigned to an A_1 Mn-CO stretching vibration by analogy with the assignments for $BrMn(CO)_5$ and $CH_3Mn(CO)_5$.

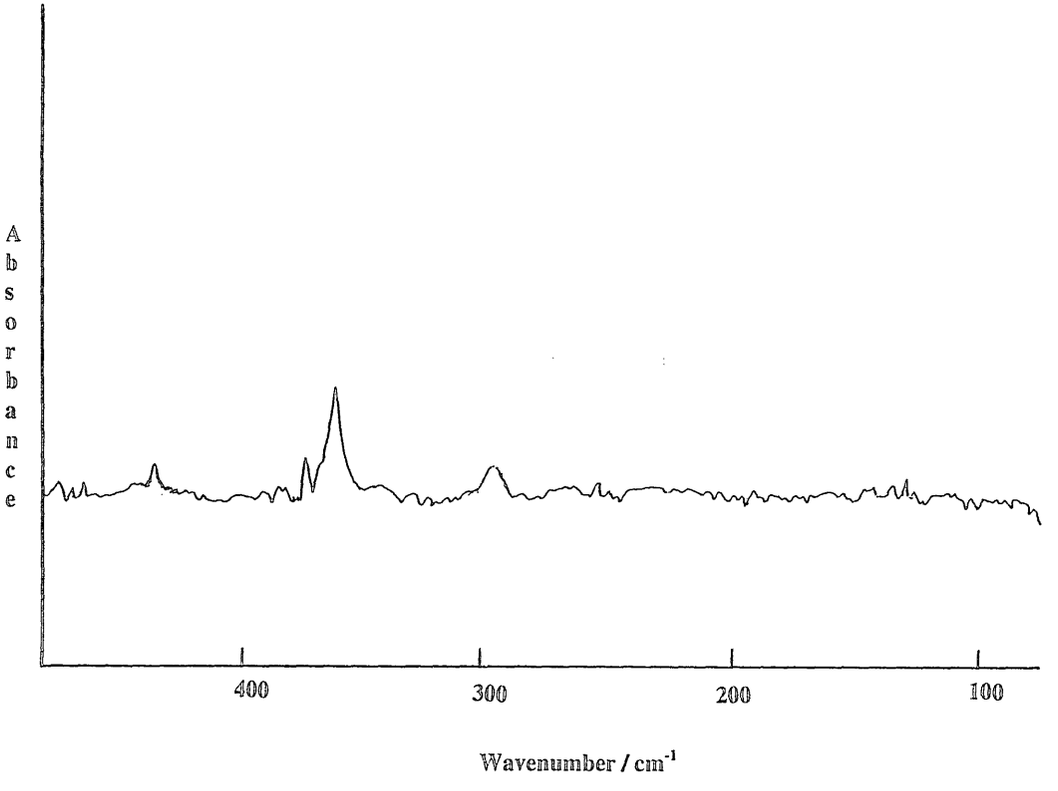

Figure 6.7: Far-infrared spectrum of $CF_3Mn(CO)_5$

Table 6.5.

Frequencies and assignments of far-IR spectrum of vapour phase $CF_3Mn(CO)_5$

Wavnumber/cm^{-1}	Assignment
296	(E) Mn-C-O bending
362	(E) Mn-CO stretching
373	(E) Mn-C-O bending
442	(A_1) Mn-CO stretching

Conclusion.

There were no major differences between the gas phase spectra in the current work and in previous studies on solutions and the solid-state, apart from frequency shifts. There was no evidence of gas phase splitting. It is difficult to make an unequivocable assignment without observing every possible band. There is no doubt that substantial mode mixing occurs in the fundamental modes in the low frequency region. Thus the Mn-C stretching motion and the Mn-C-O bending motion have a pronounced tendency to mix and one can expect some mixing of the axial and planar stretching motion in the A_1 vibrations. While a detailed diccussion of the bonding in the $XMn(CO)_5$ compounds requires a force field calculation, it is possible to make some qualitative comments concerning the observed frequencies.

It is the interesting to note in the present study how the condensed phase influences the metal-carbon stretching and metal-carbon-oxygen bending frequencies if the X (Br, Cl, H, CH_3, CF_3) is substituted on $Mn(CO)_5$. The data given in this chapter shows that the frequency shifts for $XMn(CO)_5$ from solution to vapour phase are mostly upward, are all relatively small, but are not equal. The only frequency observed involving the Mn-C bonds arises from a mixture of stretching and bending motions. Consequently, it is difficult to draw firm conclusions about changes in the Mn-C bonding. However, since the normal mode frequencies change very little from one molecule to another, it can be concluded that there is little change in the Mn-C bond strength. The Mn-X bond was found to be progressively weaker in both the stretching and bending modes as the X was changed. On the basis of the above discussion it is acceptable to assume that the Mn-C bonding in

the $XMn(CO)_5$ compounds are similar and since the same general vibrational pattern is found in the vapour and condensed phase work there is no substantial change in moving from one phase to other. Since the $XMn(CO)_5$ molecules are known to have C_{4V} symetry [11,28] in the solution and solid-state, then it is reasonable to conclude that this symmetry is maintained in the gas phase.

References.

[1]. E. W. Abel, Quart. Rew. (London), 1963, 17, 137.

[2]. F. A. Cotton and C.S. Kraihanzel, J. Am. Chem. Soc., 1962, 84, 4432.

[3]. M. A. Bennett and R. J. H.Clark, J. Chem. Soc.,1964, 5560.

[4]. C. S. Kraihanzel and F. A. Cotton, Inorg. Chem.,1963, 2, 533.

[5]. F. A. Cotton, Inorg. Chem., 1964, 3, 702.

[6]. F. A. Cotton and R. M. Wing, Inorg. Chem., 1965, 4, 1328.

[7]. D. K. Huggins and H.D. Kaesz, J. Am. Chem. Soc., 1964, 86, 2734.

[8]. L. E. Orgel, Inorg. Chem., 1962, 1, 75.

[9]. J. Lewis, A.R. Manning, J. R. Miller, M. J. Ware, and F. Nyman, Nature, 1965, 207, 142

[10]. J. Lewis, A. R. Miller, J. Chem. Soc., Sect. A, 1966, 845..

[11]. I.J.Hyams and E.R..Lippincott, Spectrochim Acta, 1969, 25A, 1845.

[12]. R.D.Closson, J.Kozikowski, T.H.Coffield, J. Org. Chem. 1957, 22,598.

[13]. (a).H.M.Seip, R.Seip. Acta Chem. Scand. 1970, 24. 3431.
(b). W.D.H.Rankin, A. Robertson. J. Organomet. Chem. 1976, 105, 331.

[14]. M.A.Andrews, J.Eckart, J.A.Goldstone, L.Passell, B.Swanson, J. Am. Chem. Soc. 1983, 105,2262.

[15]. (a.) C.Long, A.R.Morrisson, D.C.McKean, and G.P. McQuillan. J. Am. Chem. Soc. 1884, 106, 7418. (b). G.P.McQuillan, D.C.McKean, C.Long, A.R.Morrisson and I.Torto. J. Am. Chem. Soc. 1986, 108, 863.

[16]. A.B.Dempster, D.B.Powell, N.J.Ssheppard, J. Chem. Soc. A 1970, 1129.

[17]. W. Hiieber and G.Wagner, Z. Naturforsch., 1957, 12b, 47.,1958, 13b, 339.

[18]. F.A.Cotton, J.L.Down, and G.Wilkinson, J. Chem. Soc., 1959, 833.

[19]. W.E.Wilson, Z. Naturforsch.,1958, 13b, 349.

[20]. S.J.La Placa, W.C.Hamiliton, and J.A.Ibers, Inorg. Chem., 1964, 3, 1491.

[21]. D.K.Huggins and H.D.Kaesz, J. Am. Chem. Soc., 1964, 86, 2734.

[22]. P.M.Treichel and F.G.A.Ston, Adv. Organometallic Chem., 1964, 1, 143.

[23. R.B.King and M.B.Bisnette. J. Organomet. Chem., 1964, 2, 33.

[24]. F.A.Cotton and J.A.McCleverty, J.Organomet. Chem., 1965, 4,490.

[25]. M.R.Churchill, Chem. Commun., 165, 86.

[26]. M.R.Churchill, Inorg. Chem., 1965, 4, 1734.

[27]. R.Mason and D.R.Russell, Chem. Commun., 1965. 182..

[28]. V.Valenti, F. Cariati, C.Forese and G.Zerbi, Inorg. Nucl. Chem.Lett.1967, 3, 237.

[29]. F.A.Cotton, A.Musco and G. Yagupsky, Inorg. Chem. 1967, 6, 1357.

[30]. H.D.Kaesz, R.Bau, D.Hendrickson and J.M.Smith, J.Am. cHEM. Soc. 1967, 89, 2844.

[31]. P.S.Braterman, R.Bau and H.D.Kaesz, Inorg. Chem. 1967,6, 2097.

[32]. I.J.Hyams and E.R. Lippincott, J. Chem.Soc. A , 1967, 1987.

[33]. R.B.King, Organomet, Chem. Synth. 1965, 1, 147.

[34]. W.F.Edgell and W.M.Risen, Jr., J. Am. Chem. Soc., 1966, 88, 5451.

[35]. W.R.McClellan, J. Am. Chem. Soc. 1961, 83. 1598.

[36]. E.W.Abel and G.Wilkinson, J. Chem. Soc., 1959, 1501.

[37]. R.J.H.Clark and B.C.Crosse. J. Chem. Soc. A, 1969, 224.

[38]. D.M.Adams and A.Squire. J. Chem. Soc. A, 1968, 2817

[39]. W.F.Edgell, G.Asato, W.Wilson, C.Angell. J. Am.Chem. Soc., 1959, 81, 2022

[40]. R.W.Cattrall, R.J.H.Clark,. J. Organomet. Chem. 1966. 6, 167. 46.

[41]. D.K.Ottesen, H.B.Gray, L.H.Jones and M.Goldblatt, Inorg. Chem.1973, 12,1051

[42]. L.H.Jones, R.S.McDowell, M.Goldblatt. Inorg. Chem. 1969, 8, 2349.

[43]. F.A.Cotton, A.Musco, and G.Yagupsky, 1967, 6, 1357.

[44]. A.A.Cotton and R.M.Wing. J. Organomet. Chem 1967, 9. 511.

[45]. R.C.Taylor, J. Chem. Phys; 1954, 22, 714.

Chapter 7

Overall Conclusions

A gas phase mid and far-infrared study of mixtures of TMAl and DMAlH was carried out and it was observed that the properties of the mixture were not simply a superposition of those of the initial components. It was clearly shown by both gas phase FTIR and solution NMR spectroscopy that on mixing DMAlH with TMAl the predominant species is a mixed hydrogen-methyl bridged dimer, with smaller contribution from trimeric and higher species with both H and Me bridging units. The observation of two major Al-H resonances, readily ascribed to the dominant dimeric mixed bridge and trimeric dimethylalane units, is similar to that of Eisch and Rhee in the isobutyl case. However, the combined weight of our observations supports the contention that the chemical shift of these resonances is more a measure of variation in the angle subtended at the Al-H-Al centre than of the nature of the other bridging or terminal moieties, with a decrease in this angle resulting in a shift of the resonance to lower field. Indeed, this hypothesis is further supported by the observation of a weaker resonance at intermediate field in this region, which may well be due to a mixed bridge trimer. Temperature variation studies also support the above conclusion. The weakest Al-Me-Al bridge is probably that in the mixed dimer, with the result that even at the lowest temperature attainable, bridge-terminal Me exchange on the NMR timescale occurs in this species.

Both experimental and theoretical evidence points to the same conclusion, namely that the species $Me_2Al(\mu H)(\mu Me)AlMe_2$ is formed as the major component in mixture of TMA and DMAlH, and that this results from a substantial increase in strength of the Al-H-Al bridge bond. NMR results interpreted on this basis strongly

support the contention that bridge-terminal group exchange can result from a single bond dissociation and reassociation.

FTIR spectra show quite conclusively that extensive and rapid exchange of alkyl groups and hydrogen atoms occurs in gas phase mixtures of TMAA and TMGa. The tendency is for the hydrogen to migrate to the more electronegative gallium centre, and for the trimethylamine to complex preferentially with the aluminium centre, in line with the greater Lewis acidity of the latter. Some of the species thus formed are of low thermal stabilty and may decompose slowly even at room temperature. It is very evident from the FTIR spectra of TMAA/TMGa mixtures that the most prominent infrared bands are readily attributed to free dimethylgallane, Me_2GaH. This species has recently been shown to exist in the gas phase as a mixture of hydrogen bridged trimer (with strong infrared absorption at 1705 cm^{-1}) and dimer (strong bands at 1290 and 1185 cm^{-1}).

The IR LPHP studies of TMGa and TEGa mixtures were very revealing, both in their own right and in the additional light they shed on the TEGa system. The first conclusion is that at moderate temperature the products observed are consistent with the almost complete removal of Ga-bound ethyl groups and retention of methyl groups. This confirms the contention that β-elimination is strongly preferred to Ga-R bond homolysis. The products identified are entirely consistent with exchange of alkyl groups, coupled with the loss of Ga-Et groups via β-hydride elimination. The laser pyrolysis studies have provided a novel route for the production of dialkylalkylgallanes, in particular dimethylgallane. This was shown to be mainly dimeric in the vapour phase from spectroscopic evidence as

mentioned earlier. The spectra of mixtures of TMAA/TMGa and the pyrolysis products of TMGa and TEGa mixtures were found to be complex, reflecting the large number of species present. However, they can be accounted for almost quantitatively by the following simple conclusion. We assume that the mixture contains both dimeric species and trimeric species, with the former dominant, as indicated by NMR and mass spectrometric evidence, and that dialkylgallane $RR'GaH$ exists as H-bridged dimers and trimers in toluene solution, Exchange processes then lead to a statisical ditribution of all possible oligomeric forms.

The far-infrared spectra of the η-bonded metal carbonyls, butadiene iron tricarbonyl, cyclopentadienylmanganese tricarbonyl and methylcyclopentadienyl manganese tricarbonyls have been studied in the vapour phase. For butadiene iron tricarbonyl some vibrational wavenumbers show small or modest shifts relative to previous condensed phase work, but the vibrational pattern remains the same as in the liquid phase. Cyclopentadienyl manganese tricarbonyl and Methylcyclopentadienyl manganese tricarbonyl show bands assigned to skeletal vibrations at nearly identical positions in their vapour phase spectra. The methyl substituent does not appear to cause substantial splitting of the nominally degenerate modes of the $Mn(CO)_3$ group when moving from $CpMn(CO)_3$ to $MeCpMn(CO)_3$. Each vibrational mode of cyclopentadienylmanganese tricarbonyl is in turn related to the equivalent mode of $MeCpMn(CO)_3$. The ring-metal modes are shifted to higher frequency in the spectrum of $MeCpMn(CO)_3$, in agreement with trends previously noted in the spectra of ferrocene and dimethylferrocene.

Vibrational fundamentals fall in the far-infrared when atomic masses are large and/or the force resisting the deformation is small. Some vibrations of metal carbonyls fall into this catogory and given that mid-IR spectra of metal carbonyls are well-characterised, they provide good candidates for investigating low frequency vibrations. A number of metal carbonyls, e.g. $BrMn(CO)_5$, $ClMn(CO)_5$, $HMn(CO)_5$, $DMn(CO)_5$, $CH_3Mn(CO)_5$, $CD_3Mn(CO)_5$ and $CF_3Mn(CO)_5$ have been studied in the vapour phase in this work. The metal-CO stretching frequencies were found between 350-475 cm^{-1}. The metal-C-O bending frequencies were more scattered and fell between 275 and 650 cm^{-1}. The OC-M-CO bending modes have very low frequencies and occur between 50 and 150 cm^{-1}. Other vibrations were found in this region when one or more CO groups was replaced by groups in which heavy atoms or substituents were attached to the metal.

The far-infrared spectral region is notoriously difficult to work in and the spectra obtained in this work did not always exhibt good signal-to-noise ratios. Since as a consequence some bands were inevitably not strong enough to observed, it is difficult to make an unequivocable assignment of every observed band. An added difficulty is that substantial mode mixing is common in the fundamental modes in the low frequency region. Thus, for example, the totally symmetric M-C stretching and M-C-O bending motions have a pronounced tendency to mix. It is interesting to note in the present study how the condensed phase influences the metal-carbon stretching and metal-carbon-oxygen bending frequencies if X (X=Br, Cl, H, CH_3, CF_3) is substituted on $XMn(CO)_5$. The data given in chapter 6 show that the frequency shifts for $XMn(CO)_5$ from solution to vapour phase are mostly upward, are all relatively small, but are not equal. However, since the normal mode

frequencies change very little from one molecule to another, it can be concluded that there is little change in the M-C bond strength in passing from gas to condensed phase. On the basis of the above discussion it is acceptable to conclude that the Mn-C bonding in the $XMn(CO)_5$ compounds is similar and since the same general vibrational pattern is found in the vapour and condensed phase work, there is no substantial change in moving from one phase to another. Since the $XMn(CO)_5$ molecules are known to have C_{4V} symmetry in the solution and solid state, then it is reasonable to conclude that this symmetry is maintained in the gas phase.